

Determination of the Neutron and Gamma Flux Distribution in the Pressure Vessel and Cavity of a Boiling Water Reactor

Prepared by M. Asgari, M. L. Williams, and F. B. K. Kam

Oak Ridge National Laboratory

**Prepared for
U.S. Nuclear Regulatory Commission**

AVAILABILITY NOTICE

Availability of Reference Materials Cited in NRC Publications

Most documents cited in NRC publications will be available from one of the following sources:

1. The NRC Public Document Room, 2120 L Street, NW, Lower Level, Washington, DC 20555
2. The Superintendent of Documents, U.S. Government Printing Office, P.O. Box 37082, Washington, DC 20013-7082
3. The National Technical Information Service, Springfield, VA 22161

Although the listing that follows represents the majority of documents cited in NRC publications, it is not intended to be exhaustive.

Referenced documents available for inspection and copying for a fee from the NRC Public Document Room include NRC correspondence and internal NRC memoranda; NRC Office of Inspection and Enforcement bulletins, circulars, information notices, inspection and investigation notices; Licensee Event Reports; vendor reports and correspondence; Commission papers; and applicant and licensee documents and correspondence.

The following documents in the NUREG series are available for purchase from the GPO Sales Program: formal NRC staff and contractor reports, NRC-sponsored conference proceedings, and NRC booklets and brochures. Also available are Regulatory Guides, NRC regulations in the *Code of Federal Regulations*, and *Nuclear Regulatory Commission Issuances*.

Documents available from the National Technical Information Service include NUREG series reports and technical reports prepared by other federal agencies and reports prepared by the Atomic Energy Commission, forerunner agency to the Nuclear Regulatory Commission.

Documents available from public and special technical libraries include all open literature items, such as books, journal and periodical articles, and transactions. *Federal Register* notices, federal and state legislation, and congressional reports can usually be obtained from these libraries.

Documents such as theses, dissertations, foreign reports and translations, and non-NRC conference proceedings are available for purchase from the organization sponsoring the publication cited.

Single copies of NRC draft reports are available free, to the extent of supply, upon written request to the Office of Information Resources Management, Distribution Section, U.S. Nuclear Regulatory Commission, Washington, DC 20555.

Copies of industry codes and standards used in a substantive manner in the NRC regulatory process are maintained at the NRC Library, 7920 Norfolk Avenue, Bethesda, Maryland, and are available there for reference use by the public. Codes and standards are usually copyrighted and may be purchased from the originating organization or, if they are American National Standards, from the American National Standards Institute, 1430 Broadway, New York, NY 10018.

DISCLAIMER NOTICE

This report was prepared as an account of work sponsored by an agency of the United States Government. Neither the United States Government nor any agency thereof, or any of their employees, makes any warranty, expressed or implied, or assumes any legal liability of responsibility for any third party's use, or the results of such use, of any information, apparatus, product or process disclosed in this report, or represents that its use by such third party would not infringe privately owned rights.

Determination of the Neutron and Gamma Flux Distribution in the Pressure Vessel and Cavity of a Boiling Water Reactor

Manuscript Completed: August 1989
Date Published: June 1990

Prepared by
M. Asgari, M. L. Williams, and F. B. K. Kam

Oak Ridge National Laboratory
Operated by Martin Marietta Energy Systems, Inc.

Oak Ridge National Laboratory
Oak Ridge, TN 37831

Prepared for
Division of Engineering
Office of Nuclear Regulatory Research
U.S. Nuclear Regulatory Commission
Washington, DC 20555
NRC FIN B0415
Under Contract No. DE-AC05-84OR21400

ABSTRACT

The Grand Gulf Boiling Water Reactor (BWR/6), owned and operated by Mississippi Power & Light Company, has been analyzed to determine the neutron and gamma energy spectrum and flux levels in regions from the reactor vessel throughout the concrete shield wall. Several two-dimensional and one-dimensional transport calculations were performed for the Grand Gulf reactor configuration. The results from these calculations were synthesized to obtain the three-dimensional neutron flux spectra and dosimeter activities. The results from the transport calculations indicate the flux above 1 MeV peaks near the axial midplane and azimuthal angle between 40° and 45° , depending on the radial locations. The peak flux above 1 MeV incident on the vessel and at midcavity is about 1.82×10^9 and $1.07 \times 10^8 \text{ n}\cdot\text{cm}^{-2}\cdot\text{s}^{-1}$, respectively. The vessel fluence accumulated during Cycle 2 and after 32 effective full power years is about 4.41×10^{16} and $1.84 \times 10^{18} \text{ n}\cdot\text{cm}^{-2}$ respectively. The peak flux above 1 MeV at the front of the concrete shield wall, 15.24 cm (6 in.) into the concrete wall, and 30.48 cm (1 ft) into the concrete wall is about 7.91×10^7 , 7.24×10^6 , and $6.44 \times 10^5 \text{ n}\cdot\text{cm}^{-2}\cdot\text{s}^{-1}$, respectively.

The results obtained from the gamma calculations show that the peak gamma heating at the O-T location of the reactor pressure vessel has a value of $2.54 \times 10^{-3} \text{ W/g}$ of stainless steel (SS 304). The peak gamma absorbed dose rate at the midcavity is about $7.31 \times 10^3 \text{ rad/h}$ at full power operation.

CONTENTS

	<u>Page</u>
ABSTRACT	iii
LIST OF FIGURES	vi
LIST OF TABLES	ix
1. INTRODUCTION	1
2. DESCRIPTION OF THE REACTOR	3
3. CALCULATION METHODOLOGY	8
3.1 THREE-DIMENSIONAL FLUX SYNTHESIS	8
3.2 DOT-IV R- θ CALCULATION	9
3.3 DOT-IV R-Z CALCULATION	13
3.3.1 In-vessel R-Z Model	13
3.3.2 Cavity, Ex-vessel, R-Z Model	17
3.4 DOT-IV ONE-DIMENSIONAL CALCULATION.....	20
3.5 DETERMINATION OF NEUTRON SOURCE	22
4. MULTI-GROUP CROSS-SECTION LIBRARY	27
5. RESULTS	33
6. CONCLUSIONS	72
7. REFERENCES	73
APPENDIX A	75

LIST OF FIGURES

	<u>Page</u>
2.1. Cutaway view of a boiling water reactor (BWR/6)	4
2.2. Cross-sectional view of a typical BWR/6 core arrangement and core lattice	5
2.3. Cutaway view of a typical BWR/6 fuel assembly	6
3.1. One-eighth slice of the Grand Gulf reactor model used in DOT-IV R- θ calculation	10
3.2. In-vessel R-Z model used in DOT-IV calculation	14
3.3. Comparison of actual and modeled moderator void fraction distribution used in in-vessel R-Z calculation	17
3.4. Ex-vessel, cavity, R-Z model used in DOT-IV calculation	18
3.5. One-dimensional model used in DOT-IV calculation	20
3.6. Power-time histogram for Grand Gulf Cycle 2	22
5.1.a. Neutron flux above 1 MeV ($\text{n}\cdot\text{cm}^{-2}\cdot\text{s}^{-1}$) contours within the reactor vessel and the concrete shield wall based on DOT-IV R- θ calculation	36
5.1.b. Neutron flux above 1 MeV ($\text{n}\cdot\text{cm}^{-2}\cdot\text{s}^{-1}$) contours within the reactor cavity based on DOT-IV R- θ calculation	37
5.2. Displacements per atom, dpa, ($\text{dpa}\cdot\text{s}^{-1}$) contours based on DOT-IV R- θ calculation	38
5.3. Neutron flux below 0.4 eV ($\text{n}\cdot\text{cm}^{-2}\cdot\text{s}^{-1}$) contours based on DOT-IV R- θ calculation	39
5.4. Neutron flux above 1 MeV ($\text{n}\cdot\text{cm}^{-2}\cdot\text{s}^{-1}$) contours based on in-vessel DOT-IV R-Z calculation	40
5.5. Displacements per atom, dpa, ($\text{dpa}\cdot\text{s}^{-1}$) contours based on in-vessel DOT-IV R-Z calculation	41

LIST OF FIGURES
(Continued)

	<u>Page</u>
5.6. Neutron flux below 0.4 eV ($\text{n}\cdot\text{cm}^{-2}\cdot\text{s}^{-1}$) contours based on in-vessel DOT-IV R-Z calculation	42
5.7. Neutron flux above 1 MeV ($\text{n}\cdot\text{cm}^{-2}\cdot\text{s}^{-1}$) contours based on ex-vessel (cavity) DOT-IV R-Z calculation	43
5.8. Displacements per atom, dpa, ($\text{dpa}\cdot\text{s}^{-1}$) contours based on ex-vessel (cavity) DOT-IV R-Z calculation	44
5.9. Neutron flux below 0.4 eV ($\text{n}\cdot\text{cm}^{-2}\cdot\text{s}^{-1}$) contours based on ex-vessel (cavity) DOT-IV R-Z calculation	45
5.10. Gamma heating (W/g SS 304) contours based on ex-vessel (cavity) DOT-IV R-Z calculation	46
5.11. Gamma absorbed dose (rad/h) contours based on ex-vessel (cavity) DOT-IV R-Z calculation	47
5.12. Neutron energy spectra ($\text{n}\cdot\text{cm}^{-2}\cdot\text{s}^{-1}\cdot\Delta\text{u}^{-1}$) outside and center of the 3° surveillance capsule at the axial peak location	59
5.13. Neutron energy spectra ($\text{n}\cdot\text{cm}^{-2}\cdot\text{s}^{-1}\cdot\Delta\text{u}^{-1}$) at two radial locations in the RPV at the axial core midplane	60
5.14. Neutron energy spectra ($\text{n}\cdot\text{cm}^{-2}\cdot\text{s}^{-1}\cdot\Delta\text{u}^{-1}$) at two radial locations in the RPV at the axial peak	61
5.15. Neutron energy spectra ($\text{n}\cdot\text{cm}^{-2}\cdot\text{s}^{-1}\cdot\Delta\text{u}^{-1}$) at two radial locations in the RPV at the feed water nozzle elevation	62
5.16. Neutron energy spectra ($\text{n}\cdot\text{cm}^{-2}\cdot\text{s}^{-1}\cdot\Delta\text{u}^{-1}$) at midcavity and 15.24 cm into the concrete shield wall at the axial core midplane	63
5.17. Neutron energy spectra ($\text{n}\cdot\text{cm}^{-2}\cdot\text{s}^{-1}\cdot\Delta\text{u}^{-1}$) at midcavity and 15.24 cm into the concrete shield wall at the axial peak	64

LIST OF FIGURES
(Continued)

	<u>Page</u>
5.18. Neutron energy spectra ($n \cdot \text{cm}^{-2} \cdot \text{s}^{-1} \cdot \Delta u^{-1}$) at midcavity and 15.24 cm into the concrete shield wall at the feed water nozzle elevation	65
5.19. Radial variation of neutron energy spectra ($n \cdot \text{cm}^{-2} \cdot \text{s}^{-1} \cdot \Delta u^{-1}$) through the concrete shield wall at the axial core midplane	66
5.20. Gamma energy spectra ($\gamma \cdot \text{cm}^{-2} \cdot \text{s}^{-1}$) at four radial locations throughout the RPV and the concrete shield wall at the axial core midplane	67
5.21. Gamma energy spectra ($\gamma \cdot \text{cm}^{-2} \cdot \text{s}^{-1}$) at four radial locations throughout the RPV and the concrete shield wall at the axial peak	68
5.22. Gamma energy spectra ($\gamma \cdot \text{cm}^{-2} \cdot \text{s}^{-1}$) at four radial locations throughout the RPV and the concrete shield wall at the feed water nozzle elevation	69
5.23. Radial variation of the flux above 1 MeV ($n \cdot \text{cm}^{-2} \cdot \text{s}^{-1}$) at five axial locations	70
5.24. Axial variation of the flux above 1 MeV ($n \cdot \text{cm}^{-2} \cdot \text{s}^{-1}$) at five radial locations	71

LIST OF TABLES

	<u>Page</u>
2.1. Core design data for Grand Gulf reactor	7
3.1. R- θ material zones and material densities	11
3.2. R-Z material zones and material densities	15
3.3. Cavity R-Z material zones and material densities	19
3.4. One-dimensional material zones and material densities	21
3.5. X-Y relative power distribution at the core midplane	23
3.6. R-Z axial and radial burnup (MWd/Mt) distribution	24
3.7. Power-time history of Grand Gulf Cycle 2	26
4.1. SAILOR thermal correction factors based on 27-group results for absorption (f_a) and total (f_t) cross sections	28
4.2. SAILOR 47-group neutron and 20-group gamma library energy structure	29
4.3. New SAILOR P_0 cross-section identifiers	31
5.1. Spectrum-averaged cross section at center of 3° surveillance capsule for Grand Gulf Cycle 2	48
5.2. Calculated saturated activities in the Grand Gulf 3° surveillance capsule at midplane (Cycle 2)	48
5.3. Calculated saturated activities in the Grand Gulf 3° surveillance capsule at axial peak (Cycle 2)	49
5.4. Nonsaturation factors (h_{ns}) for Grand Gulf Cycle 2	49
5.5. Calculated lead factors at various radial locations through the RPV wall and cavity of Grand Gulf Cycle 2	50
5.6. Relative azimuthal variation in $\Phi(>1 \text{ MeV})$ through the RPV wall of Grand Gulf Cycle 2	51

LIST OF TABLES
(Continued)

		<u>Page</u>
5.7.	Relative azimuthal variation in $\Phi(>1 \text{ MeV})$ through the reactor cavity of Grand Gulf Cycle 2	53
5.8.	Radial variation of the total dpa, flux above 1 MeV, flux below 0.4 eV, and thermal-to-fast flux ratio at the axial core midplane and azimuthal peak	55
5.9.	Radial variation of the total dpa, flux above 1 MeV, flux below 0.4 eV, and thermal-to-fast flux ratio at the axial and azimuthal peaks	56
5.10.	Radial variation of the total dpa, flux above 1 MeV, flux below 0.4 eV, and thermal-to-fast flux ratio at the axial feed water nozzle elevation and azimuthal peak	57
5.11.	Determination of RPV peak cumulative fluence ($\text{n}\cdot\text{cm}^{-2}$) and dpa for Grand Gulf BWR/6	58
5.12.	Radial variation in gamma heating and gamma absorbed dose rate at three axial locations	58

ACKNOWLEDGMENTS

The authors would like to thank the Grand Gulf Nuclear Power Plant management and personnel, especially Pat Simpson, Ray Paterson, John Vincelli, and David Hendrix, for their overall cooperation and assistance in providing the reactor data.

This study was funded by the Louisiana State University (LSU) Center for Energy Studies and the U.S. Nuclear Regulatory Commission. This work was performed at LSU under contract number 19XSB408V with the Oak Ridge National Laboratory and served as a portion of the master's thesis in nuclear engineering for the first author.

1. INTRODUCTION

The huge initial capital investment in the construction of a nuclear power plant requires that utility companies operate the plant as long as possible before permanent shutdown in order to recover the invested capital and to provide the public with low utility rates. An important factor impacting the operating lifetime of a nuclear power reactor is the integrity of the reactor pressure vessel (RPV). The RPV is a large steel tank containing the reactor core in which heat is generated by fission. The RPV is subject to radiation embrittlement due to the continual neutron bombardment during reactor operation. This damage mechanism reduces the ability of the steel vessel to withstand severe stresses. This reduced integrity could result in the reactor vessel failure under certain accident conditions in which low-temperature, emergency coolant is injected into the RPV. The rapid change in temperature could cause a large thermal stress in the embrittled RPV, resulting in the propagation of a flaw through the vessel wall.

The U.S. Nuclear Regulatory Commission (NRC) has placed strict limits on the amount of radiation damage that an RPV can receive and still remain in operation. The NRC also requires that each utility company operating a nuclear reactor maintain an RPV surveillance program to monitor the RPV neutron fluence exposure during reactor lifetime operation. Thus, several surveillance capsules containing both metallurgical specimens of the material used in weldments and RPV, as well as dosimetry foils of different activation cross-section thresholds, have been incorporated into the design of nuclear reactors. These capsules are periodically removed and analyzed during the reactor lifetime operation. Unfortunately, the dosimeter data only provide limited information at a few selected points within the reactor. Thus, to obtain a detailed knowledge about the intensity and energy distribution of the neutron flux bombarding the RPV, it is necessary to perform neutron transport calculations in addition to the dosimetry analysis. The transport calculations provide extensive data at all points in the reactor vessel, as well as within the cavity where radiation damage to support structures may be a concern. The accuracy of the transport calculations is governed by the accuracy of the reactor model and the fundamental nuclear cross-section data.

Several earlier studies have been supported by the NRC to ascertain the expected fluence levels within the RPV and cavity of several power reactors.^{1,2} Most of these studies have been performed for pressurized water reactors (PWRs) because this type of reactor generally has a larger fluence exposure to the RPV; however, during extended lifetime operation, the radiation damage to pressure vessels in boiling water

reactors (BWRs) may also be a concern. The primary objectives of this work are to determine the cumulative fluence incident on and within the RPV, reactor cavity, and concrete reactor shield during Cycle 2 of the Grand Gulf Boiling Water Reactor (BWR/6) configuration, owned by Mississippi Power & Light (MP&L) Company, in order to provide realistic estimates for "typical" fluence levels in a BWR.

2. DESCRIPTION OF THE REACTOR

This study has been performed for the Grand Gulf BWR/6 owned by MP&L, which is located in Port Gibson, Mississippi. The BWR/6 is the latest BWR product line designed by the General Electric Corporation. These reactors have output power capabilities ranging from 600 to 1400 MW(e). Some of the BWR/6 principle design features as compared to earlier BWRs are more fuel bundles, smaller diameter fuel rods, longer active fuel length, and an 8 x 8 fuel bundle arrangement.

Figure 2.1 represents a typical BWR and its internal components. Some of the major components, as shown in Fig. 2.1, are the reactor vessel, core and internals, shroud, top guide assembly, core plate assembly, steam separator and dryer, and jet pumps. The typical plan views of the core arrangement and the lattice configuration of a BWR are shown in Fig. 2.2. The Grand Gulf reactor core consists of 800 fuel assemblies, each of which contains 64 fuel pins that are spaced and supported in a square 8 x 8 array by lower and upper tie plates. Figure 2.3 represents a typical BWR fuel assembly. Water is circulated through the reactor core producing saturated steam. The steam is then separated from the recirculated water and dried in the top of the vessel; then it is directed to the steam turbine-generator to generate electricity. The voids introduced in the core coolant by boiling affect the neutron transport and must be included in the transport model.

Table 2.1 represents some of the core design data used in modeling the reactor for analysis. It should be noted that a simplified version of the actual reactor must be used in the calculation models, because only two-dimensional (2-D) geometries can be represented in the DOT transport calculations. Also, only the nuclides that could affect the leakage of the high-energy neutrons from the core were included in the modeling of the reactor core.

ORNL DWG. NO. 89-15129

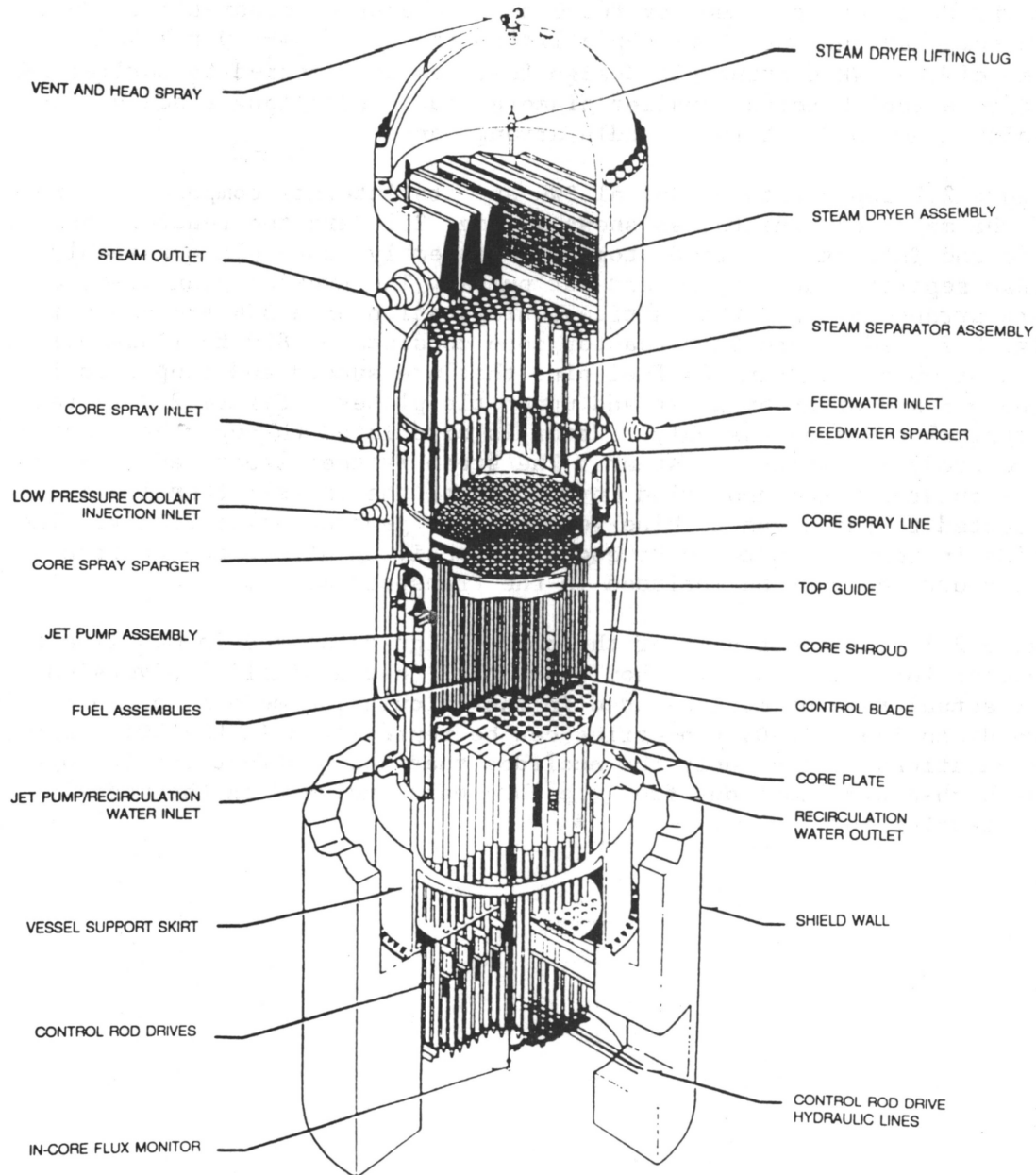


Fig. 2.1. Cutaway view of a boiling water reactor (BWR/6).
 Source: BWR/6 General Description of a Boiling Water Reactor, General Electric Company, Nuclear Energy Group, San Jose, Calif., September 1980.

ORNL DWG. NO. 89-15130

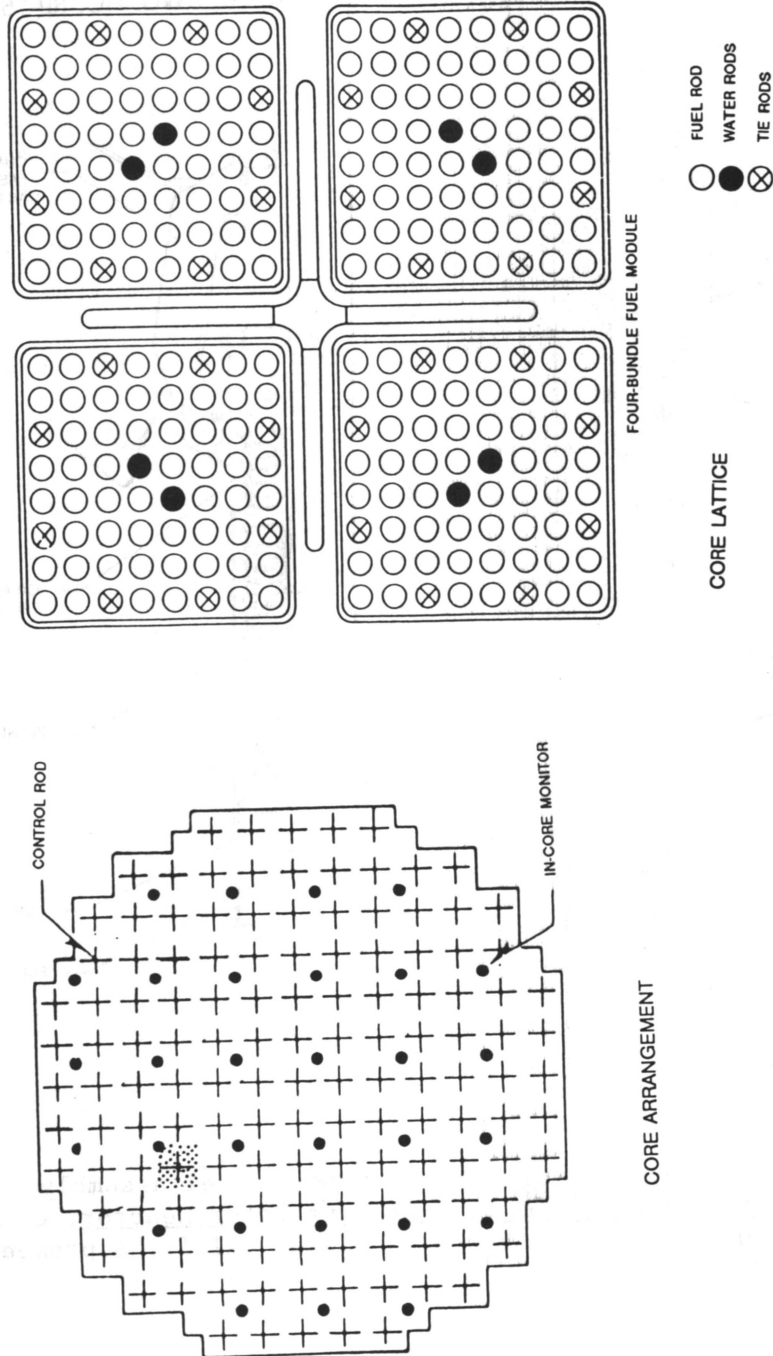


Fig. 2.2. Cross-sectional view of a typical BWR/6 core arrangement and core lattice. Source: BWR/6 General Description of a Boiling Water Reactor, General Electric Company, Nuclear Energy Group, San Jose, Calif., September 1980.

ORNL DWG. NO. 89-15131

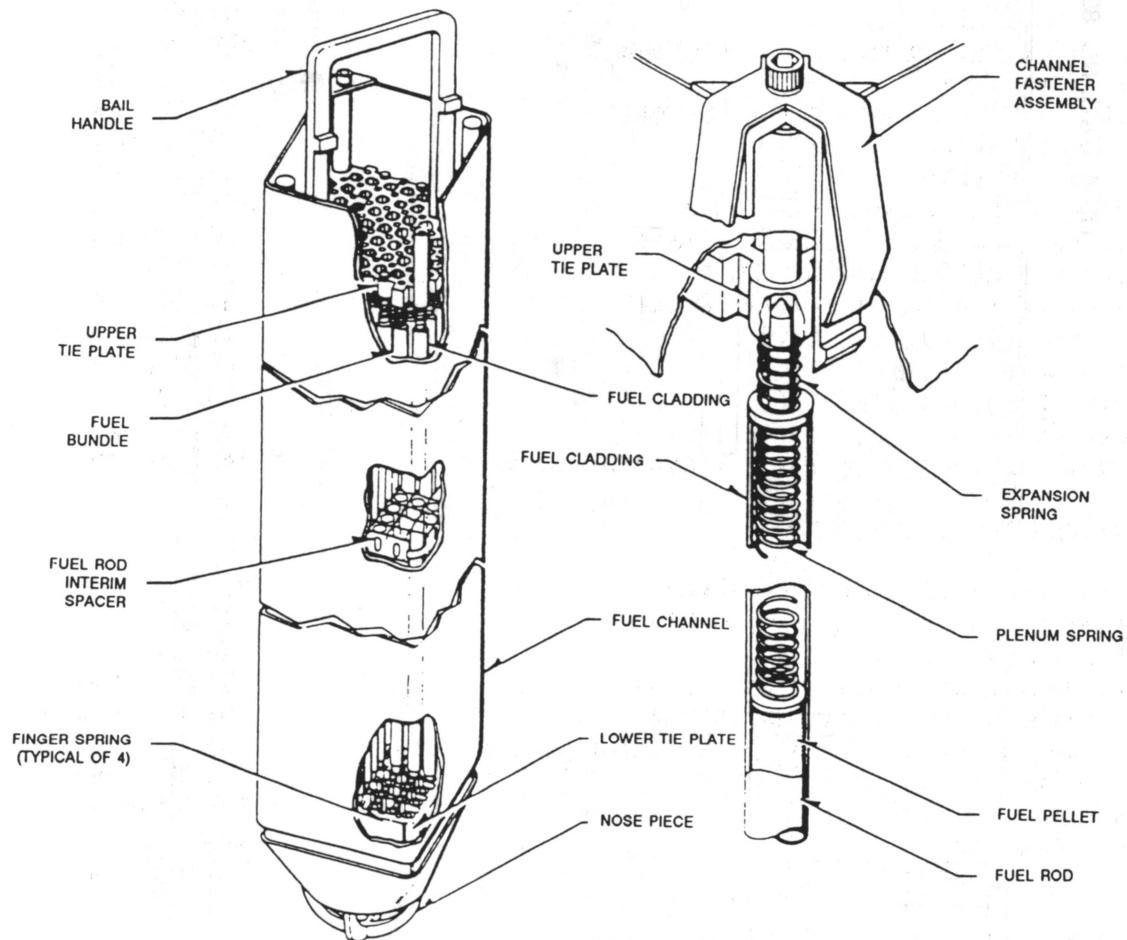


Fig. 2.3. Cutaway view of a typical BWR/6 fuel assembly.

Source: BWR/6 General Description of a Boiling Water Reactor, General Electric Company, Nuclear Energy Group, San Jose, Calif., September 1980.

Table 2.1. Core design data for Grand Gulf reactor

Reactor

Design reactor thermal power	3833	MW
Core inlet temperature	278.9	°C
Core operating pressure	7.20	MPa
Outer core diameter	486.41	cm
Radius of the shroud inner surface	270.256	cm
Shroud thickness	5.08	cm
Radius of the liner of the RPV wall	321.31	cm
Thickness of the liner	0.476	cm
RPV wall thickness	16.392	cm
Radius of the insulation liner	351.79	cm
Thickness of the insulation liner	0.159	cm
Thickness of the insulation	8.571	cm
Radius of the concrete shield wall	436.88	cm
Jet pump ID	18.212	cm
Jet pump OD	20.752	cm
Riser ID	25.40	cm
Riser OD	28.245	cm
Surveillance capsule total width/thickness	8.38/3.10	cm

Core and fuel assemblies

Total number of fuel assemblies	800	
Number of fuel rods per assembly	64	
Pitch to pitch	15.199	cm
Fuel volume fraction in the core	22.7	vol %
Moderator volume fraction in the core	61.3	vol %
Cladding and channel volume fraction in the core	15.0	vol %
Gap volume fraction	1.0	vol %
Cladding material	Zircaloy-4	
Fuel material	UO ₂	
Active core length	381.0	cm

Heat transfer and fluid flow

Core saturated temperature	287.7	°C
Total core flow	53.07	kg/h
Core channel flow	46.72	kg/h
Void fraction at the core midplane	40.50	vol %

3. CALCULATION METHODOLOGY

3.1 THREE-DIMENSIONAL FLUX SYNTHESIS

In the RPV transport calculations, it is desired to obtain the detailed three-dimensional (3-D) RPV flux distribution, since the flux varies in all three dimensions. Recently, a new computer code called "TORT"⁴ (three-dimensional Oak Ridge transport) has been developed at Oak Ridge National Laboratory (ORNL), Oak Ridge, Tennessee, for solving the 3-D transport equation but it has not been released to the public. Unfortunately, the computation costs for such calculations using 3-D transport codes like TORT are very expensive and not practical for routine applications. Therefore, most utilities and other organizations prefer the use of some other methods to obtain a good approximation to the true 3-D flux distribution.

In this study, the 3-D flux distribution will be obtained by using a computer code called DOTSYN⁵, which is a member of the LEPRICON⁶ system. This code is based on the "single-channel" synthesis method, in which "channel fluxes" for R- θ , R-Z, and R channels are used to obtain synthesized 3-D (R, θ ,Z) fluxes. In this methodology, the channel fluxes are defined as follows:

$$\Phi_{R\theta}(R, \theta) = \int_{-\infty}^{\infty} \Phi(R, \theta, Z) dZ \quad (3.1)$$

$$\Phi_{RZ}(R, Z) = \int_0^{2\pi} \Phi(R, \theta, Z) d\theta \quad (3.2)$$

$$\Phi_R(R) = \int_{-\infty}^{\infty} \int_0^{2\pi} \Phi(R, \theta, Z) d\theta dZ \quad (3.3)$$

where

$\Phi_{R\theta}(R, \theta)$ = (R- θ) channel flux

$\Phi_{RZ}(R, Z)$ = (R-Z) channel flux

$\Phi_R(R)$ = (R) channel flux

and $\Phi(R, Z, \theta)$ is assumed to be in the true 3-D flux. It should be noted that the channel fluxes for each group are related to each other in the following relation:

$$\int_0^{2\pi} \Phi_{R\theta}(R, \theta) d\theta = \int_{-\infty}^{\infty} \Phi_{RZ}(R, Z) dZ = \Phi_R(R) \quad (3.4)$$

Now the "synthesized flux" as a function of (R, θ, Z) variables can be defined by the following relation:

$$\Phi_{\text{syn}}(R, \theta, Z) = \frac{\Phi_{R\theta}(R, \theta) \cdot \Phi_{RZ}(R, Z)}{\Phi_R(R)} \quad (3.5)$$

Although Eq. (3.5) is an approximate expression, it has been shown⁵ that it produces the exact 3-D distribution if the flux is separable either azimuthally or axially. In the case where the flux is not separable, Eq. (3.5) always gives the exact axial and azimuthal integrated values (and spatial averages) of the flux at all radial points.⁵ It can also be shown that the R - θ , R - Z , one-dimensional (1-D) channel fluxes obey an equation which has an identical form as the standard R - θ , R - Z , and 1-D equations solved by the 2-D transport code DOT-IV.

Several discrete ordinates transport calculations using the DOT-IV code were performed to obtain the channel fluxes that describe radial, azimuthal, and axial flux distribution inside the reactor vessel and the reactor cavity of the Grand Gulf BWR/6 Nuclear Power Plant.

3.2 DOT-IV R - θ CALCULATION

The symmetrical fuel loading pattern in the core enables one to consider only one-eighth of the core for the R - θ calculation. The one-eighth core model corresponds to a 45° slice with reflected boundary conditions at 0° and 45° . Figure 3.1 represents an octal section of the Grand Gulf reactor at the horizontal midplane from the center of the core to beyond the biological concrete shield around the reactor cavity. The model used in the DOT-IV R - θ calculation is made up of 60 angular (θ) mesh intervals with a variable number of radial (R) mesh points for each θ coordinate, ranging from 144 to 165 radial intervals per θ . The recommended methodology described in Ref. 6 was followed in discretizing this model. The cross-sectional models of jet pumps, risers, and the surveillance capsules are included in the DOT-IV R - θ calculation to account for the significant flux perturbation effects from the presence of these reactor components. As shown in Fig. 3.1, the reactor model is made up of 14 different regions. The material composition for these regions used in the R - θ calculation are given in Table 3.1. In this calculation, a P_3 expansion of scattering cross section and an S_6 angular quadrature are used.

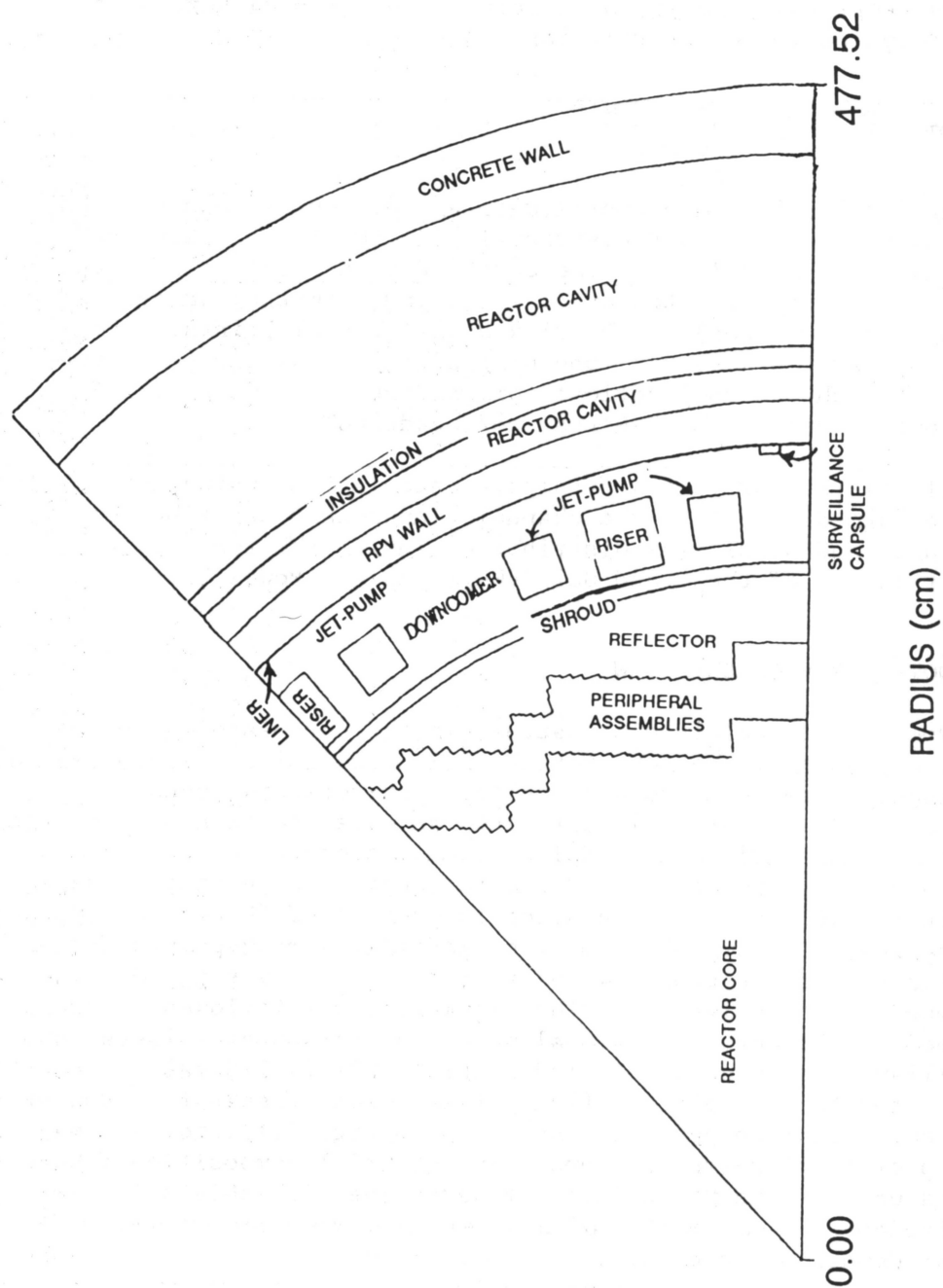


Fig. 3.1. One-eighth slice of the Grand Gulf reactor model used in DOT-IV R- θ calculation.

Table 3.1. R-θ material zones and material densities

No.	Material zone	Material/ nuclide	Atom densities (atom/b·cm)	SAILOR ID No.	Description
1	Inner-core	H	1.8307E-02	235-238	Note (2)
		O	1.9569E-02	59-62	Note (1)
		²³⁵ U	9.4546E-05	43-46	Note (1)
		²³⁸ U	5.1120E-03	47-50	Note (1)
		Zr	6.4800E-03	27-30	Note (1)
2	Outer-core	H	1.8307E-02	235-238	Note (2)
		O	1.9569E-02	59-62	Note (1)
		²³⁵ U	9.4546E-05	43-46	Note (1)
		²³⁸ U	5.1120E-03	47-50	Note (1)
		Zr	6.4800E-03	27-30	Note (1)
3	Reflector	H	4.9284E-02	235-238	Note (2)
		O	2.4642E-02	59-62	Note (1)
4	Shroud (SS 304)	Cr	1.7400E-02	239-242	Note (2)
		Mn	1.5200E-03	243-246	Note (2)
		Ni	8.5500E-03	247-250	Note (2)
		Fe	5.8300E-02	255-258	Note (2)
		C	2.3700E-04	79-82	Note (2)
		Si	8.9300E-04	107-110	Note (1)
5	Downcomer	H	5.0455E-02	235-238	Note (2)
		O	2.5228E-02	59-62	Note (1)
6	Jet-pump	H	4.1394E-02	235-238	Note (2)
		O	2.0697E-02	59-62	Note (1)
		Cr	2.7867E-03	239-242	Note (2)
		Fe	1.1456E-02	259-262	Note (2)
		Ni	1.2385E-03	247-250	Note (2)
7	Riser	H	4.2876E-02	235-238	Note (2)
		O	2.1438E-02	59-62	Note (1)
		Cr	2.3302E-03	239-242	Note (2)
		Fe	9.5801E-03	259-262	Note (2)
		Ni	1.0357E-03	247-250	Note (2)
8	S. Capsule	Steel	1.0000E+00	---	Note (3)
9	RPV liner	SS 304	1.0000E+00	---	Note (3)

Table 3.1. Continued

No.	Material zone	Material/ nuclide	Atom densities (atom/b·cm)	SAILOR ID No.	Description
10	RPV wall (steel)	Cr	1.2700E-04	239-242	Note (2)
		Mn	1.1200E-03	251-254	Note (2)
		Ni	4.4400E-04	247-250	Note (2)
		Fe	8.1900E-02	259-262	Note (2)
		C	9.8100E-04	139-142	Note (2)
		Si	3.7100E-04	107-110	Note (1)
11	Cavity	Air/O	9.6200E-06	59-62	-----
12	Insulation liner	SS 304	1.0000E+00	---	Note (3)
13	Insulation	Al	6.0603E-03	103-106	Note (1)
14	Shield wall	Concrete	1.9481E+00	195-198	Note (1)

Note (1): ID number is the same for original and modified SAILOR libraries.

Note (2): Only in modified SAILOR library.

Note (3): This material is defined in another zone.

3.3 DOT-IV R-Z CALCULATION

Two different in-vessel and ex-vessel R-Z transport calculations, respectively, were performed to determine the axial variation of neutron and gamma fluxes. The first R-Z calculation (in-vessel) models the reactor from the center of the core to the outer surface of the RPV wall. The second R-Z (ex-vessel) model extends from the inner liner of the RPV wall to beyond the shield wall. The second R-Z calculation was "bootstrapped" from the first by coupling at the inner surface of the RPV. Both models axially have the same geometry, which corresponds to the reactor region from approximately fifty centimeters below the bottom of the active fuel up to the outlet nozzle elevation. The main difference between these two runs is the order of quadrature and the axial mesh intervals. The cavity region in a BWR is relatively large. In the Grand Gulf reactor, it is 98.7-cm wide. In order to accurately treat the significant axial streaming in the large cavity region, a higher order quadrature biased in the upward and downward directions was used in the second DOT-IV R-Z calculation. The boundary fluxes at the inner surface of the RPV wall calculated in the first R-Z run were interpolated to coincide with the quadrature set and axial mesh used in the second R-Z calculation. These reformatted boundary fluxes were used as a boundary source for the second R-Z calculations.

3.3.1 In-vessel R-Z Model

The in-vessel R-Z model used for the DOT-IV calculation, as shown in Fig. 3.2, is made up of 99 and 146 axial and radial mesh intervals, respectively. Also shown in this figure are the different zones used in this calculation. The material composition for each zone is given in Table 3.2. Since the axial power distribution in the assemblies is not symmetrical with respect to the midplane of the core, the entire length of the core must be modeled in the R-Z DOT run. In addition to the axial power variation, the void distribution due to boiling also varies axially along the active core length; therefore, it is necessary to account for the presence of space-dependent voids in BWR transport calculations. In this calculation, the active core length has been divided into eight regions with a representative average moderator void fraction. Figure 3.3 compares the actual moderator void fraction distribution with model distribution used in an R-Z calculation as a function of active core height. In this calculation, a P_3 expansion of the scattering cross section, a symmetrical S_8 angular quadrature set, 47 neutron energy groups, and 20 gamma energy groups were used.

ORNL DWG. NO. 89-15133

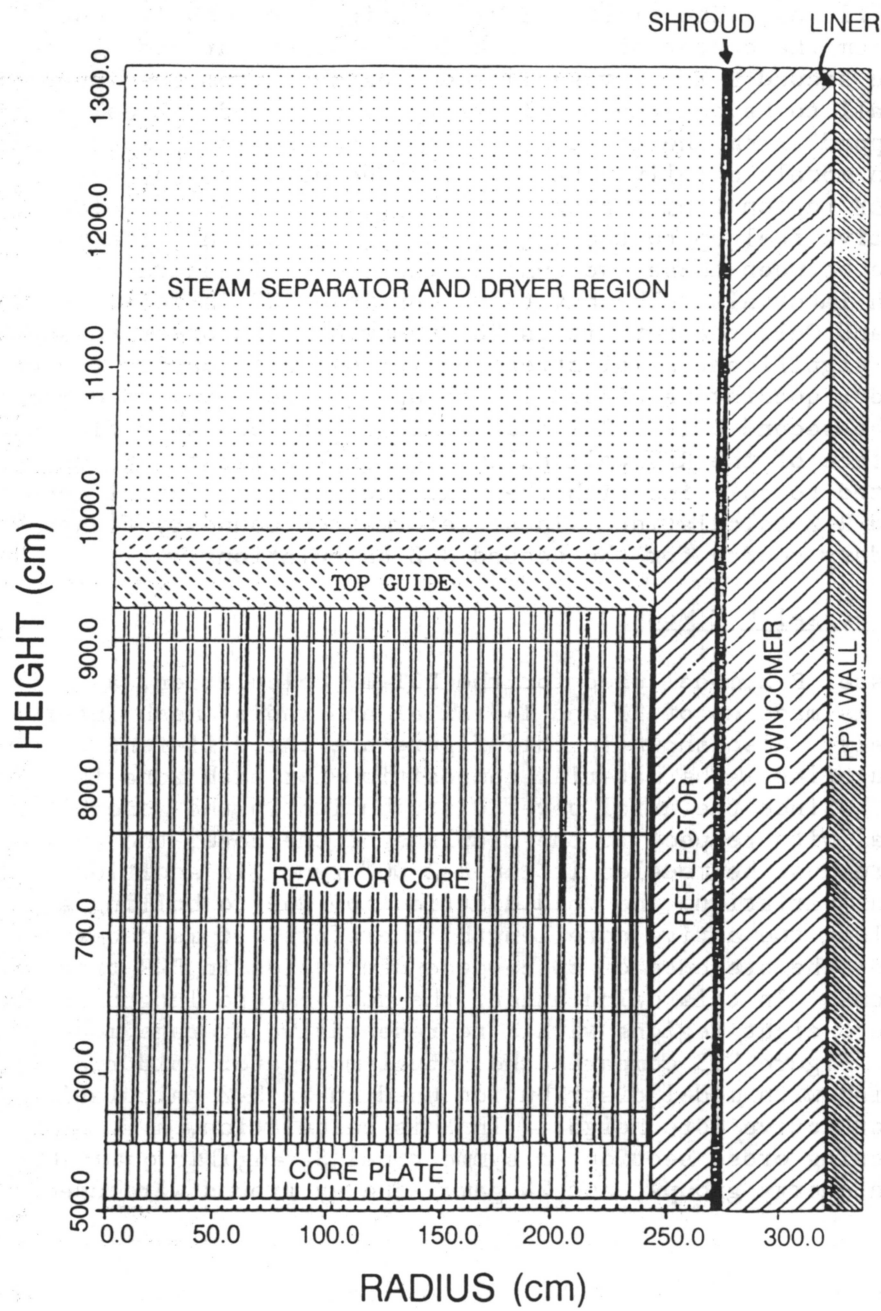


Fig. 3.2. In-vessel R-Z model used in DOT-IV calculation.

Table 3.2. R-Z material zones and material densities

No.	Material zone	Material/ nuclide	Atom densities (atom/b·cm)	SAILOR ID No.	Description
	Fuel	O	1.0415E-02	59-62	Note (1)
		²³⁵ U	9.4546E-05	43-46	Note (1)
		²³⁸ U	5.1120E-03	47-50	Note (1)
		Zr	6.4800E-03	27-30	Note (1)
	SAT.H ₂ O	H	4.9284E-02	235-238	Note (2)
		O	2.4642E-02	59-62	Note (1)
1	Core 1	Fuel	1.0000E+00	---	Note (3)
		Sat. H ₂ O	6.1320E-01	---	Note (3)
2	Core 2	Fuel	1.0000E+00	---	Note (3)
		Sat. H ₂ O	5.6300E-01	---	Note (3)
3	Core 3	Fuel	1.0000E+00	---	Note (3)
		Sat. H ₂ O	4.2850E-01	---	Note (3)
4	Core 4	Fuel	1.0000E+00	---	Note (3)
		Sat. H ₂ O	3.3030E-01	---	Note (3)
5	Core 5	Fuel	1.0000E+00	---	Note (3)
		Sat. H ₂ O	2.6800E-01	---	Note (3)
6	Core 6	Fuel	1.0000E+00	---	Note (3)
		Sat. H ₂ O	2.2560E-01	---	Note (3)
7	Core 7	Fuel	1.0000E+00	---	Note (3)
		Sat. H ₂ O	2.0870E-01	---	Note (3)
8	70% void H ₂ O and Zr	Sat. H ₂ O	2.4660E-01	---	Note (3)
		Zr	7.6896E-03	27-30	Note (1)
9	70% void H ₂ O and Zr and SS 304	Sat. H ₂ O	1.9930E-01	---	Note (3)
		Zr	7.5125E-03	27-30	Note (1)
		SS 304	1.6180E-01	183-186	Note (4)

Table 3.2. Continued

No.	Material zone	Material/ nuclide	Atom densities (atom/b·cm)	SAILOR ID No.	Description
10	70% void H ₂ O	Sat. H ₂ O	3.0000E-01	---	Note (3)
11	Reflector	Sat. H ₂ O	1.0000E+00	---	Note (3)
12	Shroud (SS 304)	Cr	1.7400E-02	239-242	Note (2)
		Mn	1.5200E-03	243-246	Note (2)
		Ni	8.5500E-03	247-250	Note (2)
		Fe	5.8300E-02	255-258	Note (2)
		C	2.3700E-04	79-82	Note (2)
		Si	8.9300E-04	107-110	Note (1)
13	Downcomer	H	5.0455E-02	235-238	Note (2)
		O	2.5228E-02	59-62	Note (1)
14	RPV liner	SS 304	1.0000E+00	---	Note (4)
15	RPV wall (steel)	Cr	1.2700E-04	239-242	Note (2)
		Mn	1.1200E-03	251-254	Note (2)
		Ni	4.4400E-04	247-250	Note (2)
		Fe	8.1900E-02	259-262	Note (2)
		C	9.8100E-04	139-142	Note (2)
		Si	3.7100E-04	107-110	Note (1)
16	Inlet region	Sat. H ₂ O	7.1860E-01	---	Note (3)
		Zr	7.9747E-03	27-30	Note (1)
		SS 304	1.1350E-01	---	Note (4)
17	Core plate	Sat. H ₂ O	9.4640E-01	---	Note (3)
		SS 304	7.5600E-02	---	Note (4)

Note (1): ID number is the same for original and modified SAILOR libraries.

Note (2): Only in modified SAILOR library.

Note (3): This material has already been defined to be mixed with other material(s).

Note (4): This material is defined in another zone.

ORNL DWG. NO. 89-15134

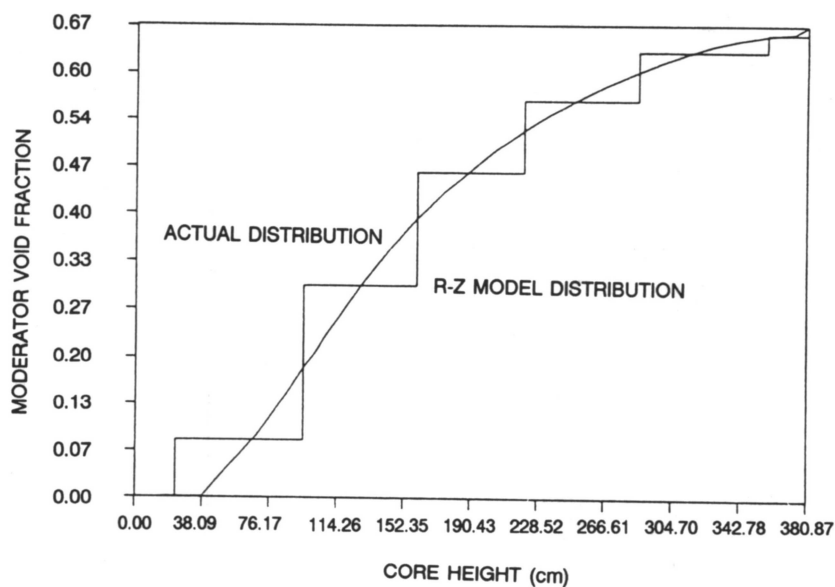


Fig. 3.3. Comparison of actual and modeled moderator void fraction distribution used in in-vessel R-Z calculation.

3.3.2 Cavity, Ex-vessel, R-Z Model

The cavity region is the void space between the RPV wall and the concrete shield wall. The calculation of the neutron and gamma flux in the Grand Gulf reactor cavity was performed using a somewhat simplified geometry. The cavity R-Z model consists of 198 axial and 40 radial mesh intervals and 130 angular directions. The R-Z model used in this calculation is shown in Fig. 3.4. The material composition for each region is given in Table 3.3. In this calculation, a P_3 expansion of scattering cross section, 47 neutron energy groups, and 20 gamma energy groups were used.

ORNL DWG. NO. 89-15135

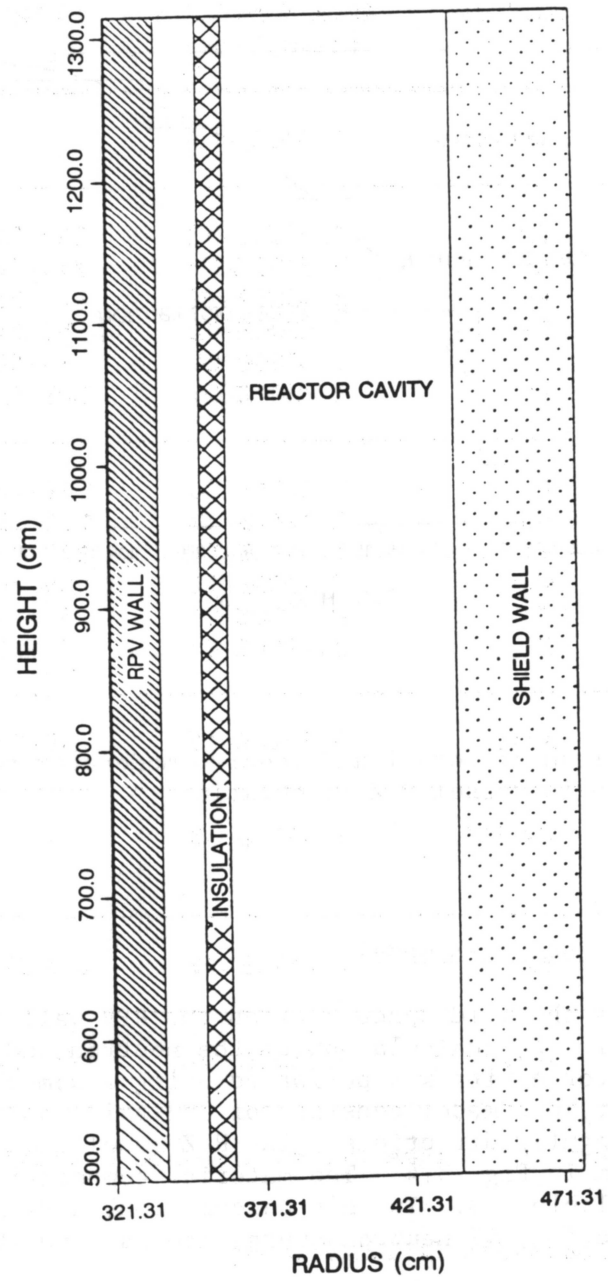


Fig. 3.4. Ex-vessel, cavity, R-Z model used in DOT-IV calculation.

Table 3.3. Cavity R-Z material zones and material densities

No.	Material zone	Material/ nuclide	Atom densities (atom/b·cm)	SAILOR ID No.	Description
1	Absorber	Absorber	1.0000E+06	---	-----
2	Shroud (SS 304)	Cr	1.7400E-02	239-242	Note (2)
		Mn	1.5200E-03	243-246	Note (2)
		Ni	8.5500E-03	247-250	Note (2)
		Fe	5.8300E-02	255-258	Note (2)
		C	2.3700E-04	79-82	Note (2)
		Si	8.9300E-04	107-110	Note (1)
3	RPV wall (steel)	Cr	1.2700E-04	239-242	Note (2)
		Mn	1.1200E-03	251-254	Note (2)
		Ni	4.4400E-04	247-250	Note (2)
		Fe	8.1900E-02	259-262	Note (2)
		C	9.8100E-04	139-142	Note (2)
		Si	3.7100E-04	107-110	Note (1)
4	Cavity	Air/O	9.6200E-06	59-62	Note (1)
5	Insulation liner	SS 304	1.0000E+00	---	Note (3)
6	Insulation	Al	6.0603E-03	103-106	Note (1)
7	Shield wall	Concrete	1.9481E+00	195-198	Note (1)

Note (1): ID number is the same for original and modified SAILOR libraries.

Note (2): Only in modified SAILOR library.

Note (3): This material is defined in another zone.

3.4 DOT-IV ONE-DIMENSIONAL CALCULATION

The 1-D model used in this calculation is shown in Fig. 3.5. This model consists of 168 radial mesh intervals, one axial mesh interval, and ten material regions. The material composition of each region is given in Table 3.4. In this calculation, the P_3 expansion of scattering cross section, S_6 angular quadrature, 47 neutron energy groups, and 20 gamma energy groups have been used.

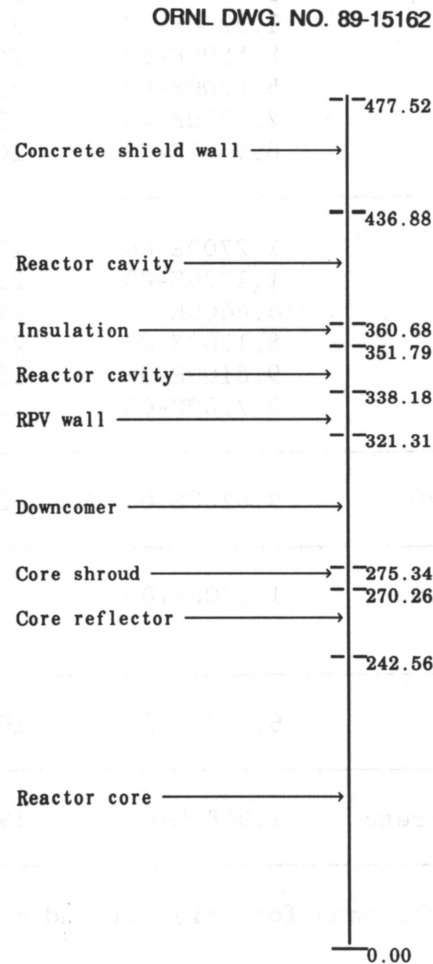


Fig. 3.5. One-dimensional model used in DOT-IV calculation (distance is in cm).

Table 3.4. One-dimensional material zones and material densities

No.	Material zone	Material/ nuclide	Atom densities (atom/b·cm)	SAILOR ID No.	Description
1	Core	H	1.8307E-02	235-238	Note (2)
		O	1.9569E-02	59-62	Note (1)
		²³⁵ U	9.4546E-05	43-46	Note (1)
		²³⁸ U	5.1120E-03	47-50	Note (1)
		Zr	6.4800E-03	27-30	Note (1)
2	Reflector	H	4.9284E-02	235-238	Note (2)
		O	2.4642E-02	59-62	Note (1)
3	Shroud (SS 304)	Cr	1.7400E-02	239-242	Note (2)
		Mn	1.5200E-03	243-246	Note (2)
		Ni	8.5500E-03	247-250	Note (2)
		Fe	5.8300E-02	255-258	Note (2)
		C	2.3700E-04	79-82	Note (2)
		Si	8.9300E-04	107-110	Note (1)
4	Downcomer	H	5.0455E-02	235-238	Note (2)
		O	2.5228E-02	59-62	Note (1)
5	RPV liner	SS 304	1.0000E+00	---	Note (3)
6	RPV wall (steel)	Cr	1.2700E-04	239-242	Note (2)
		Mn	1.1200E-03	251-254	Note (2)
		Ni	4.4400E-04	247-250	Note (2)
		Fe	8.1900E-02	259-262	Note (2)
		C	9.8100E-04	139-142	Note (2)
		Si	3.7100E-04	107-110	Note (1)
7	Cavity	Air/O	9.6200E-06	59-62	Note (1)
8	Insulation liner	SS 304	1.0000E+00	---	Note (3)
9	Insulation	Al	6.0603E-03	103-106	Note (1)
10	Shield wall	Concrete	1.9481E+00	195-198	Note (1)

Note (1): ID number is the same for original and modified SAILOR libraries.

Note (2): Only in modified SAILOR library.

Note (3): This material is defined in another zone.

3.5 DETERMINATION OF NEUTRON SOURCE

Calculation of neutron source for DOT-IV R- θ run was performed using DOTSOR code, a module of the LEPRICON⁶ system. The function of this code is to generate the R- θ source for DOT-IV transport calculation based on the given X-Y core power distribution. Table 3.5 represents the average assembly-wise power during Cycle 2 of the Grand Gulf reactor. The one-fourth core X-Y power density values are converted to a neutron source density, and the X-Y source distribution is then mapped into the one-eighth core R- θ mesh used in the DOT-IV.

For the in-vessel R-Z calculation, the axial burn-up distributions, as shown in Table 3.6, are used to calculate the relative axial distribution. All the data presented in Tables 3.5 and 3.6 were obtained from the Reactor Engineering Division of the Grand Gulf Nuclear Station. Since the axial burn-up distribution varies radially from the inner core assemblies to the peripheral assemblies, the average axial distributions at three regions (inner core, next-to-the-last assembly, and peripheral assembly) were used to represent the burnup distribution for the reactor core. The 1-D source was obtained by integrating the R-Z source over Z. Figure 3.6 shows the power-time histogram of Grand Gulf during Cycle 2 as provided by MP&L. This figure illustrates the monthly and cumulative thermal load factor for Cycle 2. The load factor is the ratio of the actual thermal energy generated during the month or cycle over the energy that would have been generated by full power operation during the month or cycle. The monthly power-time history from this figure is tabulated in Table 3.7.

ORNL DWG. NO. 89-15136

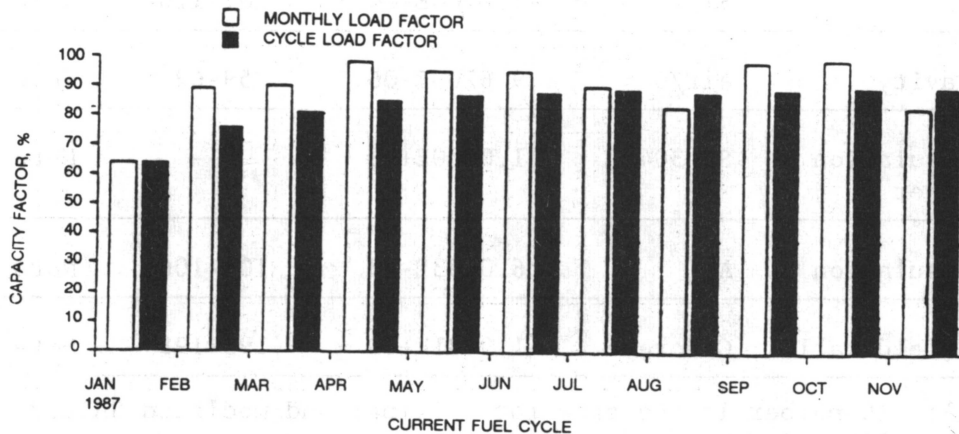


Fig. 3.6. Power-time histogram for Grand Gulf Cycle 2.

Table 3.5. X-Y relative power distribution at the core midplane.

[illegible]

Table 3.6. R-Z axial and radial burnup (MWd/Mt) distribution

Height ^a (cm)	Inner core ^b average	Adjacent to peripheral average	Peripheral ^d average
3.810	0.7635	0.5475	0.2875
11.430	2.4275	1.6985	0.8404
19.050	4.2285	2.9056	1.3712
26.480	5.5202	3.7752	1.7533
33.720	6.3026	4.3073	1.9864
40.960	6.9432	4.7555	2.1849
48.200	7.3665	5.0754	2.3302
55.440	7.7337	5.3671	2.4659
62.680	7.9636	5.5900	2.5784
69.910	8.1749	5.8010	2.6869
77.150	8.3051	5.9605	2.7792
84.390	8.4306	6.1158	2.8699
91.630	8.5024	6.2207	2.9432
98.850	8.5739	6.3253	3.0162
106.050	8.6205	6.3784	3.0673
113.240	8.6663	6.4299	3.1176
120.440	8.6907	6.4398	3.1502
127.640	8.7115	6.4426	3.1797
134.830	8.7014	6.4228	3.1924
142.030	8.6801	6.3948	3.1991
149.230	8.6434	6.3554	3.1975
156.420	8.5971	6.3091	3.1908
163.070	8.5526	6.2661	3.1838
169.160	8.5098	6.2268	3.1765
175.260	8.4670	6.1875	3.1692
181.360	8.4342	6.1518	3.1632
187.450	8.4014	6.1162	3.1572
193.550	8.3726	6.0828	3.1512
199.640	8.3478	6.0518	3.1452
205.740	8.3230	6.0208	3.1392
211.840	8.3090	5.9921	3.1335
217.930	8.2950	5.9635	3.1278
224.580	8.2795	5.9299	3.1191
231.780	8.2625	5.8913	3.1073
238.970	8.2397	5.8488	3.0929
246.170	8.2076	5.8000	3.0744
253.370	8.1730	5.7463	3.0530

Table 3.6. Continued

Height ^a (cm)	Inner core ^b average	Adjacent to ^c peripheral average	Peripheral ^d average
260.560	8.1315	5.6791	3.0235
267.780	8.0842	5.6070	2.9908
274.960	8.0060	5.5092	2.9410
282.150	7.9256	5.4099	2.8903
289.370	7.7754	5.2626	2.8149
296.610	7.6249	5.1149	2.7393
303.850	7.3745	4.9075	2.6312
311.090	7.1156	4.6949	2.5204
318.330	6.7399	4.4215	2.3804
325.560	6.3386	4.1349	2.2341
332.800	5.8335	3.7917	2.0551
340.040	5.2862	3.4255	1.8627
347.280	4.6913	2.9865	1.6291
354.520	3.8744	2.4999	1.3686
361.950	2.8917	1.8529	1.0244
369.570	1.6712	1.0454	0.5964
377.190	0.5305	0.3208	0.1913

^aActive core height in cm (0.0 cm = bottom of active core and
381 cm = top of active core).

^bAveraged over inner-core assemblies.

^cAveraged over row of assemblies adjacent to peripheral assemblies.

^dAveraged over peripheral assemblies.

Table 3.7. Power-time history of Grand Gulf Cycle 2

Month/year	Days of irradiation	Power fraction
1/87	31	0.640
2/87	28	0.890
3/87	31	0.900
4/87	30	0.990
5/87	31	0.960
6/87	30	0.960
7/87	31	0.900
8/87	31	0.820
9/87	30	0.990
10/87	31	0.990
11/87	7	0.820

4. MULTI-GROUP CROSS-SECTION LIBRARY

The nuclear cross-section library is one of the essential ingredients in nuclear analysis. The accuracy of the cross-section data is one of the primary factors that governs the accuracy of the calculated pressure vessel fluence. There are several multi-group cross-section libraries currently available for light water reactor (LWR) shielding analysis. A new version of the SAILOR nuclear cross-section library has been used to obtain all the nuclear data necessary for the calculations in this study. The new SAILOR library is a modified version of the original SAILOR.⁷ In the new SAILOR library, the thermal cross-section values for Fe, Cr, Mn, Ni, and H have been modified from those in the original SAILOR to incorporate a more realistic thermal spectrum. Also, in this library, the iron inelastic cross section was based on a more recent, and much improved evaluation performed by Peter Fu of ORNL. The present analysis is one of the first to employ the new Fu iron cross-section data.

The original SAILOR cross-section library assumed a Maxwellian thermal spectrum at 300°K in averaging the thermal values in the energy range below 0.4 eV. In order to obtain a more realistic thermal spectrum, a transport calculation utilizing seven thermal groups with upscatter in the range below 0.4 eV has been performed for a 1-D PWR model using the 27-group CSRL Criticality Library (based on ENDF/B-V). Results of this analysis were used to correct the thermal group cross sections of the water and ex-core structural materials in SAILOR to improve the calculation of the thermal neutron flux as well as gamma production in RPV transport calculations. The correction factors were obtained by:

1. Collapsing the 27-group absorption cross sections into the appropriate two thermal groups corresponding to the energy intervals (0, 0.1) and (0.1, 0.4) using the calculated multi-group thermal spectrum;
2. Dividing the new absorption cross sections by the original SAILOR values to get a correction factor (f_a) for the neutron thermal absorption and thermal neutron gamma production cross sections:

$$f_a = \frac{(\sigma_{ag})_{\text{new}}}{(\sigma_{ag})_{\text{original}}} ; \quad \text{and}$$

3. Assuming a constant scatter cross section in the thermal range, the correction factor for the total cross section is calculated,

$$f_t = 1 + (f_a - 1) \left[\frac{\sigma_{ag}}{\sigma_{tg}} \right]_{\text{original}}$$

Table 4.1 gives the correction factors computed for the absorption and total cross section, and applied in the modified SAILOR library.

This library, like the original SAILOR, consists of 47 neutron energy groups and 20 gamma energy groups. Table 4.2 shows the neutron and gamma energy group structure for this library. Table 4.3 lists the contents of the new SAILOR library. The compositions of the macroscopic mixtures used in the various zones in the DOT-IV runs are given in Tables 3.1 to 3.4. A code called GIP was used to obtain the macroscopic cross sections used in the DOT-IV calculations. Reaction rates have been calculated for the following selected dosimeter activities from the SAILOR "activity material": $^{54}\text{Fe}(n,p)^{54}\text{Mn}$, $^{58}\text{Ni}(n,p)^{58}\text{Co}$, $^{237}\text{Np}(n,f)^{137}\text{Cs}$, $^{238}\text{U}(n,f)^{137}\text{Cs}$, $^{46}\text{Ti}(n,p)^{46}\text{Sc}$, total flux, flux above 1.0 MeV, flux under 0.1 MeV, flux under 0.4 eV (thermal flux).

The $^{63}\text{Cu}(n,\alpha)^{60}\text{Co}$ activity cross sections in the SAILOR library have been previously observed to produce poor results. In this analysis the $^{63}\text{Cu}(n,\alpha)$ cross sections were obtained from a more accurate data set that was available at ORNL.

Table 4.1. SAILOR thermal correction factors based on 27-group results for absorption (f_a) and total (f_t) cross sections

Nuclide	Group 46 (0.1 - 0.4 eV)		Group 47 (0.0 - 0.1 eV)	
	f_a	f_t	f_a	f_t
H	1.00	1.00	0.91	1.00
Cr*	1.06*	1.01	0.79*	0.91
Ni	1.07	1.01	0.78	0.96
Mn	1.06	1.04	0.80	0.82
Fu-Fe	0.97	1.00	0.96	0.99

*The Cr results are estimated from the other values because an error was found in the Cr data in the 27-group CSRL Library.

Table 4.2. SAILOR 47-group neutron and 20-group gamma library energy structure

Energy group	Upper limit (MeV)	Lower limit (MeV)
<u>Neutron groups</u>		
1	1.733E+01	1.419E+01
2	1.419E+01	1.221E+01
3	1.221E+01	1.000E+01
4	1.000E+01	8.607E+00
5	8.607E+00	7.408E+00
6	7.408E+00	6.065E+01
7	6.065E+00	4.966E+01
8	4.966E+00	3.679E+01
9	3.679E+00	3.012E+00
10	3.012E+00	2.725E+00
11	2.725E+00	2.466E+00
12	2.466E+00	2.365E+00
13	2.365E+00	2.346E+00
14	2.346E+00	2.231E+00
15	2.231E+00	1.920E+00
16	1.920E+00	1.653E+00
17	1.653E+00	1.353E+00
18	1.353E+00	1.003E+00
19	1.003E+00	8.208E-01
20	8.208E-01	7.427E-01
21	7.427E-01	6.081E-01
22	6.081E-01	4.979E-01
23	4.979E-01	3.688E-01
24	3.688E-01	2.972E-01
25	2.972E-01	1.832E-01
26	1.832E-01	1.111E-01
27	1.111E-01	6.738E-02
28	6.738E-02	4.087E-02
29	4.087E-02	3.183E-02
30	3.183E-02	2.606E-02
31	2.606E-02	2.418E-02
32	2.418E-02	2.188E-02
33	2.188E-02	1.503E-02
34	1.503E-02	7.102E-03
35	7.102E-03	3.355E-03

Table 4.2. Continued

Energy group	Upper limit (MeV)	Lower limit (MeV)
<u>Neutron groups (continued)</u>		
36	3.355E-03	1.585E-03
37	1.585E-03	4.540E-04
38	4.540E-04	2.144E-04
39	2.144E-04	1.013E-04
40	1.013E-04	3.727E-05
41	3.727E-05	1.068E-05
42	1.068E-05	5.043E-06
43	5.043E-06	1.855E-06
44	1.855E-06	8.764E-07
45	8.764E-07	4.140E-07
46	4.140E-07	1.000E-07
47	1.000E-07	1.000E-11
<u>Gamma groups</u>		
1	1.400E+01	1.000E+01
2	1.000E+01	8.000E+00
3	8.000E+00	7.000E+00
4	7.000E+00	6.000E+00
5	6.000E+00	5.000E+00
6	5.000E+00	4.000E+00
7	4.000E+00	3.000E+00
8	3.000E+00	2.000E+00
9	2.000E+00	1.500E+00
10	1.500E+00	1.000E-01
11	1.000E+00	8.000E-01
12	8.000E-01	7.000E-01
13	7.000E-01	6.000E-01
14	6.000E-01	4.000E-01
15	4.000E-01	2.000E-01
16	2.000E-01	1.000E-01
17	1.000E-01	6.000E-02
18	6.000E-02	3.000E-02
19	3.000E-02	2.000E-02
20	2.000E-02	1.000E-02

Table 4.3. New SAILOR P₀ cross-section identifiers

ID	Description		
1	ENDF/B-IV	Dosimetry file	Flat weighting
2	ENDF/B-IV	Dosimetry file	1/4-T pressure vessel
3	Hydrogen	PWR core	47 N/20 G SAILWR library
7	B-10	PWR core	47 N/20 G SAILWR library
11	Oxygen	PWR core	47 N/20 G SAILWR library
15	Chromium	PWR core	47 N/20 G SAILWR library
19	Iron	PWR core	47 N/20 G SAILWR library
23	Nickel	PWR core	47 N/20 G SAILWR library
27	Zirconium	PWR core	47 N/20 G SAILWR library
31	U-235	PWR core	47 N/20 G SAILWR library
35	U-238	PWR core	47 N/20 G SAILWR library
39	Oxygen	PWR core fuel	47 N/20 G SAILWR library
43	U-235	BWR core	47 N/20 G SAILWR library
47	U-238	BWR core	47 N/20 G SAILWR library
51	Oxygen	BWR core fuel	47 N/20 G SAILWR library
55	Hydrogen	PWR downcomer	47 N/20 G SAILWR library
59	Oxygen	PWR downcomer	47 N/20 G SAILWR library
63	Chromium	PWR downcomer	47 N/20 G SAILWR library
67	Mn-55	PWR downcomer	47 N/20 G SAILWR library
71	Iron	PWR downcomer	47 N/20 G SAILWR library
75	Nickel	PWR downcomer	47 N/20 G SAILWR library
79	Carbon	PWR downcomer	47 N/20 G SAILWR library
83	Hydrogen	Concrete weighting	47 N/20 G SAILWR library
87	Carbon	Concrete weighting	47 N/20 G SAILWR library
91	Oxygen	Concrete weighting	47 N/20 G SAILWR library
95	Sodium	Concrete weighting	47 N/20 G SAILWR library
99	Magnesium	Concrete weighting	47 N/20 G SAILWR library
103	Aluminum	Concrete weighting	47 N/20 G SAILWR library
107	Silicon	Concrete weighting	47 N/20 G SAILWR library
111	Potassium	Concrete weighting	47 N/20 G SAILWR library
115	Calcium	Concrete weighting	47 N/20 G SAILWR library
119	Iron	Concrete weighting	47 N/20 G SAILWR library
123	Chromium	1/4-T pressure vessel	47 N/20 G SAILWR library
127	Mn-55	1/4-T pressure vessel	47 N/20 G SAILWR library
131	Iron	1/4-T pressure vessel	47 N/20 G SAILWR library
135	Nickel	1/4-T pressure vessel	47 N/20 G SAILWR library
139	Carbon	1/4-T pressure vessel	47 N/20 G SAILWR library
143	U-235	PWR mixed oxide fuel	47 N/20 G SAILWR library
147	U-236	PWR mixed oxide fuel	47 N/20 G SAILWR library
151	U-238	PWR mixed oxide fuel	47 N/20 G SAILWR library

Table 4.3. Continued

ID	Description		
155	Pu-239	PWR mixed oxide fuel	47 N/20 G SAILWR library
159	Pu-240	PWR mixed oxide fuel	47 N/20 G SAILWR library
163	Pu-241	PWR mixed oxide fuel	47 N/20 G SAILWR library
167	Pu-242	PWR mixed oxide fuel	47 N/20 G SAILWR library
171	Np-237	PWR mixed oxide fuel	47 N/20 G SAILWR library
175	Oxygen	PWR mixed oxide fuel	47 N/20 G SAILWR library
179	Water	at 1.0 g/cc	47 N/20 G SAILWR library
183	SS 304	at 7.38 g/cc	47 N/20 G SAILWR library
187	A-533-B	low-carbon steel at 7.38 g/cc	47 N/20 G SAILWR library
191	A-508	class 2 steel	47 N/20 G SAILWR library
195	ANSI	standard concrete type 04 at 2.31 g/cc	47 N/20 G SAILWR library
199	Zircaloy-4	at 6.56 g/cc	47 N/20 G SAILWR library
203	UO ₂ .711	w/o U-235 10.412 g/cc BWR	47 N/20 G SAILWR library
207	UO ₂ 1.76	w/o U-235 10.412 g/cc BWR	47 N/20 G SAILWR library
211	UO ₂ 2.10	w/o U-235 10.412 g/cc BWR	47 N/20 G SAILWR library
215	UO ₂ 2.23	w/o U-235 10.412 g/cc BWR	47 N/20 G SAILWR library
219	UO ₂ 2.60	w/o U-235 10.412 g/cc BWR	47 N/20 G SAILWR library
223	UO ₂ 3.00	w/o U-235 10.412 g/cc BWR	47 N/20 G SAILWR library
227	UO ₂ 3.30	w/o U-235 10.412 g/cc BWR	47 N/20 G SAILWR library
231	UO ₂ 92.5	w/o U-235 10.412 g/cc BWR	47 N/20 G SAILWR library
235	Hydrogen		Revised SAILOR*
239	Chromium		Revised SAILOR*
243	Mn-55	Downcomer	Revised SAILOR*
247	Nickel		Revised SAILOR*
251	Mn-55	RPV	Revised SAILOR*
255	Iron	Fu SS 304	Revised SAILOR**
259	Iron	Fu RPV	Revised SAILOR**

*Modified thermal groups (M. L. Williams, June 1988).

**New thermal cross sections (M. L. Williams, June 1988).

5. RESULTS

Figures 5.1 through 5.3 represent the radial and azimuthal variation of the calculated flux above 1 MeV, dpa, and thermal flux, respectively. Figures 5.1.a and 5.1.b show the same quantity at two different regions, inside the RPV and in the cavity vicinity, respectively. Figures 5.4 through 5.6 represent the radial and axial variation in flux above 1 MeV, dpa, and thermal flux, respectively, as obtained from in-vessel R-Z transport calculations. Figures 5.7 through 5.9 are similar type plots obtained from ex-vessel R-Z calculations for the cavity and concrete shield regions. Figures 5.10 and 5.11 are also based on ex-vessel R-Z calculations and show gamma heating and gamma dose contours, respectively, in the cavity.

Table 5.1 shows the calculated spectrum-averaged cross section for several reactions at the center of the 3° surveillance capsule at the axial core midplane and peak locations. Tables 5.2 and 5.3 show the calculated saturated activities within the 3° surveillance capsule at the axial core midplane and peak locations, respectively. Table 5.4 shows the calculated nonsaturation factors for several dosimeters based on the Cycle 2 power-time history. Table 5.5 shows the lead factors at various radial locations through the RPV wall and cavity region. Tables 5.6 and 5.7 show the relative azimuthal variation in flux above 1 MeV through the pressure vessel (PV) wall and cavity region, respectively. In Tables 5.8 through 5.10, the radial variation total dpa, flux above 1 MeV, thermal flux, and thermal-to-fast flux ratio are tabulated at three axial locations of core midplane, peak, and feed water nozzle elevation, respectively. Table 5.11 shows the peak cumulative total dpa and fluence based on axial and azimuthal peak flux above 1 MeV during Cycle 2 and after 32 effective full power years (EFPY) at different locations through the RPV wall. Table 5.12 shows the radial variation in gamma heating and gamma absorbed dose rate obtained in transport calculations at three axial locations of core midplane, peak, and feed water nozzle elevation, respectively. Several more tables of calculational results are presented in Appendix A.

Figure 5.12 shows the absolute neutron spectrum outside the 3° surveillance capsule in the downcomer region and in the center of the surveillance capsule at the axial peak location. Figures 5.13 through 5.15 represent the neutron spectrum at two radial locations of 1/4-T and 3/4-T of PV wall at axial core midplane, peak, and feed water nozzle elevation, respectively. Figures 5.16 through 5.18 are similar type plots, except at the radial locations of reactor midcavity and 15.24 cm (6 in.) into the concrete shield wall. Figure 5.19 illustrates the variation of the neutron spectrum through the concrete shield wall at the core midplane. Figures 5.20 through 5.22 show the absolute gamma spectrum at four radial locations of 1/2-T, 3/4-T, reactor midcavity, and 15.24 cm (6 in.) into the concrete shield wall at the axial core midplane, peak, and feed water nozzle elevation, respectively. Figure 5.23 shows radial variation of flux above 1 MeV at five axial locations of bottom, midplane, top of active core,

peak, and feed water nozzle elevation. Finally, Figure 5.24 shows axial variation of flux above 1 MeV at five radial locations of 1/4-T, 1/2-T, 3/4-T, 1-T, and midcavity.

The flux in the RPV of this BWR/6 reactor was found to peak at an azimuthal angle between 40° and 45° depending on the radial location. Tables 5.7 and 5.8 illustrate the azimuthal variation of the flux above 1 MeV at several points through the PV wall and the cavity region at the core axial mid-plane. There is a factor of 1.76 variation in the azimuthal dependence of the flux above 1 MeV at 0-T of PV. This factor has a value of 1.67 at the reactor midcavity. As shown in these tables, the azimuthal variation of the flux above 1 MeV also depends slightly on the radial location. From the R-Z transport calculations, the flux was found to peak near, but slightly above the core midplane even though the source in the core peaked near the bottom of the core. The combined effects of a bottom-peaked source distribution and a top-peaked moderator void fraction seem to compensate, and account for the location of the R-Z flux peak. Figure 5.24 illustrates the axial variation of the flux above 1 MeV at several points within the RPV wall and the cavity region. The flux above 1 MeV at the midcavity and at the elevation corresponding to the top of the core and the inlet feed water nozzle are factors of 2.74 and 49.5 lower than the core midplane value, respectively.

The flux above 1 MeV incident on the vessel wetted surface at the peak azimuthal and axial location is about $1.819 \times 10^9 \text{ n}\cdot\text{cm}^{-2}\cdot\text{s}^{-1}$. The flux ($E > 1 \text{ MeV}$) incident on the vessel at the peak azimuthal and core axial midplane is about $1.749 \times 10^9 \text{ n}\cdot\text{cm}^{-2}\cdot\text{s}^{-1}$. The peak flux ($E > 1 \text{ MeV}$) is reduced to a value of $7.911 \times 10^7 \text{ n}\cdot\text{cm}^{-2}\cdot\text{s}^{-1}$ at the front of the concrete shield wall. Based on the calculated peak flux above 1 MeV, the total fluence due to 280.37 effective full power days of Cycle 2 at wetted surface of RPV, is about $4.406 \times 10^{16} \text{ n}\cdot\text{cm}^{-2}$. Based on this fluence rate, the projected cumulative fluence after 32 EFPY is about $1.838 \times 10^{18} \text{ n}\cdot\text{cm}^{-2}$.

As shown in Tables A.2.a through A.2.h of Appendix A, at the 0-T peak location, about 81.1% of the total dpa is due to flux ($E > 1 \text{ MeV}$), 16.5% is due to flux ($0.1 < E < 1.0 \text{ MeV}$) and less than 1% is due to thermal neutrons; the remainder percentage is due to neutrons in the energy range (0.1 eV, 0.1 MeV). At 3/4-T of the PV and at midcavity, these values change to 52.9%, 41%, and 0.0% and 48.8%, 45.8%, and 0.3%, respectively. The thermal energy neutron flux contribution increases through the concrete shield wall. At the radial location corresponding to 30.48 cm into the concrete, where the thermal-to-fast flux ratio has a value of 24.8, about 14.3% of the total dpa is due to thermal flux. Tables A.3.a through A.3.h show that at 0-T, 3/4-T, and axial feed water nozzle elevation, the percent of contribution of flux ($E > 1 \text{ MeV}$), flux ($0.1 < E < 1 \text{ MeV}$), and thermal flux to the total dpa are 83.8, 13.8, and 1.0 and 14.2, 69.7, and 0.2, respectively. At 30.48 cm into the concrete, where the thermal-to-flux above 1 MeV ratio is 208.4, about 59% of the total dpa is due to thermal flux. It should be noted that the magnitude of the total dpa at this point is only about 2.0×10^{-05} times that at the peak 1/4-T value.

Figure 5.7 illustrates the axial streaming of the flux ($E > 1$ MeV) in the cavity region. As seen in this figure, at the axial locations above the top of the core, the high-energy neutrons entering through the outer surface of the vessel and penetrating back into the RPV wall cause an increase in the flux above 1 MeV from inner-to-outer RPV wall. This effect can be easily seen in Fig. 5.23. In this figure at the axial elevation corresponding to the inlet feed water nozzle, the flux above 1 MeV actually increases from the inside to the outside of the RPV wall instead of decreasing, as occurs within the axial active core elevation. The dpa contours, Fig. 5.8, show a similar behavior. Figure 5.9 shows the behavior of the thermal flux in the cavity and in the concrete shield wall regions. As seen in this figure, the fast neutrons leaking from the vessel are thermalized as they enter the concrete shield and generate a localized thermal source within the wall. The thermal neutrons emerging from the concrete shield travel across the cavity and strike the RPV wall at the outer surface causing a peak in the thermal flux in this vicinity. Figure 5.12 clearly illustrates the change in neutron spectra due to the presence of the surveillance capsule. In this figure, at the outside of the surveillance capsule, the neutron energy spectrum follows the same behavior as the Maxwellian distribution in thermal energy range, $1/E$, in the epithermal region and fission spectra at the high-energy range. Whereas at the center of the surveillance capsule, this behavior is perturbed due to the presence of iron in the surveillance capsule, which eliminates the thermal component. Thus, it is important to include the surveillance capsule in the reactor model when performing transport calculations to account for the flux perturbation.

The gamma calculation results have been presented in terms of gamma spectra, gamma heating source, and gamma absorbed dose rate throughout the vessel, reactor cavity, and concrete shield wall. The gamma heating source values can be used in determining the temperature of the structural components if a thermal analysis is performed. The peak gamma heating at three radial locations of 0-T, 3/4-T, and the front of the concrete shield wall has values of 2.544×10^{-03} , 6.073×10^{-05} , and 1.700×10^{-05} W/g SS 304, respectively, as shown in Table 5.12. The gamma absorbed dose data can be used in the quantitative determination of the radiation exposure to any instrumentation and wiring located in the cavity or concrete shield wall. Table 5.12 shows that the gamma absorbed dose rate at the midcavity is about 7.310×10^3 rad/h during full power operation.

ORNL DWG. NO. 89-15150

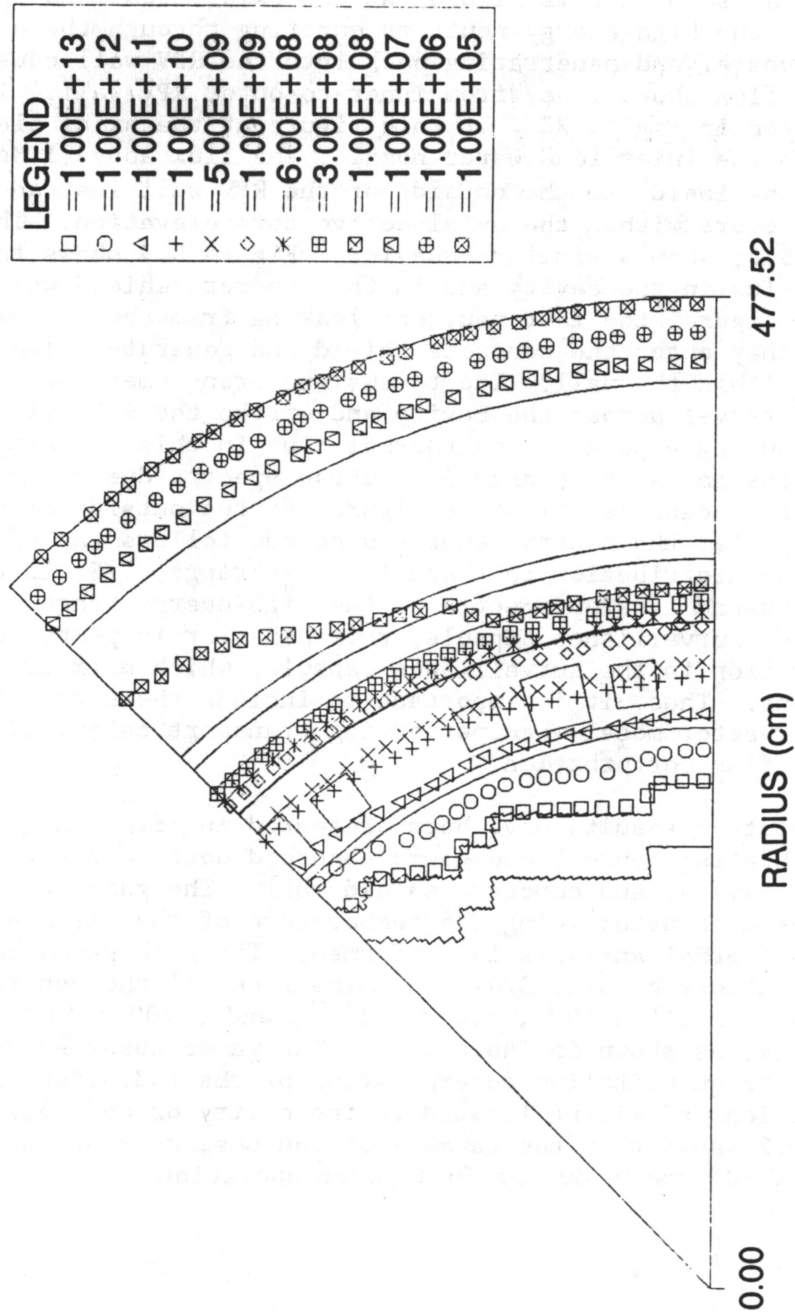


Fig. 5.1.a. Neutron flux above 1 MeV ($\text{n} \cdot \text{cm}^{-2} \cdot \text{s}^{-1}$) contours within the reactor vessel and the concrete shield wall based on DOT-IV R-0 calculation.

ORNL DWG. NO. 89-15151

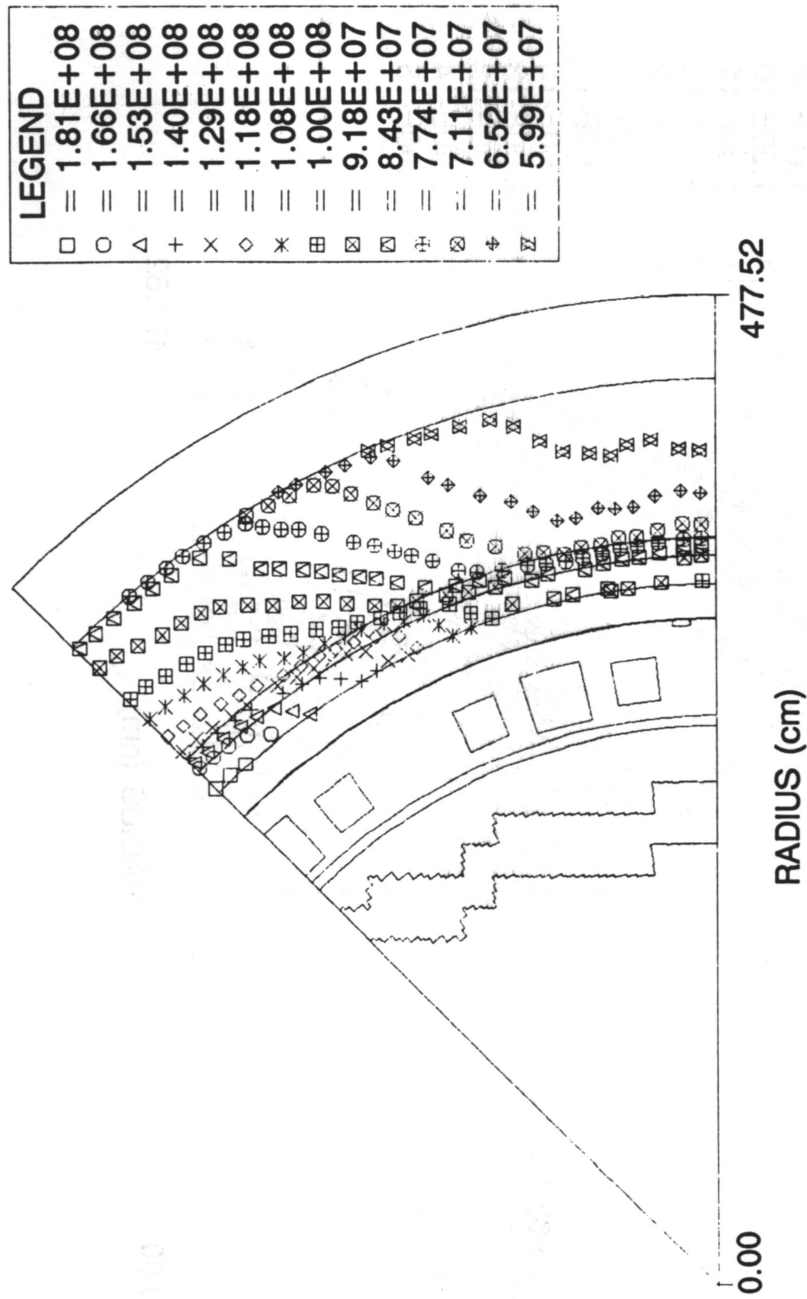


Fig. 5.1.b. Neutron flux above 1 MeV ($\text{n}\cdot\text{cm}^{-2}\cdot\text{s}^{-1}$) contours within the reactor cavity based on DOT-IV R- θ calculation.

ORNL DWG. NO. 89-15152

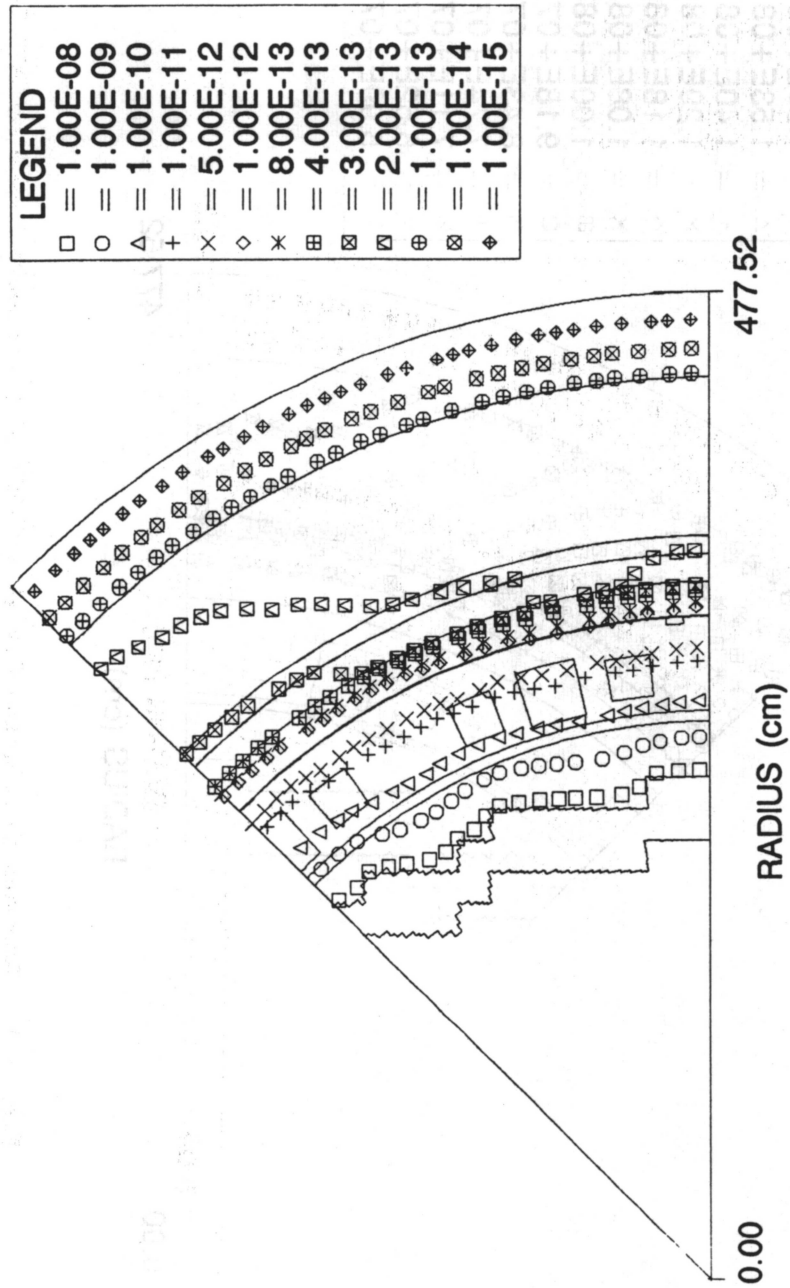


Fig. 5.2. Displacements per atom, dpa, ($\text{dpa} \cdot \text{s}^{-1}$) contours based on DOT-IV R- θ calculation.

ORNL DWG. NO. 89-15153



Fig. 5.3. Neutron flux below 0.4 eV ($\text{n}\cdot\text{cm}^{-2}\cdot\text{s}^{-1}$) contours based on DOT-IV R-θ calculation.

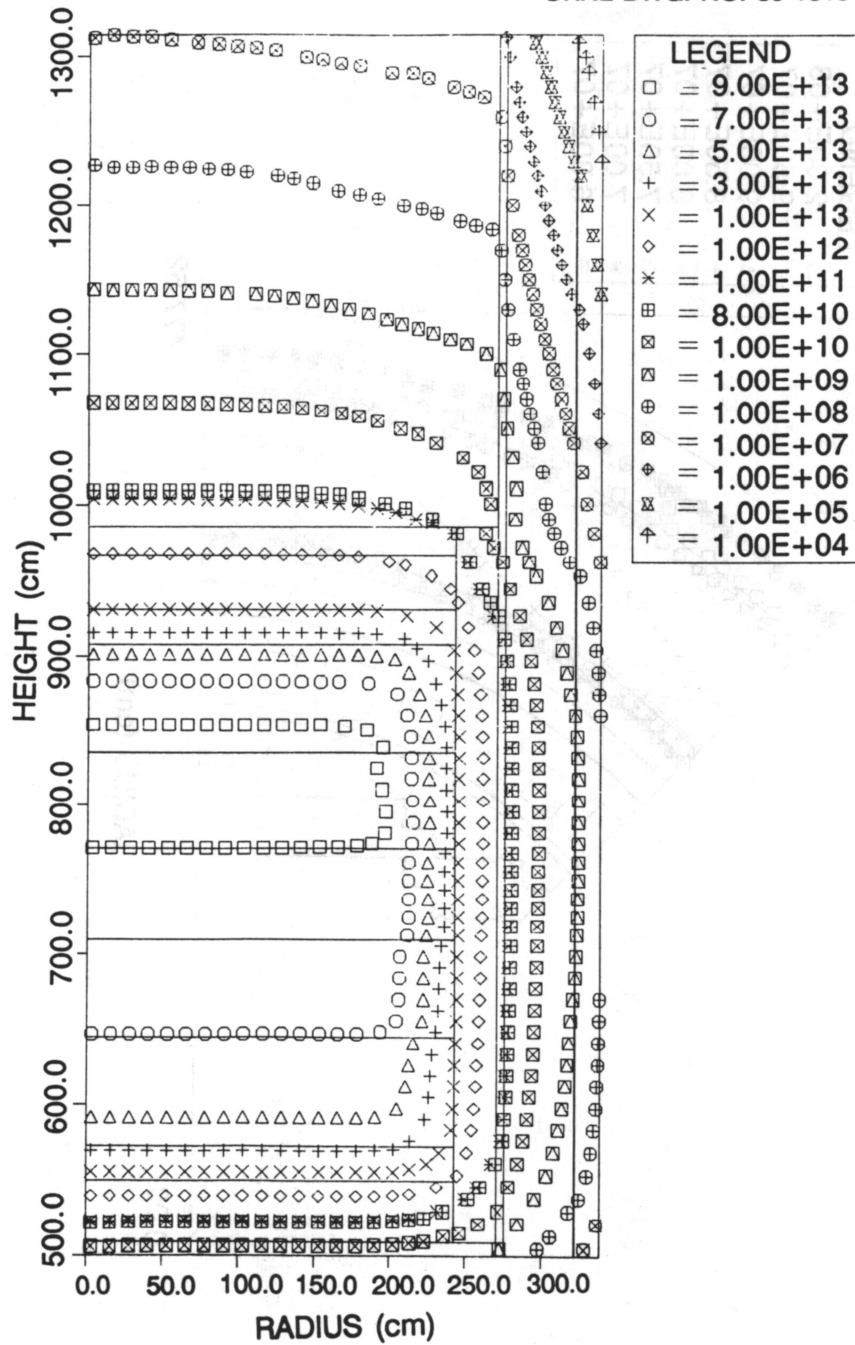


Fig. 5.4. Neutron flux above 1 MeV ($\text{n} \cdot \text{cm}^{-2} \cdot \text{s}^{-1}$) contours based on in-vessel DOT-IV R-Z calculation.

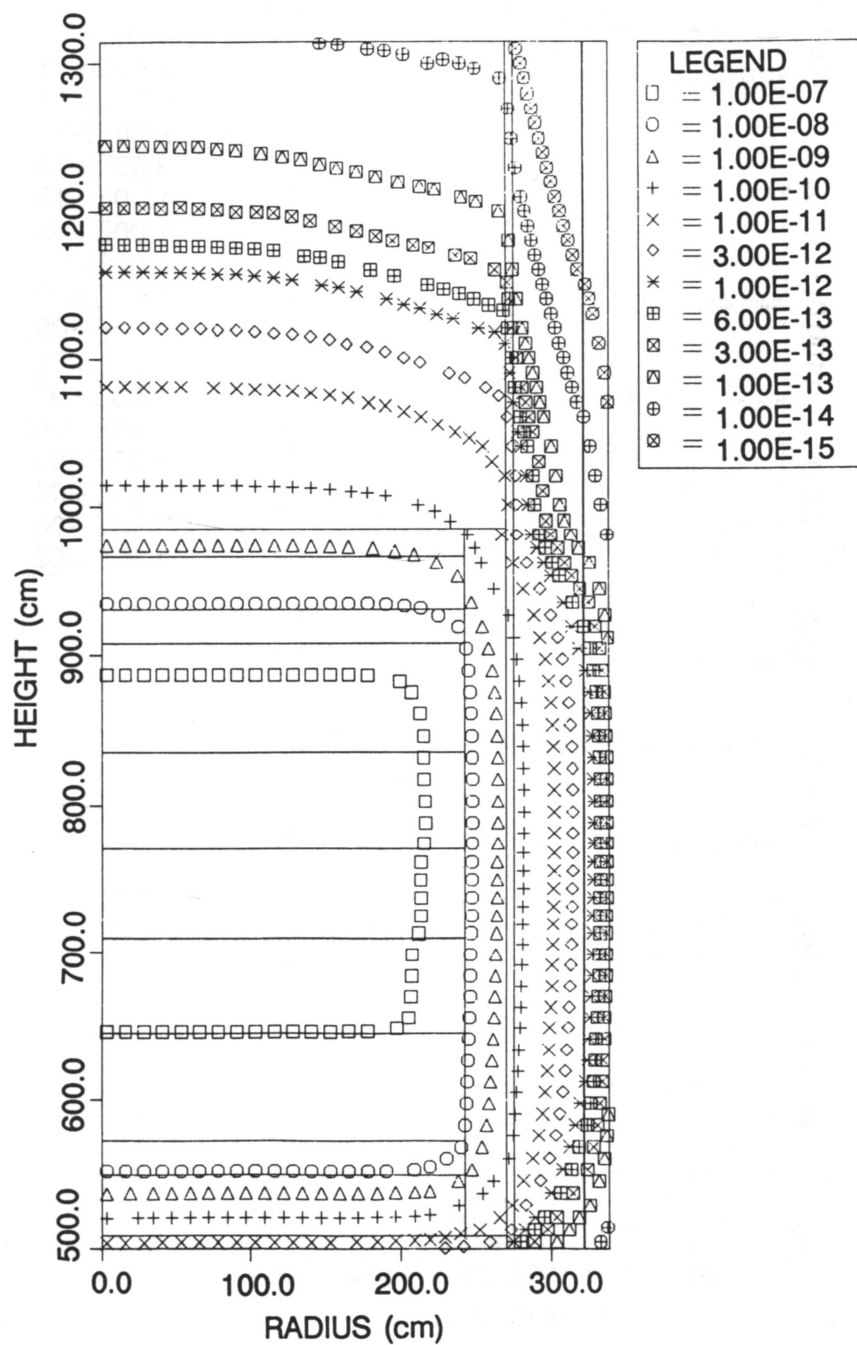


Fig. 5.5. Displacements per atom, dpa, ($\text{dpa} \cdot \text{s}^{-1}$) contours based on in-vessel DOT-IV R-Z calculation.

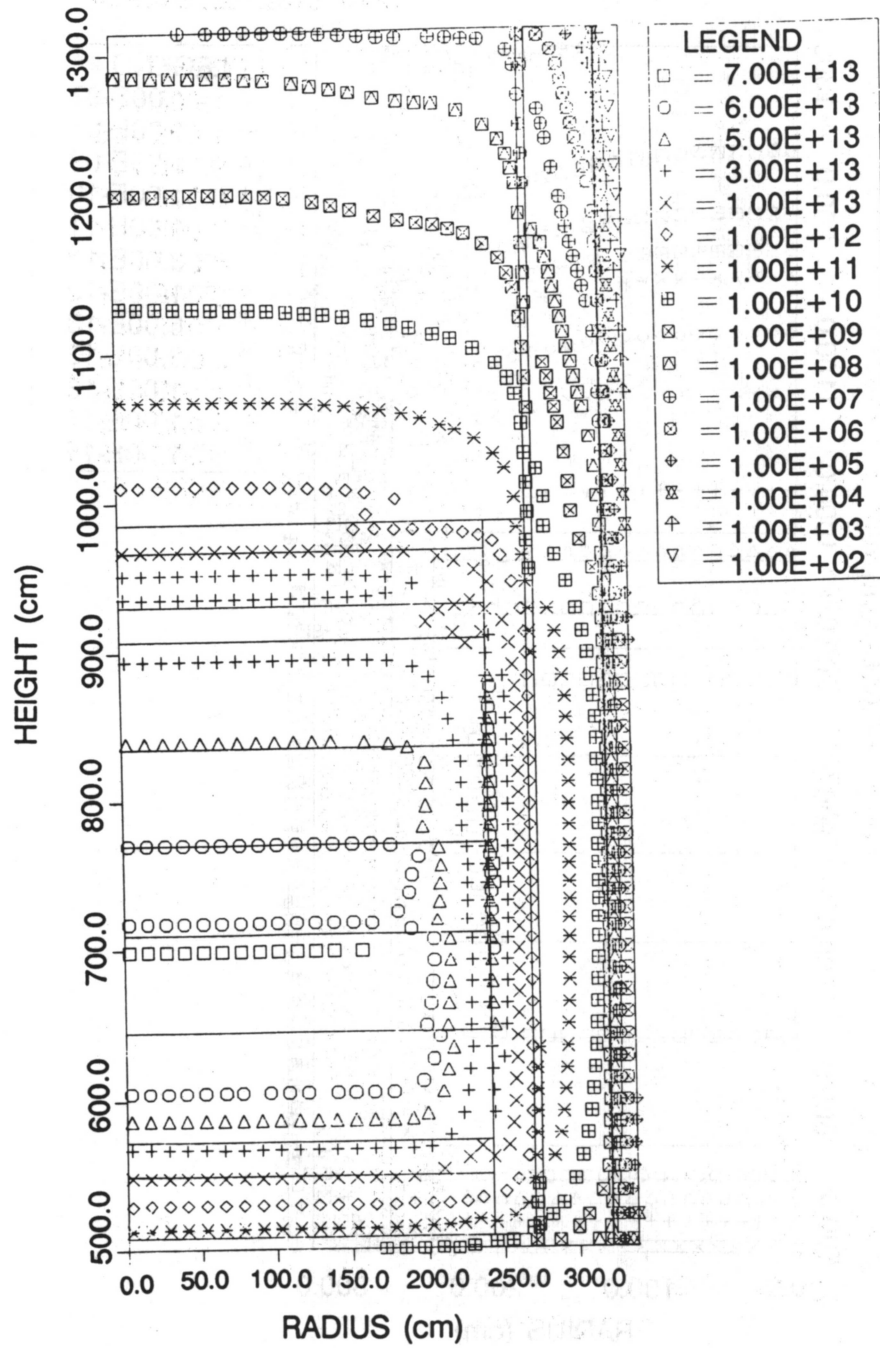


Fig. 5.6. Neutron flux below 0.4 eV ($\text{n}\cdot\text{cm}^{-2}\cdot\text{s}^{-1}$) contours based on in-vessel DOT-IV R-Z calculation.

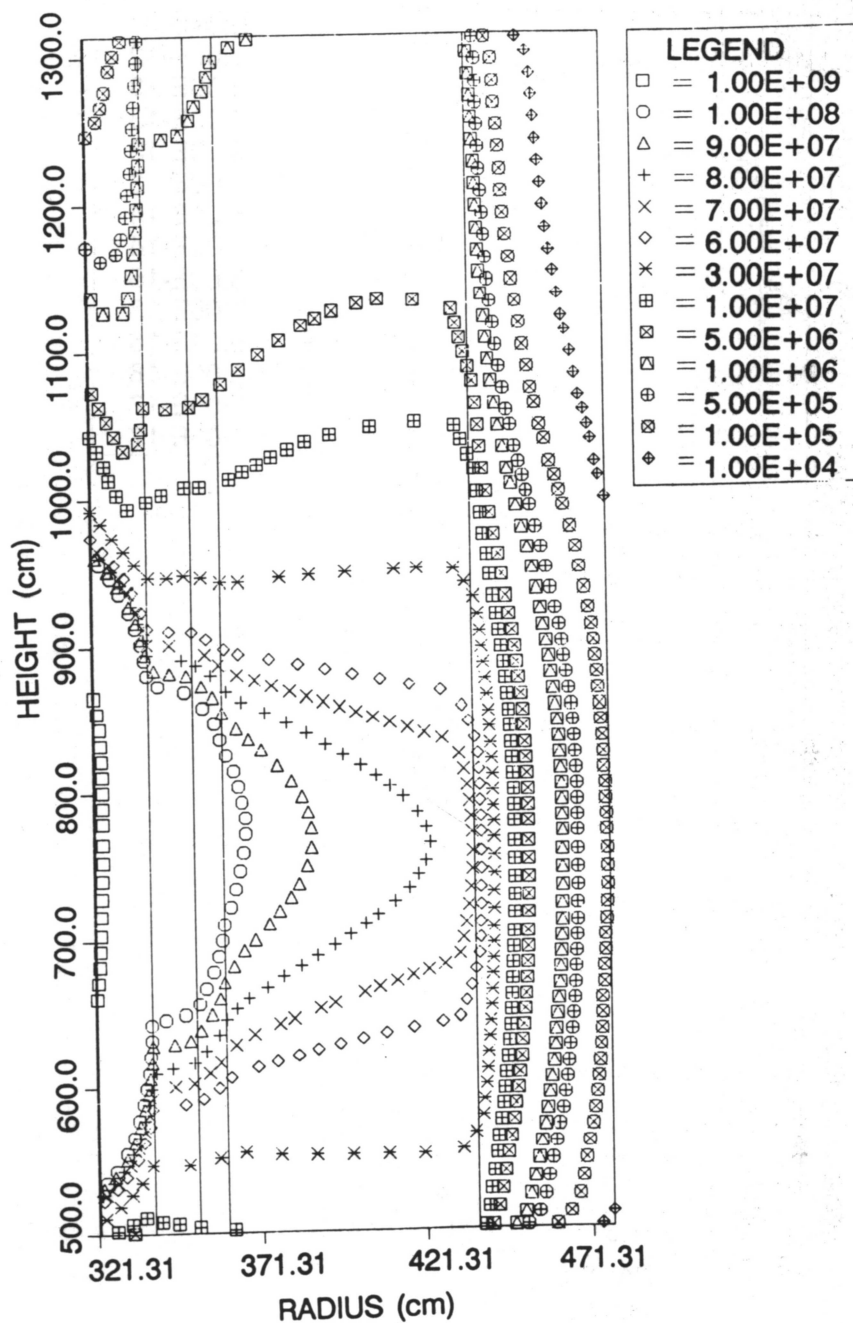


Fig. 5.7. Neutron flux above 1 MeV ($\text{n}\cdot\text{cm}^{-2}\cdot\text{s}^{-1}$) contours based on ex-vessel (cavity) DOT-IV R-Z calculation.

ORNL DWG. NO. 89-15158

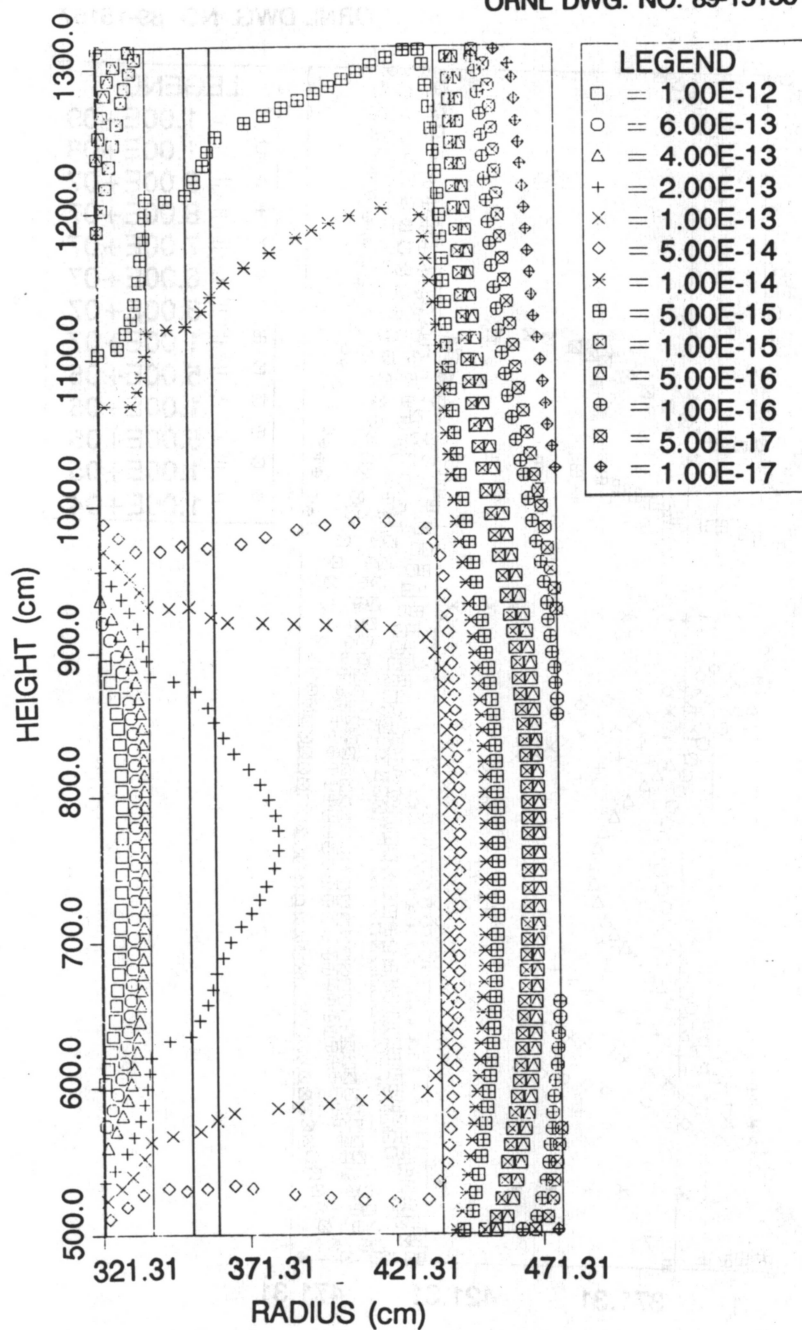


Fig. 5.8. Displacements per atom, dpa, ($\text{dpa} \cdot \text{s}^{-1}$) contours based on ex-vessel (cavity) DOT-IV R-Z calculation.

ORNL DWG. NO. 89-15159

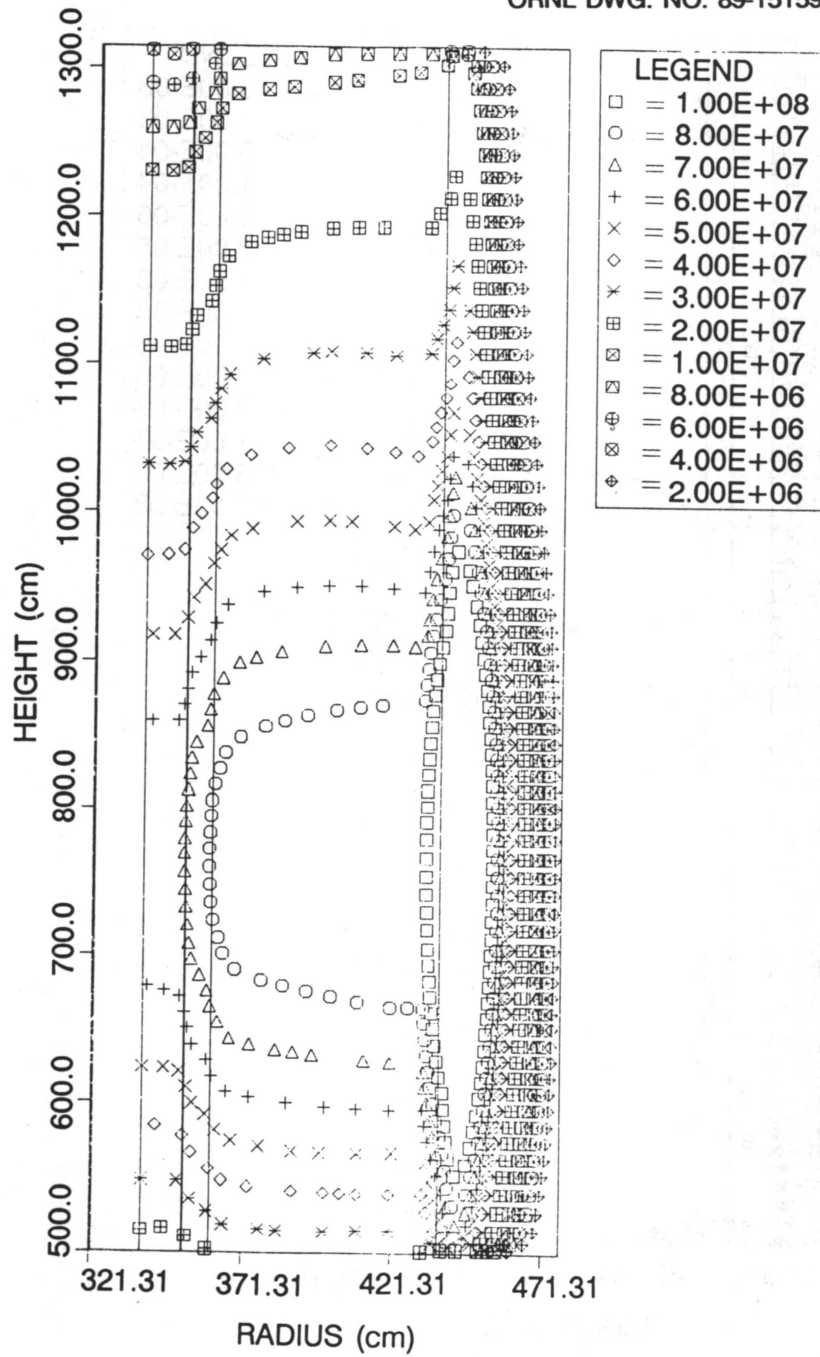


Fig. 5.9. Neutron flux below 0.4 eV ($\text{n}\cdot\text{cm}^{-2}\cdot\text{s}^{-1}$) contours based on ex-vessel (cavity) DOT-IV R-Z calculation.

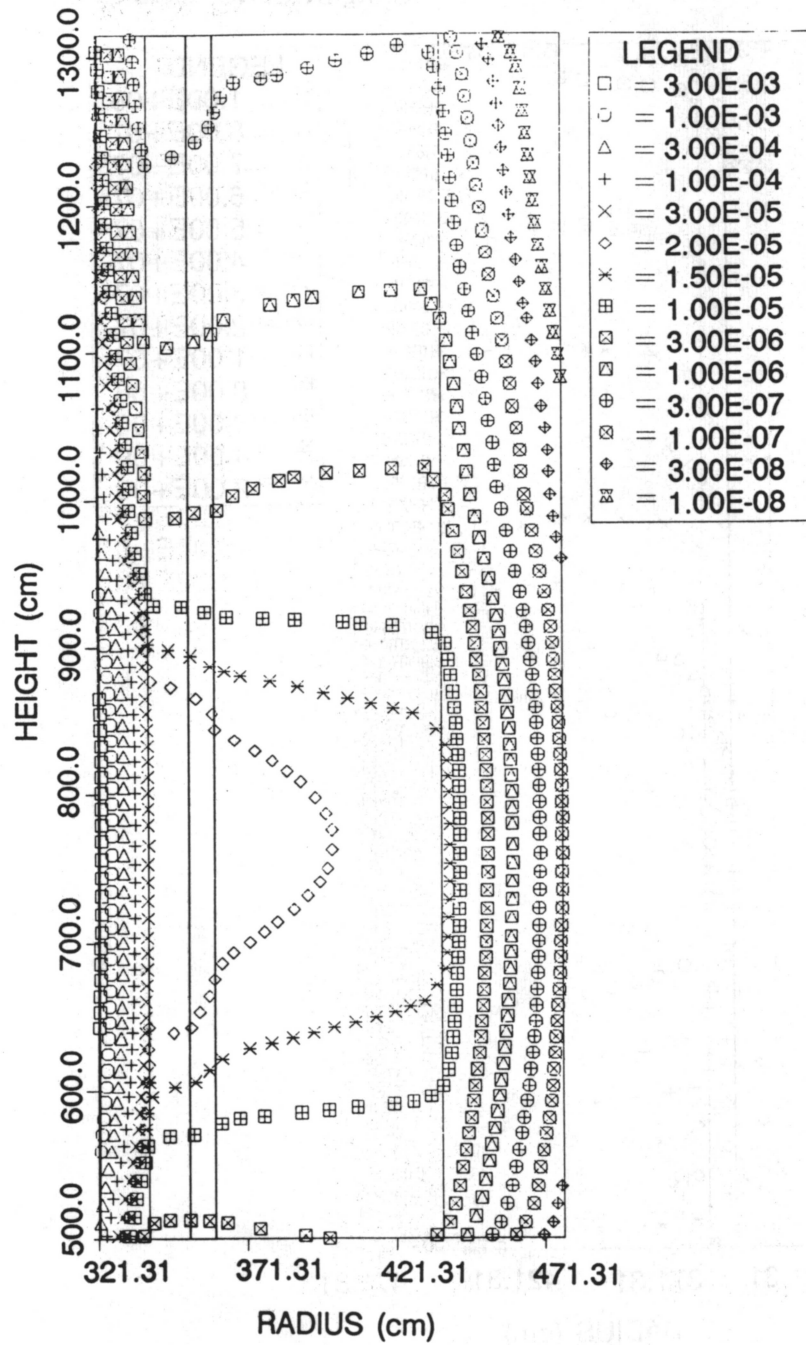


Fig. 5.10. Gamma heating (W/g SS 304) contours based on ex-vessel (cavity) DOT-IV R-Z calculation.

ORNL DWG. NO. 89-15161

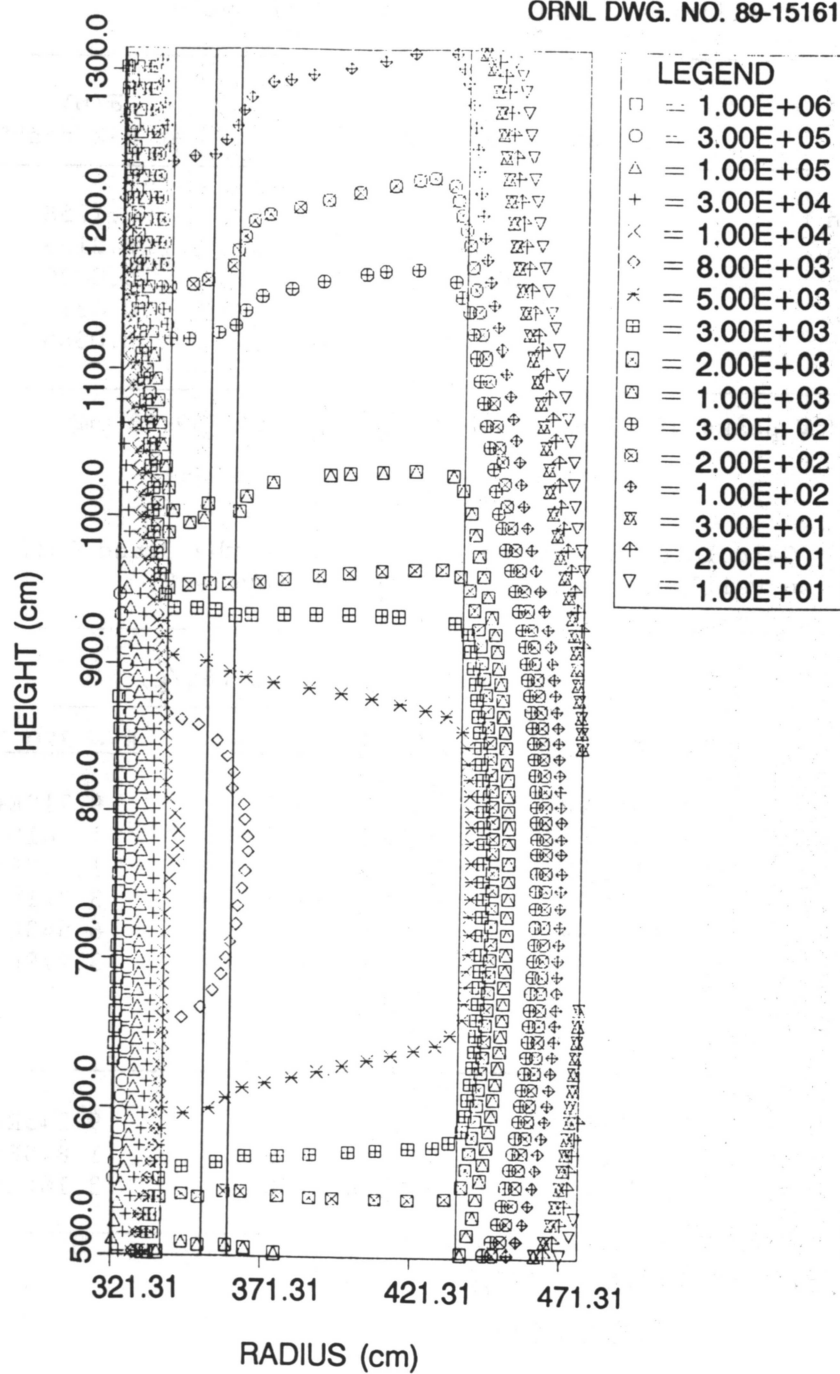


Fig. 5.11. Gamma absorbed dose (rad/h) contours based on ex-vessel (cavity) DOT-IV R-Z calculation.

Table 5.1. Spectrum-averaged cross section at center of 3° surveillance capsule for Grand Gulf Cycle 2

Reaction	$\bar{\sigma}(b)$ at midplane	$\bar{\sigma}(b)$ at R-Z peak ^a
$^{54}\text{Fe}(n,p)^{54}\text{Mn}$	0.1762	0.1758
$^{58}\text{Ni}(n,p)^{58}\text{Co}$	0.2163	0.2159
$^{63}\text{Cu}(n,\alpha)^{60}\text{Co}$	0.0030	0.0030
$^{238}\text{U}(n,f)^{137}\text{Cs}$	0.4817	0.4813
$^{46}\text{Ti}(n,p)^{46}\text{Sc}$	0.0366	0.0365

^aR-Z $\Phi > 1$ MeV peaks 48.47 cm above the midplane (739.93 cm).

Table 5.2. Calculated saturated activities in the Grand Gulf 3° surveillance capsule at midplane (Cycle 2)

Dosimeter	Saturated activities (Bq/g)		
	R = 318.73 cm	R = 319.76 cm	R = 320.79 cm
$^{54}\text{Fe}(n,p)^{54}\text{Mn}$	1.331E+05*	1.148E+05	9.719E+04
$^{58}\text{Ni}(n,p)^{58}\text{Co}$	1.821E+06	1.578E+06	1.341E+06
$^{63}\text{Cu}(n,\alpha)^{60}\text{Co}$	2.411E+04	2.063E+04	1.749E+04
$^{237}\text{Np}(n,f)^{137}\text{Cs}$	3.860E+05	3.633E+05	3.321E+05
$^{238}\text{U}(n,f)^{137}\text{Cs}$	8.470E+04	7.612E+04	6.643E+04
$^{46}\text{Ti}(n,p)^{46}\text{Sc}$	4.534E+04	3.882E+04	3.279E+04
Flux	$\Phi(E) \text{ n}\cdot\text{cm}^{-2}\cdot\text{s}^{-1}$		
$\Phi(E > 1.0 \text{ MeV})$	1.117E+09	1.041E+09	9.343E+08
$\Phi(E > 0.1 \text{ MeV})$	1.948E+09	1.937E+09	1.845E+09
$\Phi(E < 0.4 \text{ eV})$	1.278E+09	5.948E+08	3.164E+08

*Read as 1.331×10^5 .

Table 5.3. Calculated saturated activities in the Grand Gulf 3° surveillance capsule axial peak (Cycle 2)

Dosimeter	Saturated activities (Bq/g)		
	R = 318.73 cm	R = 319.76 cm	R = 320.79 cm
$^{54}\text{Fe}(n,p)^{54}\text{Mn}$	1.382E+05*	1.191E+05	1.009E+05
$^{58}\text{Ni}(n,p)^{58}\text{Co}$	1.891E+06	1.638E+06	1.392E+06
$^{63}\text{Cu}(n,\alpha)^{60}\text{Co}$	2.493E+04	2.133E+04	1.808E+04
$^{237}\text{Np}(n,f)^{137}\text{Cs}$	4.019E+05	3.783E+05	3.458E+05
$^{238}\text{U}(n,f)^{137}\text{Cs}$	8.804E+04	7.912E+04	6.904E+04
$^{46}\text{Ti}(n,p)^{46}\text{Sc}$	4.700E+04	4.023E+04	3.398E+04
Flux	$\Phi(E) \text{ n}\cdot\text{cm}^{-2}\cdot\text{s}^{-1}$		
$\Phi(E > 1.0 \text{ MeV})$	1.162E+09	1.083E+09	9.718E+08
$\Phi(E > 0.1 \text{ MeV})$	2.027E+09	2.016E+09	1.919E+09
$\Phi(E < 0.4 \text{ eV})$	1.334E+09	6.204E+08	3.301E+08

*Read as 1.382×10^5 .

Table 5.4. Nonsaturation factors (h_{ns}) for Grand Gulf Cycle 2

Dosimeter	h_{ns}^a
$^{54}\text{Fe}(n,p)^{54}\text{Mn}$	0.45375
$^{58}\text{Ni}(n,p)^{58}\text{Co}$	0.88525
$^{63}\text{Cu}(n,\alpha)^{60}\text{Co}$	0.09566
$^{238}\text{U}(n,f)^{137}\text{Cs}$	0.01747
$^{46}\text{Ti}(n,p)^{46}\text{Sc}$	0.85613
$^{181}\text{Ta}(n,\gamma)^{182}\text{Ta}$	0.79033

$$^a \quad h_{ns} = \sum_j P_j (1 - e^{-\lambda T_j}) e^{-\lambda(T-t_j)}$$

Table 5.5. Calculated lead factors at various radial locations through the RPV wall and cavity of Grand Gulf Cycle 2

Location ^a	Lead factor ^b
0-T	0.613
1/4-T	0.904
1/2-T	1.519
3/4-T	2.661
1-T	5.450
1/2-CW	9.702
1-CW	13.232

^aLocation within the RPV or in the cavity (i.e., 1/2-T = one-half RPV wall thickness and 1/2-CW = one-half cavity width = middle of cavity, etc.).

$$^b\text{Lead factor} = \frac{\Phi_{sc}(> 1)}{\Phi_1(> 1)}$$

where Φ_{sc} is the calculated flux at the center of the 3° surveillance capsule, and Φ_1 is the maximum calculated flux incident at the indicated locations.

Table 5.6. Relative azimuthal variation^a in $\Phi(>1 \text{ MeV})$
through the RPV wall of Grand Gulf Cycle 2

J	$\bar{\theta}$	0-T	1/4-T ^b	1/2-T ^b	3/4-T ^b
1	1.1245E+00	0.5349	0.5317	0.5311	0.5335
2	2.4995E+00	0.4945	0.4831	0.4946	0.5055
3	3.0000E+00	0.4841	0.4634	0.4777	0.4911
4	3.5005E+00	0.4711	0.4576	0.4689	0.4812
5	4.3755E+00	0.4756	0.4649	0.4662	0.4736
6	5.2390E+00	0.4492	0.4522	0.4550	0.4629
7	5.9890E+00	0.4239	0.4334	0.4419	0.4529
8	6.7500E+00	0.4076	0.4183	0.4302	0.4437
9	7.1250E+00	0.4009	0.4118	0.4248	0.4391
10	7.3250E+00	0.3978	0.4084	0.4220	0.4365
11	7.5950E+00	0.3921	0.4032	0.4174	0.4324
12	8.1300E+00	0.3864	0.3972	0.4111	0.4261
13	8.5350E+00	0.3889	0.3970	0.4092	0.4235
14	8.7460E+00	0.3881	0.3963	0.4075	0.4214
15	9.2070E+00	0.3878	0.3953	0.4050	0.4180
16	1.0261E+01	0.3929	0.3965	0.4028	0.4141
17	1.1624E+01	0.3868	0.3901	0.3963	0.4082
18	1.3124E+01	0.3670	0.3774	0.3890	0.4044
19	1.4500E+01	0.3736	0.3838	0.3969	0.4135
20	1.5500E+01	0.3896	0.4010	0.4141	0.4303
21	1.6500E+01	0.4181	0.4290	0.4402	0.4541
22	1.7376E+01	0.4526	0.4598	0.4669	0.4774
23	1.8376E+01	0.4868	0.4878	0.4910	0.4990
24	1.9500E+01	0.4997	0.5013	0.5053	0.5140
25	2.0239E+01	0.4966	0.5026	0.5105	0.5213
26	2.1239E+01	0.4990	0.5088	0.5195	0.5324
27	2.2500E+01	0.5113	0.5236	0.5364	0.5507
28	2.3500E+01	0.5333	0.5455	0.5584	0.5722
29	2.4261E+01	0.5591	0.5683	0.5795	0.5922
30	2.4636E+01	0.5709	0.5798	0.5911	0.6035
31	2.5017E+01	0.5852	0.5920	0.6030	0.6151
32	2.5517E+01	0.6041	0.6099	0.6198	0.6313
33	2.5875E+01	0.6179	0.6245	0.6335	0.6441
34	2.6566E+01	0.6470	0.6511	0.6577	0.6665
35	2.7566E+01	0.6695	0.6775	0.6856	0.6942
36	2.8301E+01	0.6835	0.6934	0.7034	0.7129
37	2.8801E+01	0.6932	0.7035	0.7149	0.7251
38	2.9250E+01	0.7009	0.7119	0.7245	0.7353
39	2.9745E+01	0.7091	0.7208	0.7338	0.7454

Table 5.6. Continued

J	$\bar{\theta}$	0-T	1/4-T ^b	1/2-T ^b	3/4-T ^b
40	3.0256E+01	0.7171	0.7296	0.7434	0.7551
41	3.0761E+01	0.7259	0.7382	0.7524	0.7641
42	3.1250E+01	0.7343	0.7468	0.7606	0.7720
43	3.1608E+01	0.7416	0.7537	0.7668	0.7776
44	3.2108E+01	0.7484	0.7599	0.7724	0.7832
45	3.3000E+01	0.7609	0.7707	0.7815	0.7916
46	3.3690E+01	0.7664	0.7759	0.7861	0.7964
47	3.4440E+01	0.7692	0.7792	0.7912	0.8030
48	3.5239E+01	0.7689	0.7825	0.7983	0.8123
49	3.6027E+01	0.7734	0.7923	0.8108	0.8263
50	3.7288E+01	0.8089	0.8292	0.8475	0.8616
51	3.8761E+01	0.8844	0.8983	0.9095	0.9167
52	3.9761E+01	0.9427	0.9482	0.9515	0.9527
53	4.0236E+01	0.9642	0.9678	0.9692	0.9688
54	4.0986E+01	1.0000	0.9952	0.9921	0.9890
55	4.1874E+01	0.9979	1.0000	1.0000	0.9987
56	4.2510E+01	0.9839	0.9937	0.9986	1.0000
57	4.3386E+01	0.9618	0.9782	0.9907	0.9974
58	4.4250E+01	0.9474	0.9654	0.9837	0.9949
59	4.4725E+01	0.9419	0.9603	0.9826	0.9956
60	4.4975E+01	0.9422	0.9640	0.9853	0.9982

^aPeak values are normalized to unity.

^bLocation within the RPV (i.e., 1/2-T = one-half RPV wall thickness).

Table 5.7. Relative azimuthal variation^a in $\Phi(>1 \text{ MeV})$
through the reactor cavity of Grand Gulf Cycle 2

J	$\bar{\theta}$	0-CW ^b	1/2-CW ^b	1-CW ^b
1	1.1245E+00	0.5121	0.5986	0.6279
2	2.4995E+00	0.4973	0.5939	0.6095
3	3.0000E+00	0.4882	0.5950	0.6071
4	3.5005E+00	0.4806	0.5957	0.6130
5	4.3755E+00	0.4706	0.5939	0.6233
6	5.2390E+00	0.4654	0.5918	0.6215
7	5.9890E+00	0.4564	0.5896	0.6231
8	6.7500E+00	0.4532	0.5897	0.6161
9	7.1250E+00	0.4546	0.5898	0.6071
10	7.3250E+00	0.4591	0.5898	0.6051
11	7.5950E+00	0.4468	0.5899	0.6117
12	8.1300E+00	0.4395	0.5898	0.6158
13	8.5350E+00	0.4501	0.5901	0.6113
14	8.7460E+00	0.4400	0.5898	0.6131
15	9.2070E+00	0.4325	0.5891	0.6243
16	1.0261E+01	0.4289	0.5886	0.6369
17	1.1624E+01	0.4256	0.5932	0.6474
18	1.3124E+01	0.4256	0.5999	0.6560
19	1.4500E+01	0.4349	0.6120	0.6639
20	1.5500E+01	0.4485	0.6203	0.6682
21	1.6500E+01	0.4671	0.6287	0.6729
22	1.7376E+01	0.4834	0.6367	0.6774
23	1.8376E+01	0.5010	0.6479	0.6892
24	1.9500E+01	0.5135	0.6626	0.6991
25	2.0239E+01	0.5250	0.6735	0.7057
26	2.1239E+01	0.5327	0.6879	0.7284
27	2.2500E+01	0.5497	0.7069	0.7486
28	2.3500E+01	0.5677	0.7233	0.7588
29	2.4261E+01	0.5864	0.7369	0.7591
30	2.4636E+01	0.6049	0.7431	0.7573
31	2.5017E+01	0.6052	0.7486	0.7670
32	2.5517E+01	0.6198	0.7556	0.7732
33	2.5875E+01	0.6367	0.7609	0.7790
34	2.6566E+01	0.6432	0.7728	0.8011
35	2.7566E+01	0.6660	0.7903	0.8134
36	2.8301E+01	0.6842	0.8038	0.8127
37	2.8801E+01	0.6992	0.8133	0.8137
38	2.9250E+01	0.7064	0.8217	0.8208
39	2.9745E+01	0.7152	0.8303	0.8299

Table 5.7. Continued

J	$\bar{\theta}$	0-CW ^b	1/2-CW ^b	1-CW ^b
40	3.0256E+01	0.7232	0.8388	0.8393
41	3.0761E+01	0.7323	0.8467	0.8488
42	3.1250E+01	0.7389	0.8542	0.8570
43	3.1608E+01	0.7564	0.8597	0.8629
44	3.2108E+01	0.7448	0.8671	0.8872
45	3.3000E+01	0.7525	0.8802	0.9091
46	3.3690E+01	0.7654	0.8918	0.9154
47	3.4440E+01	0.7646	0.9030	0.9337
48	3.5239E+01	0.7799	0.9172	0.9400
49	3.6027E+01	0.7866	0.9273	0.9555
50	3.7288E+01	0.8143	0.9426	0.9726
51	3.8761E+01	0.8540	0.9585	0.9764
52	3.9761E+01	0.8857	0.9648	0.9613
53	4.0236E+01	0.8980	0.9678	0.9623
54	4.0986E+01	0.9064	0.9751	0.9803
55	4.1874E+01	0.9159	0.9809	0.9817
56	4.2510E+01	0.9231	0.9855	0.9833
57	4.3386E+01	0.9186	0.9947	1.0000
58	4.4250E+01	0.9257	0.9982	0.9875
59	4.4725E+01	0.9290	0.9996	0.9757
60	4.4975E+01	1.0000	1.0000	0.9686

^aPeak values are normalized to unity.

^bLocation in the cavity (i.e., 1/2-CW = one-half cavity width = middle of the cavity, etc.).

Table 5.8. Radial variation of the total dpa, flux >1 MeV, flux <0.4 eV, and thermal-to-fast flux ratio at the axial core midplane and azimuthal peak

Radius ^a (cm)	Total dpa (dpa·s ⁻¹)	Fast flux (n·cm ⁻² ·s ⁻¹)	Thermal flux (n·cm ⁻² ·s ⁻¹)	Ratio ^b (ΦTh/ΦF)
321.310	2.680E-12	1.749E+09	3.131E+09	1.790
321.790	2.615E-12	1.712E+09	2.180E+09	1.273
322.700	2.445E-12	1.604E+09	1.204E+09	0.751
324.500	2.113E-12	1.355E+09	2.957E+08	0.218
325.888	1.838E-12	1.153E+09	1.289E+08	0.112
326.340	1.749E-12	1.087E+09	7.738E+07	0.071
328.200	1.434E-12	8.585E+08	2.462E+07	0.029
329.990	1.178E-12	6.768E+08	9.329E+07	0.014
331.810	9.610E-13	5.278E+08	5.016E+06	0.010
333.630	7.726E-13	4.064E+08	5.334E+06	0.013
334.080	7.322E-13	3.820E+08	7.024E+06	0.018
335.500	6.049E-13	3.055E+08	1.295E+07	0.042
337.300	4.502E-13	2.189E+08	4.132E+07	0.189
338.182	3.831E-13	1.845E+08	6.312E+07	0.342
340.460	3.695E-13	1.754E+08	6.381E+07	0.364
360.610	2.783E-13	1.344E+08	7.782E+07	0.579
377.000	2.372E-13	1.133E+08	8.328E+07	0.735
387.530	2.227E-13	1.056E+08	8.432E+07	0.798
409.660	2.032E-13	9.477E+07	8.692E+07	0.917
420.550	1.968E-13	9.092E+07	8.808E+07	0.969
436.880	1.721E-13	7.843E+07	1.409E+08	1.797
438.200	1.664E-13	7.576E+07	1.549E+08	2.044
443.200	6.355E-14	3.191E+07	2.669E+08	8.365
448.300	2.416E-14	1.315E+07	2.172E+08	16.515
452.120	1.279E-14	7.130E+06	1.501E+08	21.047
455.900	6.618E-15	3.740E+06	9.169E+07	24.512
461.000	2.820E-15	1.616E+06	4.186E+07	25.899
467.400	1.094E-15	6.360E+05	1.582E+07	24.875
470.000	6.679E-16	3.971E+05	8.738E+06	22.003

^aRefer to the reactor one-dimensional model shown in Fig. 3.5.

^bThermal-to-fast flux ratio.

Table 5.9. Radial variation of the total dpa, flux >1 MeV, flux <0.4 eV, and thermal-to-fast flux ratio at the axial and azimuthal peak

Radius ^a (cm)	Total dpa (dpa·s ⁻¹)	Fast flux (n·cm ⁻² ·s ⁻¹)	Thermal flux (n·cm ⁻² ·s ⁻¹)	Ratio ^b (ΦTh/ΦF)
321.310	2.786E-12	1.819E+09	3.265E+09	1.795
321.790	2.718E-12	1.781E+09	2.273E+09	1.277
322.700	2.542E-12	1.668E+09	1.256E+09	0.753
324.500	2.196E-12	1.409E+09	3.077E+08	0.218
325.888	1.911E-12	1.199E+09	1.344E+08	0.112
326.340	1.817E-12	1.130E+09	8.077E+07	0.071
328.200	1.489E-12	8.924E+08	2.567E+07	0.029
329.990	1.223E-12	7.036E+08	9.655E+07	0.014
331.810	9.967E-13	5.482E+08	5.183E+06	0.009
333.630	8.003E-13	4.217E+08	5.402E+06	0.013
334.080	7.583E-13	3.964E+08	7.097E+06	0.018
335.500	6.259E-13	3.170E+08	1.305E+07	0.041
337.300	4.642E-13	2.263E+08	4.171E+07	0.184
338.182	3.949E-13	1.910E+08	6.377E+07	0.334
340.460	3.797E-13	1.808E+08	6.442E+07	0.356
360.610	2.843E-13	1.376E+08	7.846E+07	0.570
377.000	2.413E-13	1.156E+08	8.407E+07	0.728
387.530	2.259E-13	1.073E+08	8.517E+07	0.793
409.660	2.051E-13	9.583E+07	8.775E+07	0.916
420.550	1.985E-13	9.185E+07	8.889E+07	0.968
436.880	1.735E-13	7.911E+07	1.422E+08	1.797
438.200	1.677E-13	7.642E+07	1.563E+08	2.045
443.200	6.417E-14	3.225E+07	2.692E+08	8.348
448.300	2.447E-14	1.334E+07	2.191E+08	16.431
452.120	1.298E-14	7.243E+06	1.514E+08	20.907
455.900	6.720E-15	3.797E+06	9.256E+07	24.378
461.000	2.859E-15	1.637E+06	4.230E+07	25.843
467.400	1.107E-15	6.442E+05	1.600E+07	24.831
470.000	6.638E-16	3.923E+05	8.839E+06	22.530

^aRefer to the reactor one-dimensional model shown in Fig. 3.5.

^bThermal-to-fast flux ratio.

Table 5.10. Radial variation of the total dpa, flux >1 MeV, flux <0.4 eV, and thermal-to-fast flux ratio at the axial feed water nozzle elevation and azimuthal peak

Radius ^a (cm)	Total dpa (dpa·s ⁻¹)	Fast flux (n·cm ⁻² ·s ⁻¹)	Thermal flux (n·cm ⁻² ·s ⁻¹)	Ratio ^b (ΦTh/ΦF)
321.310	1.154E-16	7.259E+04	1.094E+05	1.507
321.790	1.126E-16	7.110E+04	7.575E+04	1.066
322.700	1.048E-16	6.650E+04	4.254E+04	0.640
324.500	9.808E-16	1.429E+05	3.470E+04	0.243
325.888	1.161E-15	1.586E+05	4.150E+04	0.262
326.340	1.217E-15	1.635E+05	4.377E+04	0.268
328.200	1.459E-15	1.944E+05	7.167E+04	0.369
329.990	1.710E-15	2.370E+05	1.222E+05	0.516
331.810	2.000E-15	3.010E+05	2.211E+05	0.736
333.630	2.328E-15	3.936E+05	4.837E+05	1.229
334.080	2.438E-15	4.331E+05	7.165E+05	1.654
335.500	2.795E-15	5.620E+05	1.515E+06	2.695
337.300	3.568E-15	8.808E+05	4.794E+06	5.443
338.182	4.376E-15	1.270E+06	7.799E+06	6.139
340.460	4.324E-15	1.228E+06	7.834E+06	6.378
360.610	5.688E-15	1.745E+06	1.070E+07	6.131
377.000	6.130E-15	1.958E+06	1.219E+07	6.230
387.530	6.505E-15	2.134E+06	1.260E+07	5.904
409.660	7.482E-15	2.604E+06	1.305E+07	5.011
420.550	7.961E-15	2.827E+06	1.315E+07	4.651
436.880	4.880E-15	1.663E+06	1.477E+07	8.880
438.200	4.033E-15	1.339E+06	1.519E+07	11.341
443.200	8.801E-16	2.442E+05	1.751E+07	71.720
448.300	2.693E-16	7.402E+04	1.117E+07	150.916
452.120	1.306E-16	3.507E+04	6.705E+06	191.172
455.900	6.189E-17	1.636E+04	3.575E+06	218.535
461.000	2.311E-17	6.165E+03	1.394E+06	226.129
467.400	7.850E-18	2.219E+03	4.625E+05	208.423
470.000	4.094E-18	1.239E+03	2.300E+05	185.645

^aRefer to the reactor one-dimensional model shown in Fig. 3.5.

^bThermal-to-fast flux ratio.

Table 5.11. Determination of RPV peak cumulative fluence ($n \cdot cm^{-2}$) and dpa for Grand Gulf BWR/6

Radial location	Cycle 2 ^a		32 EFPY ^b	
	fluence	dpa	fluence	dpa
RPV wetted surface	4.406E+16	6.749E-05	1.838E+18	2.815E-03
0-T RPV	4.314E+16	6.584E-05	1.800E+18	2.747E-03
1/4-T RPV	2.904E+16	4.629E-05	1.212E+18	1.931E-03
1/2-T RPV	1.704E+16	2.983E-05	7.110E+17	1.236E-03
3/4-T RPV	9.602E+15	1.837E-05	4.006E+17	7.663E-04
1-T RPV	4.627E+15	9.566E-06	1.930E+17	3.991E-04

^aCycle 2 was about 280.37 full power days = 2.422×10^{07} seconds.

^b32 EFPY amounts to 11,696 full power days = 1.011×10^{09} seconds.

Table 5.12. Radial variation in gamma heating^a and gamma absorbed dose^b rate at three axial locations

Radius (cm)	Core midplane		Peak		F.W.N. ^c	
	γ heating	γ dose	γ heating	γ dose	γ heating	γ dose
321.790	2.463E-3	8.866E+5	2.544E-3	9.158E+5	9.639E-6	3.470E+3
325.888	7.905E-4	2.846E+5	8.163E-4	2.939E+5	3.037E-6	1.093E+6
329.990	2.722E-4	9.799E+4	2.818E-4	1.015E+5	1.030E-6	3.709E+2
334.080	5.894E-5	2.122E+4	6.073E-5	2.186E+4	2.837E-7	1.021E+2
338.182	2.769E-5	9.968E+3	2.840E-5	1.022E+4	2.457E-7	8.847E+1
360.610	2.174E-5	7.827E+3	2.214E-5	7.970E+3	3.519E-7	1.267E+2
387.530	2.000E-5	7.210E+3	2.030E-5	7.310E+3	3.900E-7	1.390E+2
420.500	1.840E-5	6.620E+3	1.874E-5	6.620E+3	4.400E-7	1.590E+2
436.880	1.695E-5	6.102E+3	1.700E-5	6.094E+3	3.089E-7	1.112E+2
452.120	2.601E-6	9.364E+2	2.605E-6	9.378E+3	4.409E-8	1.587E+1
467.400	3.000E-7	1.080E+2	3.028E-6	1.090E+3	4.985E-9	1.795E+0

^aGamma heating (W/g SS 304).

^bGamma absorbed dose rate (rad/h).

^cFeed water nozzle elevation (517.0 cm above the midplane).

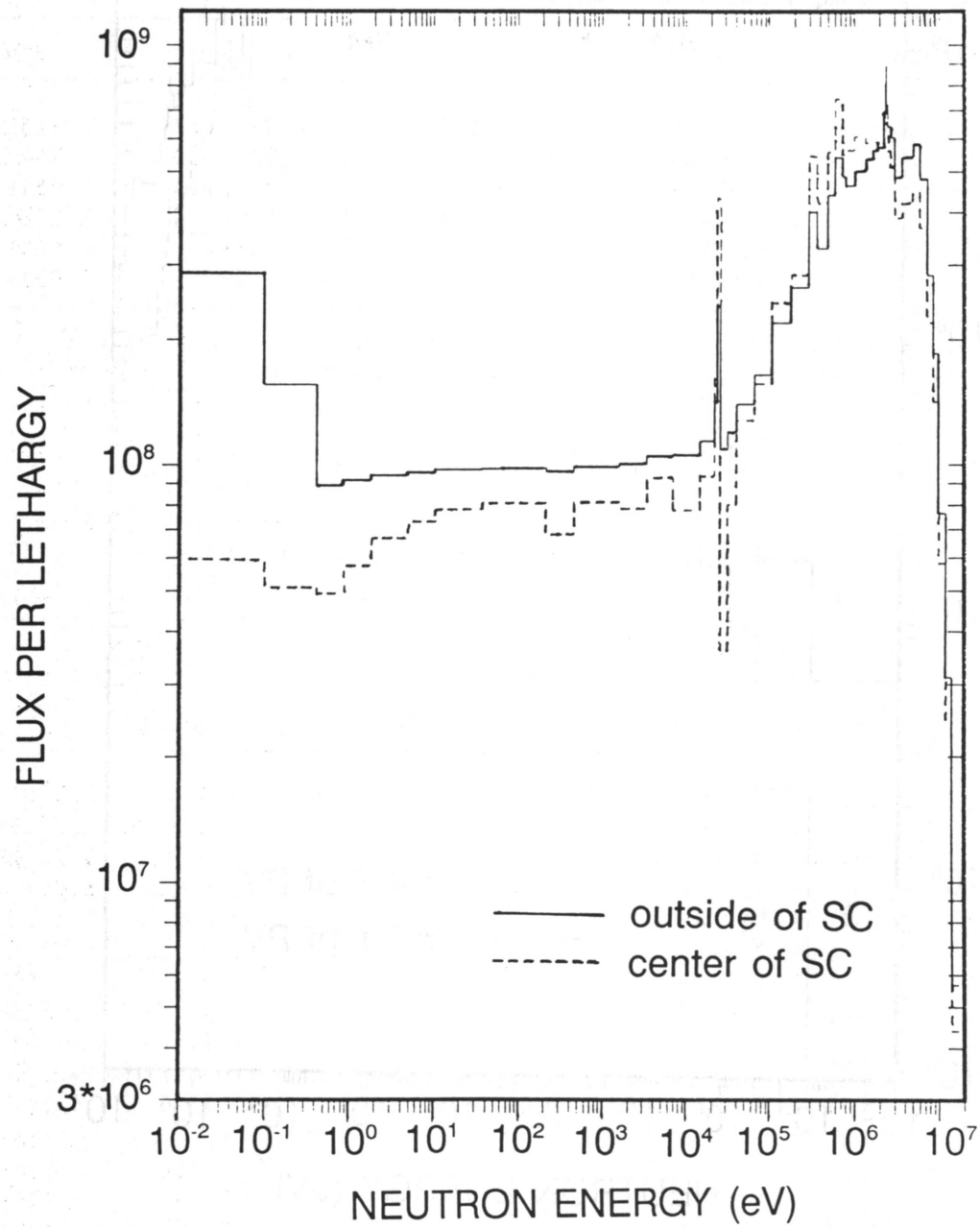


Fig. 5.12. Neutron energy spectra ($\text{n} \cdot \text{cm}^{-2} \cdot \text{s}^{-1} \cdot \Delta u^{-1}$) outside and center of the 3° surveillance capsule at the axial peak location.

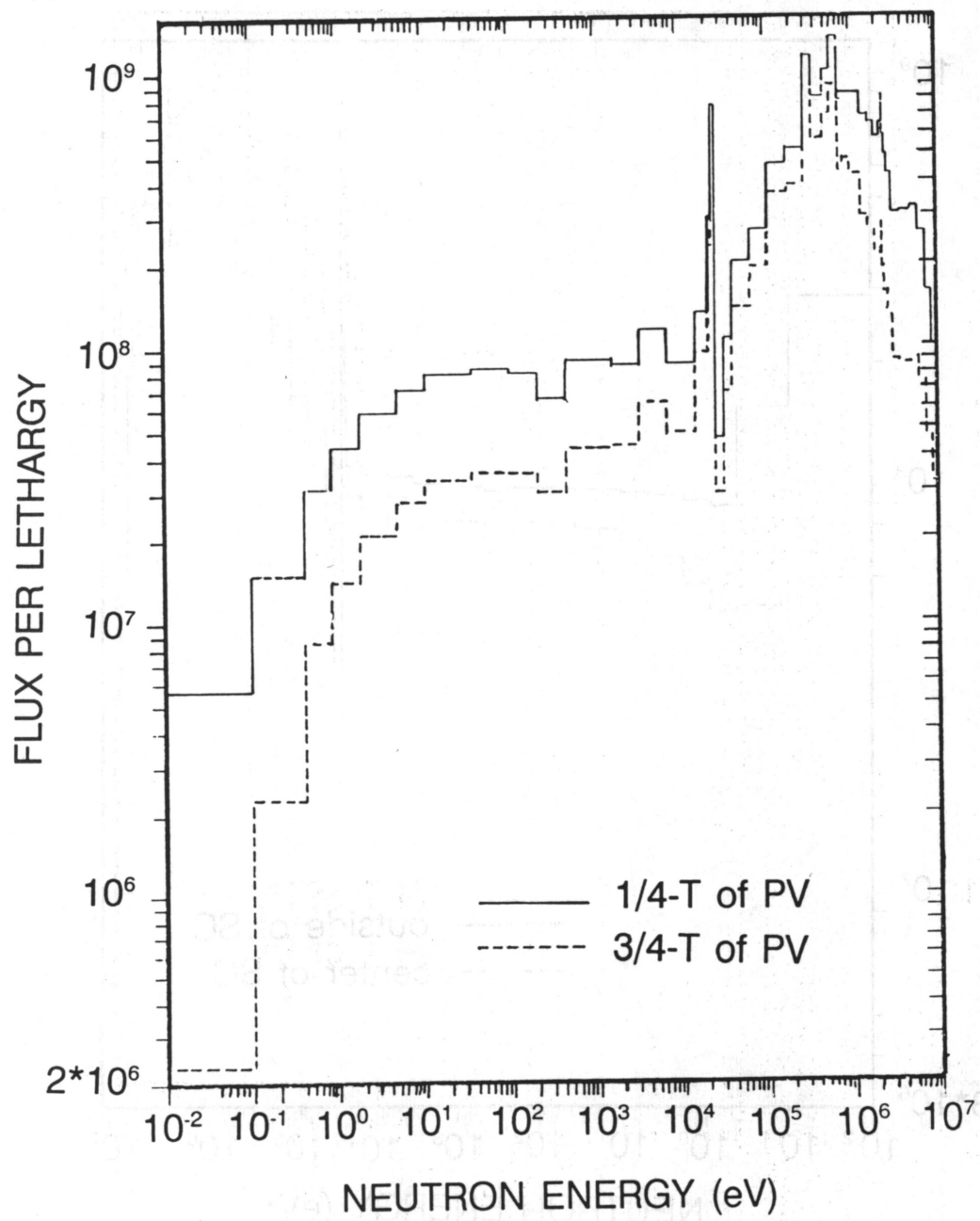


Fig. 5.13. Neutron energy spectra ($\text{n} \cdot \text{cm}^{-2} \cdot \text{s}^{-1} \cdot \Delta u^{-1}$) at two radial locations in the RPV at the axial core midplane.

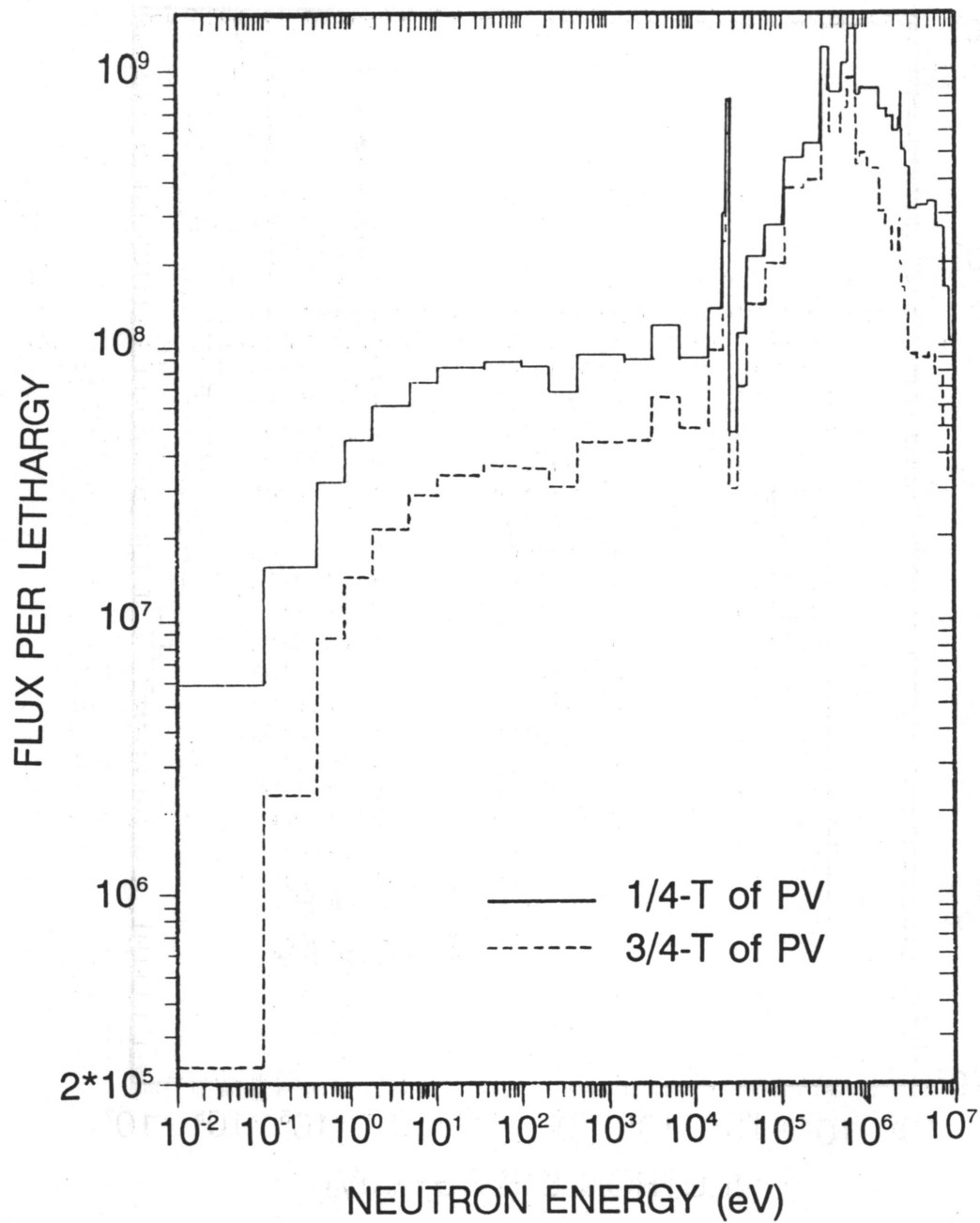


Fig. 5.14. Neutron energy spectra ($\text{n} \cdot \text{cm}^{-2} \cdot \text{s}^{-1} \cdot \Delta u^{-1}$) at two radial locations in the RPV at the axial peak.

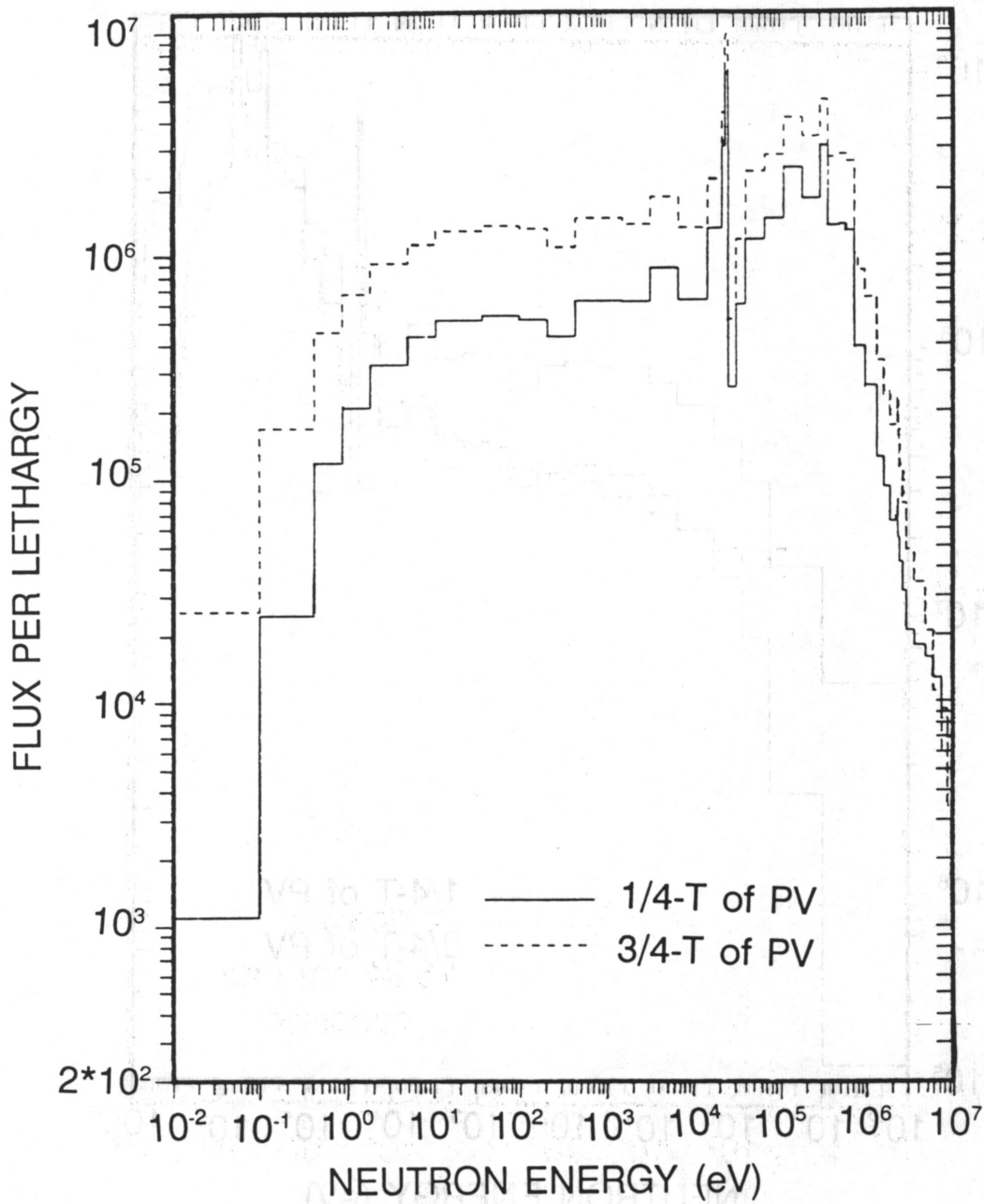


Fig. 5.15. Neutron energy spectra ($\text{n} \cdot \text{cm}^{-2} \cdot \text{s}^{-1} \cdot \Delta u^{-1}$) at two radial locations in the RPV at the feed water nozzle elevation.

ORNL DWG. NO. 89-15141

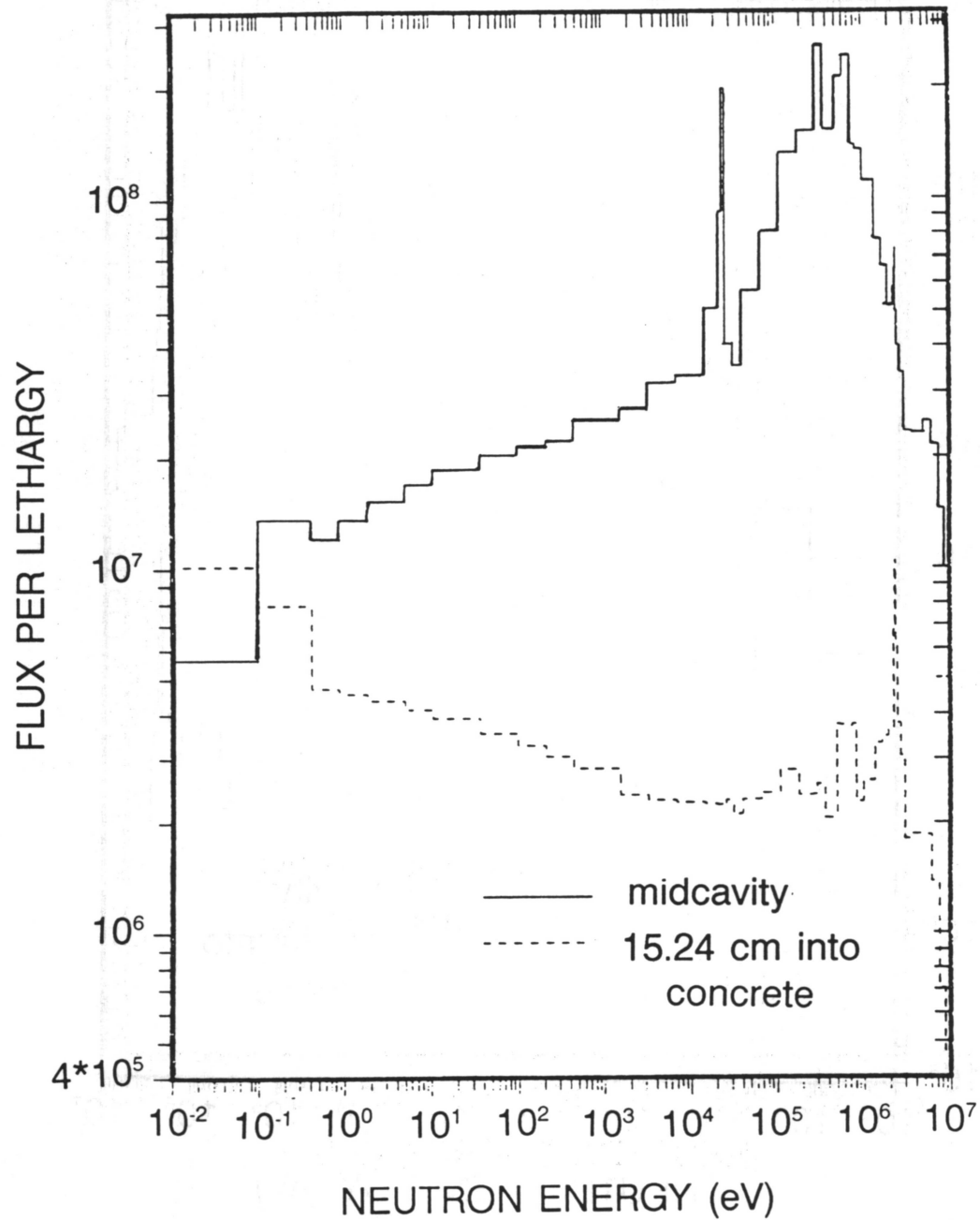


Fig. 5.16. Neutron energy spectra ($\text{n} \cdot \text{cm}^{-2} \cdot \text{s}^{-1} \cdot \Delta u^{-1}$) at midcavity and 15.24 cm into the concrete shield wall at the axial core midplane.

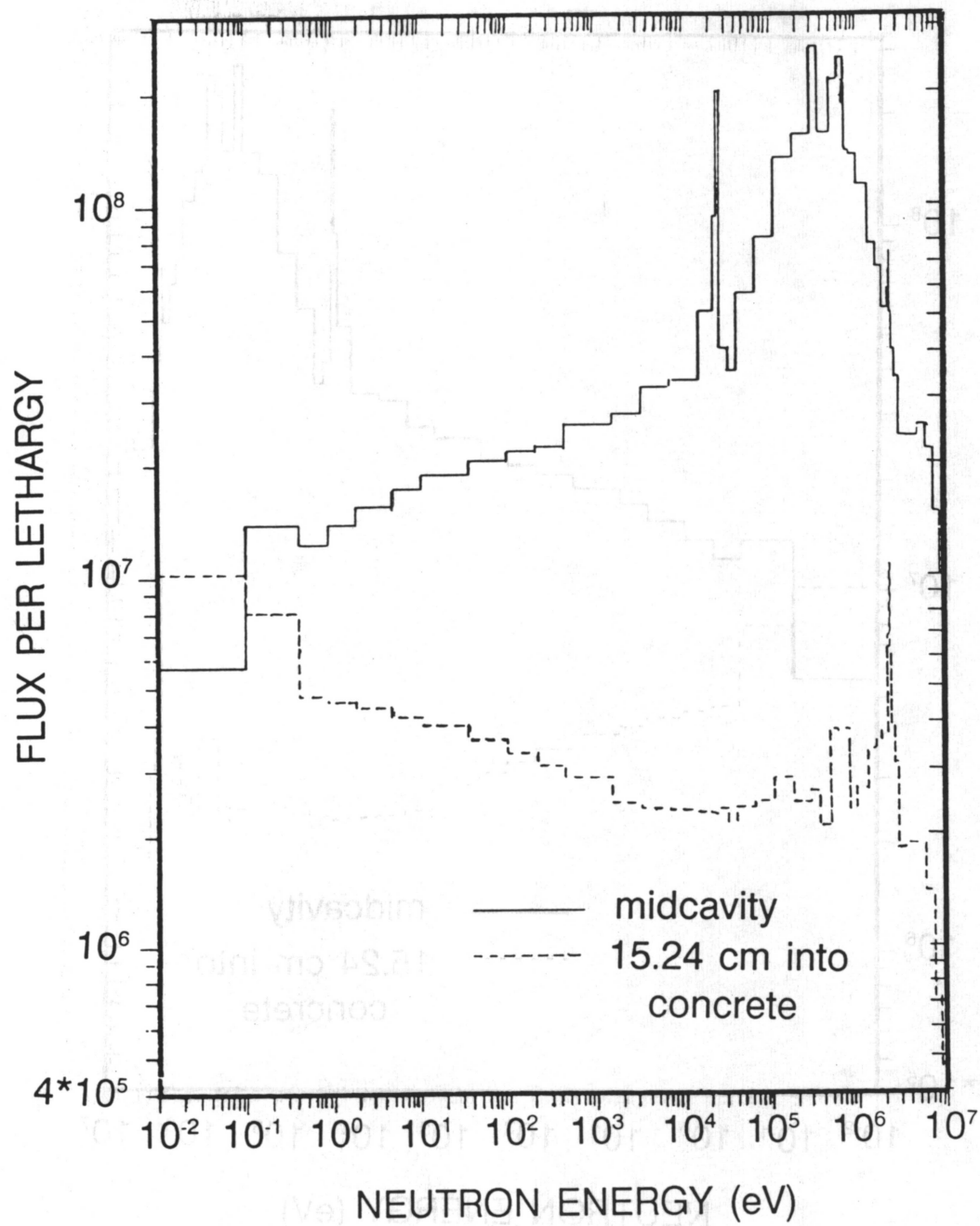


Fig. 5.17. Neutron energy spectra ($\text{n} \cdot \text{cm}^{-2} \cdot \text{s}^{-1} \cdot \Delta u^{-1}$) at midcavity and 15.24 cm into the concrete shield wall at the axial peak.

ORNL DWG. NO. 89-15143

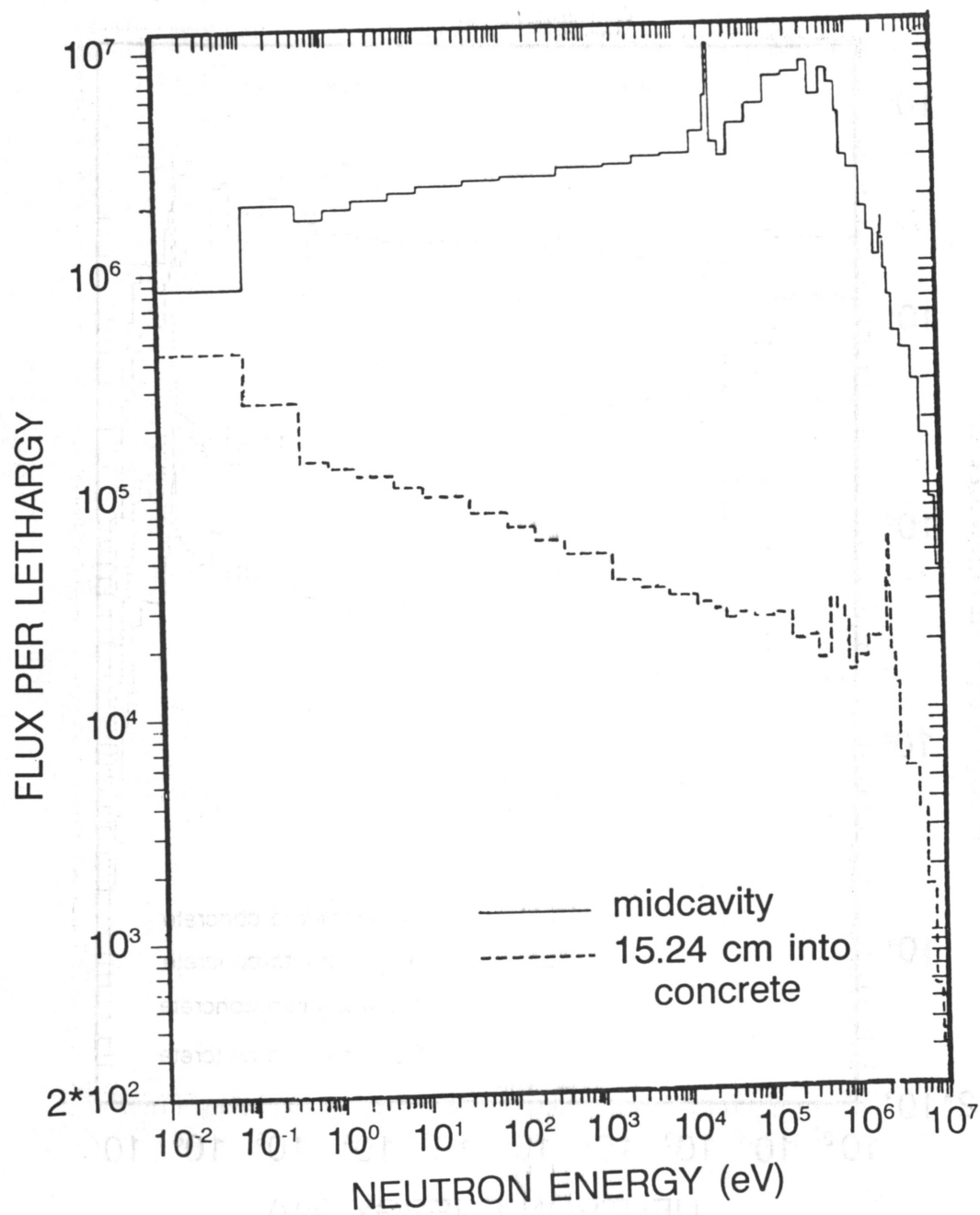


Fig. 5.18. Neutron energy spectra ($\text{n} \cdot \text{cm}^{-2} \cdot \text{s}^{-1} \cdot \Delta u^{-1}$) at midcavity and 15.24 cm into the concrete shield wall at the feed water nozzle elevation.

ORNL DWG. NO. 89-15144

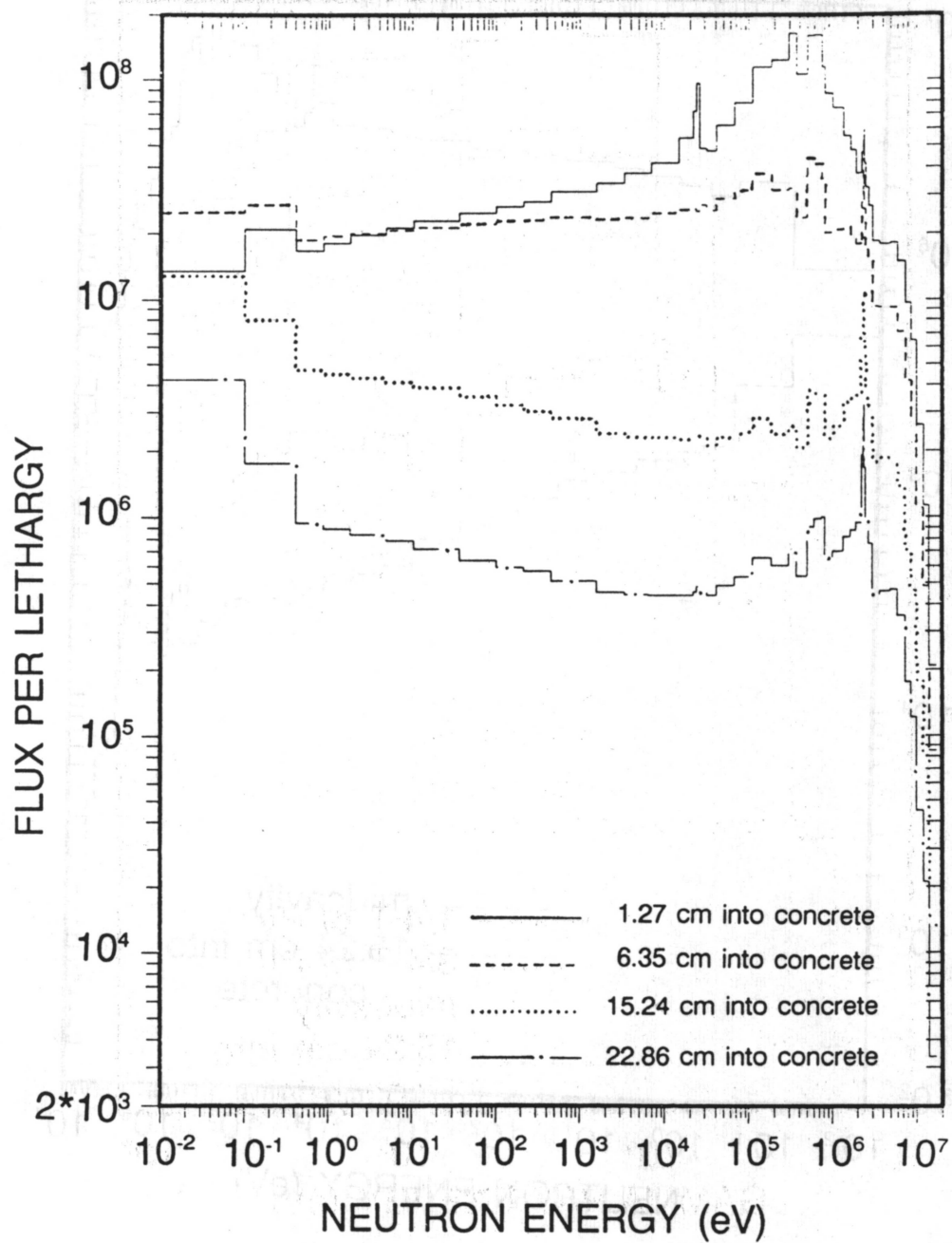


Fig. 5.19. Radial variation of neutron energy spectra ($\text{n} \cdot \text{cm}^{-2} \cdot \text{s}^{-1} \cdot \Delta u^{-1}$) through the concrete shield wall at the axial core midplane.

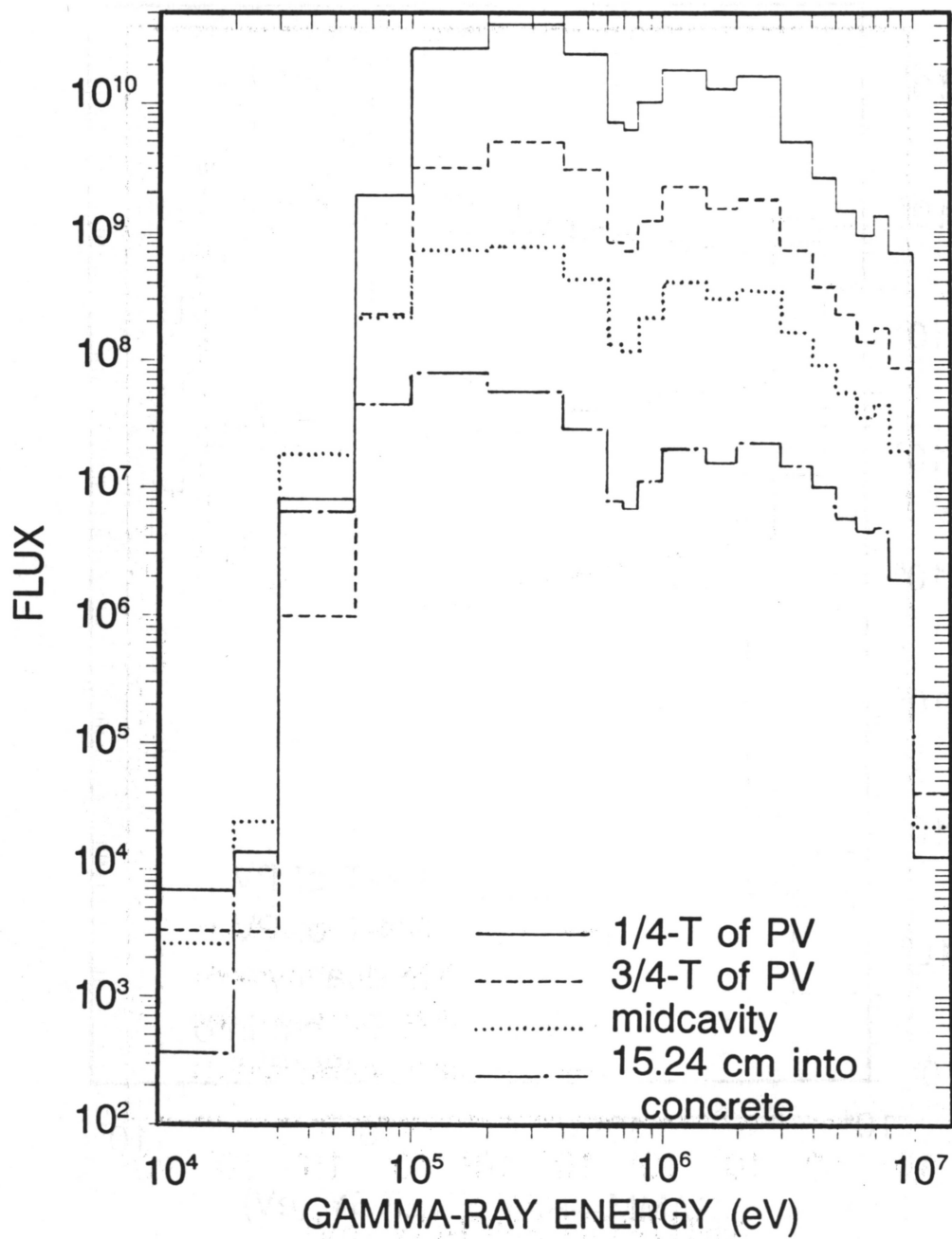


Fig. 5.20. Gamma energy spectra ($\gamma \cdot \text{cm}^{-2} \cdot \text{s}^{-1}$) at four radial locations throughout the RPV and the concrete shield wall at the axial core midplane.

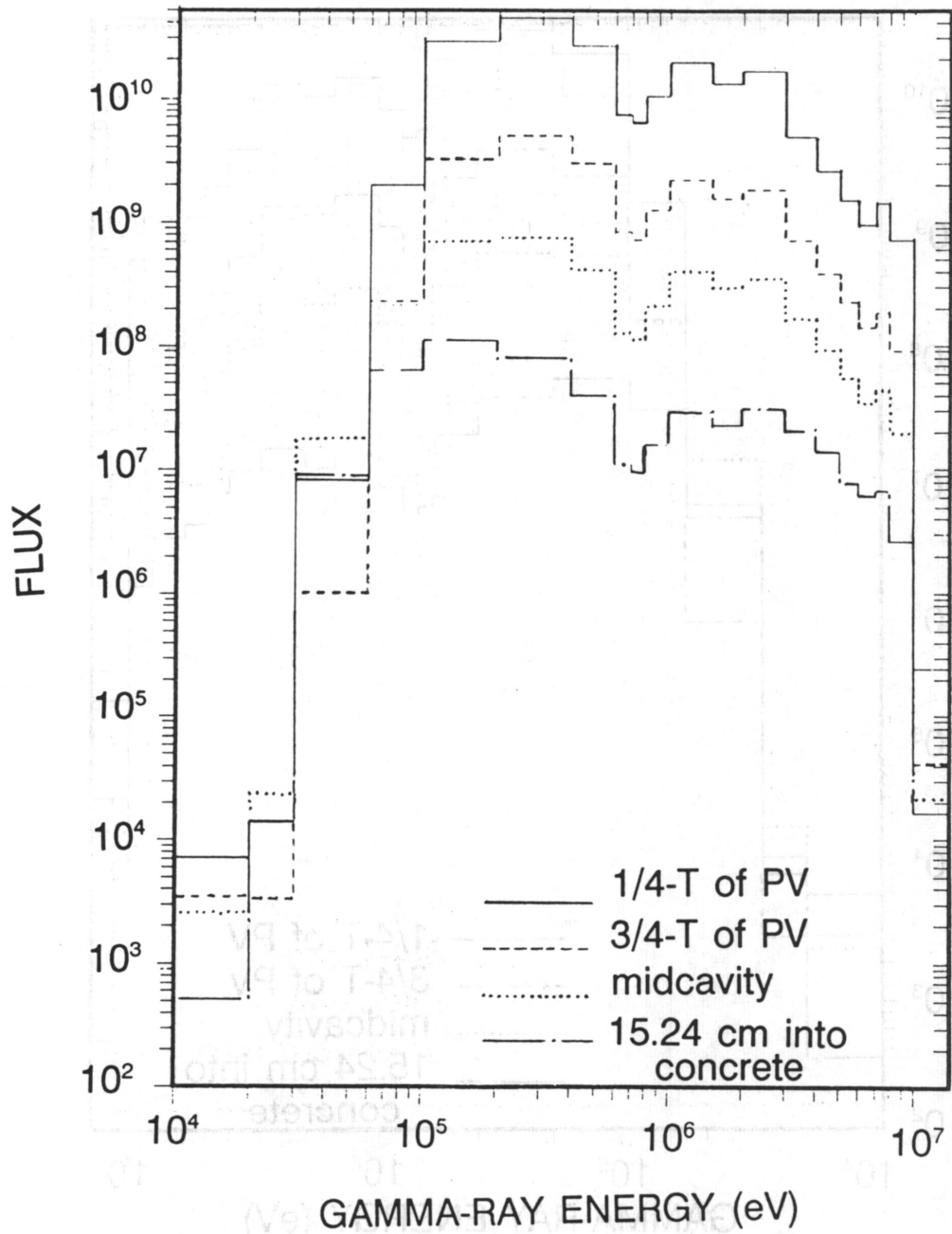


Fig. 5.21. Gamma energy spectra ($\gamma \cdot \text{cm}^{-2} \cdot \text{s}^{-1}$) at four radial locations throughout the RPV and the concrete shield wall at the axial peak.

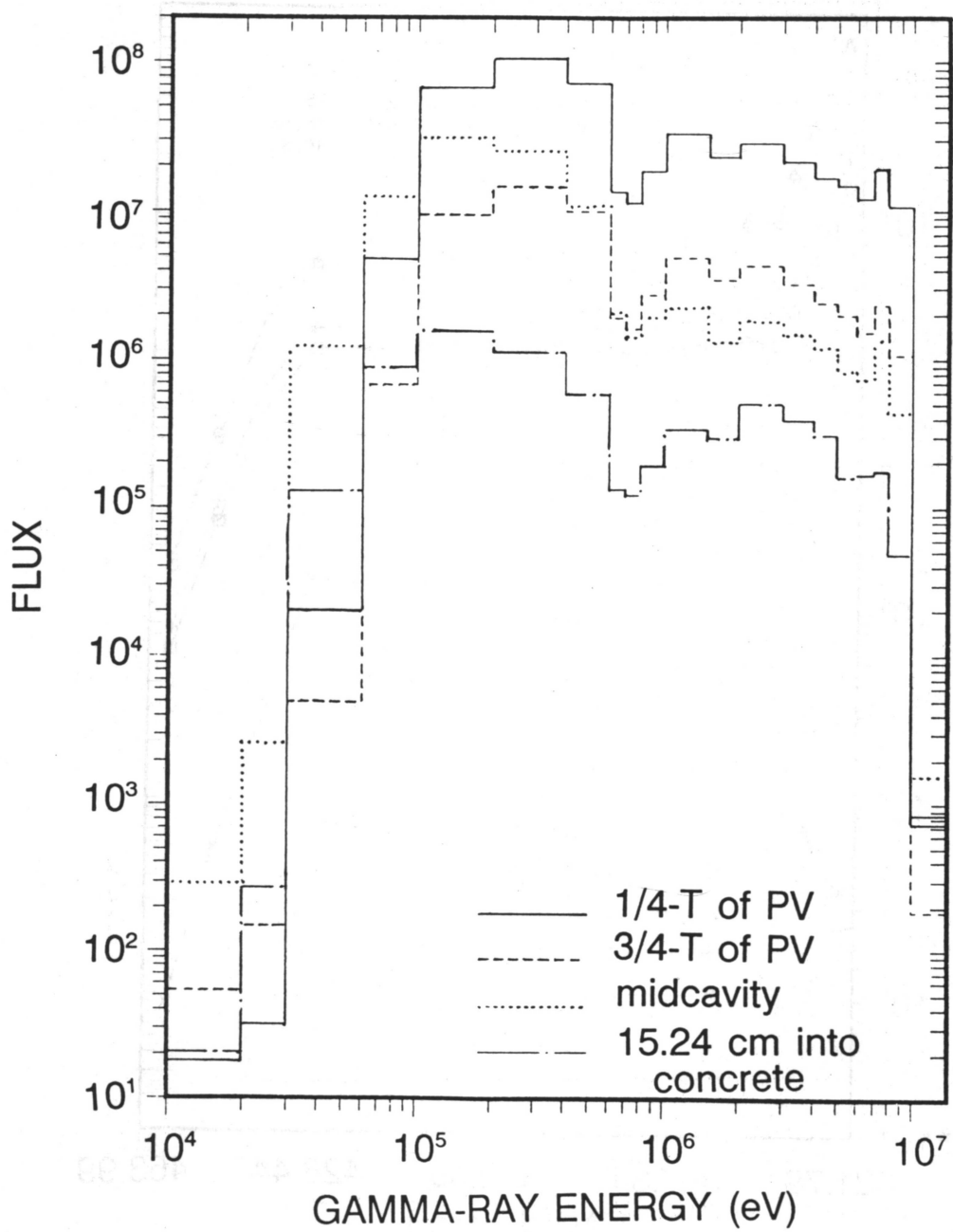


Fig. 5.22. Gamma energy spectra ($\gamma \cdot \text{cm}^{-2} \cdot \text{s}^{-1}$) at four radial locations throughout the RPV and the concrete shield wall at the feed water nozzle elevation.

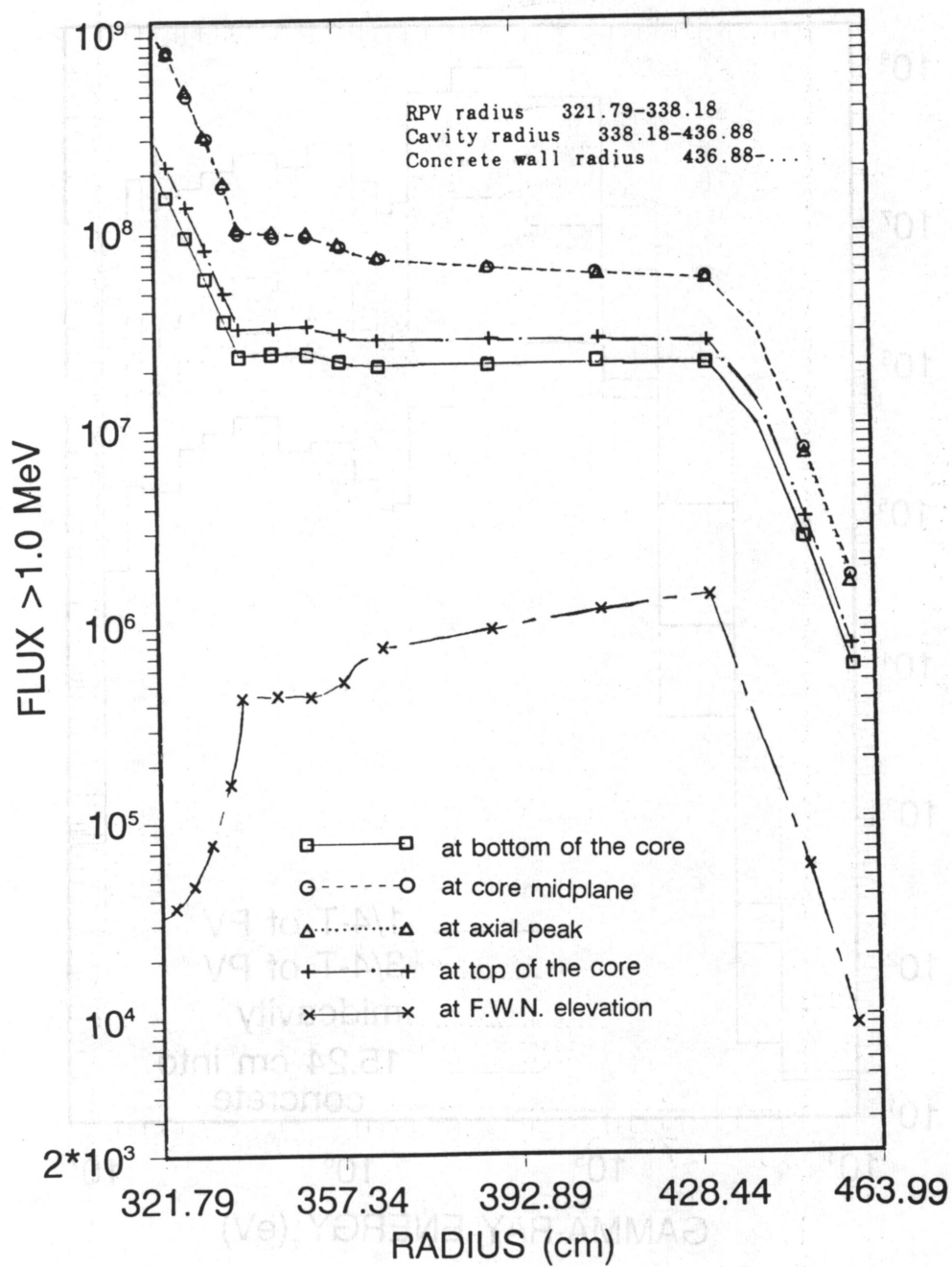


Fig. 5.23. Radial variation of the flux above 1 MeV ($\text{n}\cdot\text{cm}^{-2}\cdot\text{s}^{-1}$) at five radial locations.

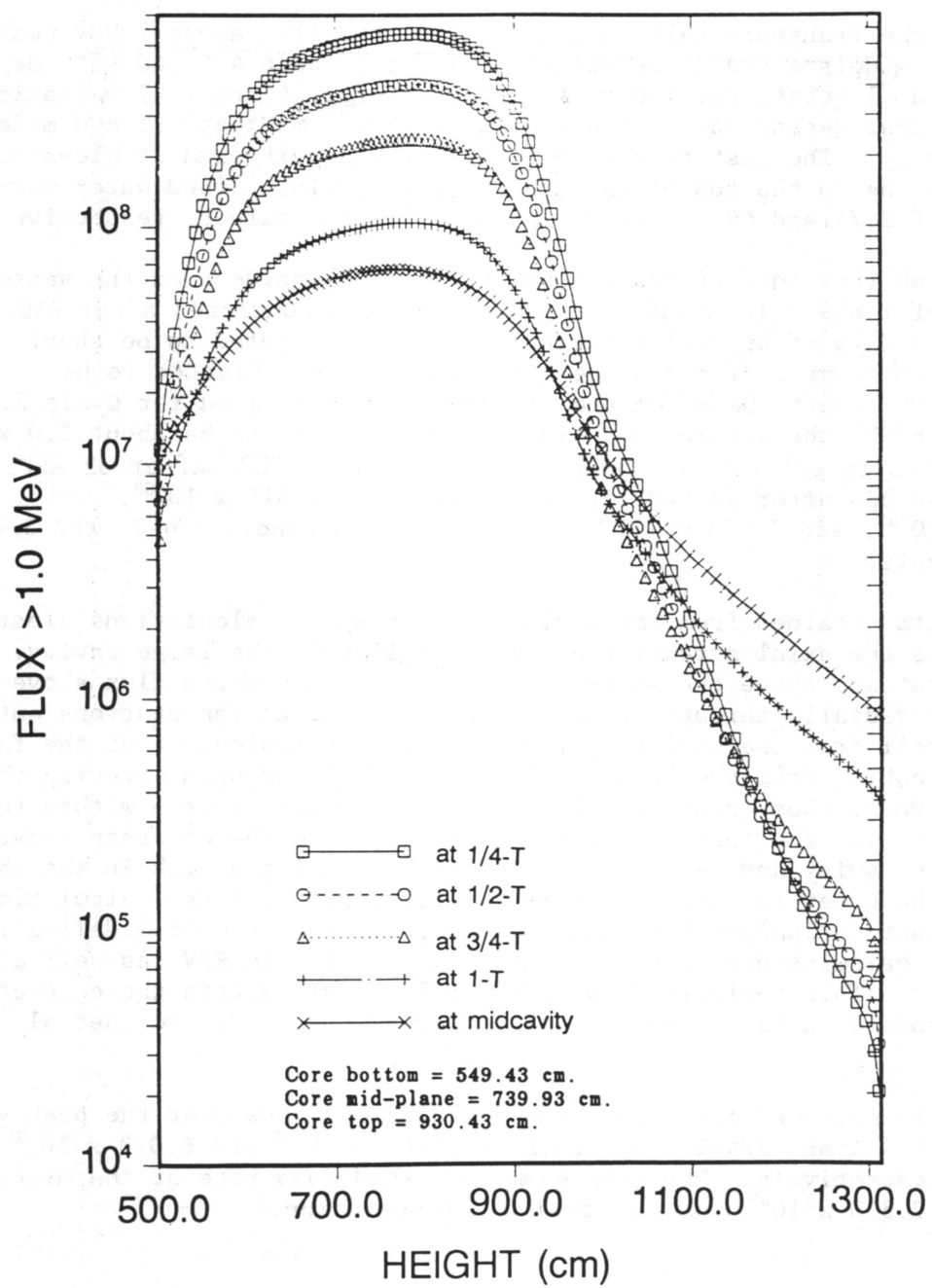


Fig. 5.24. Axial variation of the flux above 1 MeV ($\text{n}\cdot\text{cm}^{-2}\cdot\text{s}^{-1}$) at five radial locations.

6. CONCLUSIONS

Based on the transport calculation results, the flux above 1 MeV peaks near the axial midplane and at an azimuthal angle between 40° and 45°, depending on the radial locations. There is a factor of 1.76 and 1.67 variation in the azimuthal dependence of the fast flux ($E > 1$ MeV) at 0-T and midcavity, respectively. The fast flux ($E > 1$ MeV) at midcavity and at elevations corresponding to the top of the active core and inlet feed water nozzle are factors of 2.74 and 49.5 lower than core midplane values, respectively.

At the peak location, the fast flux ($E > 1$ MeV) incident on the vessel has a value of $1.819 \times 10^9 \text{ n}\cdot\text{cm}^{-2}\cdot\text{s}^{-1}$. The fluence accumulated after 280.37 full power days of operation during Cycle 2 is computed to be about $4.406 \times 10^{16} \text{ n}\cdot\text{cm}^{-2}$. The fluence after 32 EFPY is estimated to be $1.838 \times 10^{18} \text{ n}\cdot\text{cm}^{-2}$, based on the fluence rate calculated for Cycle 2. After 50 EFPY, the accumulated fluence is projected to be about $3.0 \times 10^{18} \text{ n}\cdot\text{cm}^{-2}$ which is still lower than observed for most PWRs after 32 EFPY. The cumulative dpa after 32 EFPY is estimated to be 2.815×10^{-03} , 1.931×10^{-03} , and 7.663×10^{-04} for RPV wetted surface, 1/4-T, and 3/4-T, respectively.

The results obtained from the cavity R-Z transport calculations clearly illustrate the axial streaming of the fast flux in the large cavity. At axial locations above the active core height, the neutron flux above 1 MeV increases radially throughout the vessel wall due to the neutrons entering the RPV wall from the cavity. Also, the results indicate that the fast neutron leaking from the vessel wall are thermalized upon entering the concrete wall, thus creating a large thermal neutron source within the concrete wall. The thermal neutrons emerging from the concrete travel across the cavity and re-enter the RPV wall, causing a peak in the thermal flux at the outer surface of the RPV wall. Based on these calculations, it is important to include the concrete shield in the reactor modeling for transport calculations of the thermal flux within the RPV, as well as in the cavity. This analysis shows that at locations within the concrete reactor shield, a large fraction of the fatal dpa is due to thermal neutrons.

The results obtained from the gamma calculations show that the peak gamma heating at 0-T and 3/4-T had values of 2.544×10^{-03} and $6.073 \times 10^{-05} \text{ W/g SS 304}$, respectively. The peak gamma absorbed dose rate at the midcavity is about $7.310 \times 10^{03} \text{ rad/h}$ at full power operation.

7. REFERENCES

1. R. E. Maerker, *Nucl. Sci. Eng.* 96(4), 263 (August 1987).
2. Calculation of Neutron Energy Spectra in the Core and Cavity of a PWR (ANO-1), Topical Report, NP-3776, Electric Power Research Institute, Palo Alto, Calif., December 1984.
3. BWR/6 General Description of a Boiling Water Reactor, General Electric Company, Nuclear Energy Group, San Jose, Calif., September 1980.
4. W. A. Rhoades and R. L. Childs, The TORT Three-Dimensional Discrete Ordinates Neutron/Photon Transport Code, ORNL-6268, Oak Ridge Natl. Lab., Oak Ridge, Tenn., November 1987.
5. P. Chowdhury, M. L. Williams, and F. B. K. Kam, Development of a Three-Dimensional Flux Synthesis Program and Comparison with 3-D Transport Theory Results, NUREG/CR-4984, ORNL/TM-10503, Oak Ridge Natl. Lab., Oak Ridge, Tenn., January 1988.
6. R. E. Maerker, M. L. Williams, and B. L. Broadhead, "Summary Documentation of Workshop on LWR Pressure Vessel Fluence Calculations with LEPRICON Code System," meeting held at Palo Alto, Calif., April 18-19, 1983.
7. G. L. Simmons and R. Roussin, RSIC Data Library Collection (DLC-76) - SAILOR - Coupled, Self-shielded, 47 Neutron, 20 Gamma-ray, P₃, Cross Section Library for Light Water Reactors, Radiation Shielding Information Center, Oak Ridge, Tenn., 1985.

APPENDIX A. ABSOLUTE CALCULATED NEUTRON FLUX SPECTRA AND DPA RATE

The definitions used in the following tables are

G = energy group

Energy = upper energy in MeV for corresponding group

Group flux = flux in $\text{n}\cdot\text{cm}^{-2}\cdot\text{s}^{-1}$ for corresponding energy group (Φ_g)

Cumulative flux = summed over the group flux, in $\text{n}\cdot\text{cm}^{-2}\cdot\text{s}^{-1}$ ($\Sigma\Phi_g$)

$$\Sigma\Phi_g = \sum_{g=1}^G \Phi_g$$

Group dpa rate = displacements per atom per second, $\text{dpa}\cdot\text{s}^{-1}$, for corresponding group [$(\text{dpa})_g$]

Cumulative dpa rate = summed over the group dpa, in $\text{dpa}\cdot\text{s}^{-1}$, [$\Sigma(\text{dpa})_g$]

$$[\Sigma(\text{dpa})_g] = \sum_{g=1}^G [(\text{dpa})_g]$$

dpa fraction = the ratio of cumulative dpa rate to total dpa rate

$$\frac{[\Sigma(\text{dpa})_g]}{\sum_{g=1}^{47} [(\text{dpa})_g]}$$

Table A.1.a. Absolute calculated neutron flux spectra
and dpa rate at the center of 3° surveillance capsule
and core axial peak of Grand Gulf Cycle 2

G	Energy (MeV)	Group flux	Cumulative flux	Group dpa rate	Cumulative dpa rate	dpa fraction
1	1.733E+01	8.550E+05	8.550E+05	2.498E-15	2.498E-15	1.590E-03
2	1.419E+01	3.545E+06	4.400E+06	9.379E-15	1.188E-14	7.558E-03
3	1.221E+01	1.129E+07	1.569E+07	2.719E-14	3.907E-14	2.486E-02
4	1.000E+01	2.052E+07	3.621E+07	4.554E-14	8.461E-14	5.384E-02
5	8.607E+00	3.166E+07	6.787E+07	6.607E-14	1.507E-13	9.588E-02
6	7.408E+00	7.078E+07	1.386E+08	1.375E-13	2.882E-13	1.834E-01
7	6.065E+00	8.608E+07	2.247E+08	1.536E-13	4.418E-13	2.811E-01
8	4.966E+00	1.209E+08	3.456E+08	1.899E-13	6.317E-13	4.020E-01
9	3.679E+00	7.468E+07	4.203E+08	1.023E-13	7.340E-13	4.671E-01
10	3.012E+00	4.934E+07	4.696E+08	6.271E-14	7.967E-13	5.070E-01
11	2.725E+00	5.386E+07	5.235E+08	6.867E-14	8.654E-13	5.507E-01
12	2.466E+00	2.594E+07	5.494E+08	3.040E-14	8.958E-13	5.700E-01
13	2.365E+00	6.350E+06	5.558E+08	6.960E-15	9.028E-13	5.744E-01
14	2.346E+00	3.160E+07	5.874E+08	3.290E-14	9.357E-13	5.954E-01
15	2.231E+00	8.189E+07	6.693E+08	8.467E-14	1.020E-12	6.492E-01
16	1.920E+00	8.466E+07	7.539E+08	6.886E-14	1.089E-12	6.931E-01
17	1.653E+00	1.129E+08	8.669E+08	9.148E-14	1.181E-12	7.513E-01
18	1.353E+00	1.742E+08	1.041E+09	9.761E-14	1.278E-12	8.134E-01
19	1.003E+00	1.080E+08	1.149E+09	3.957E-14	1.318E-12	8.386E-01
20	8.208E-01	5.251E+07	1.202E+09	2.945E-14	1.347E-12	8.573E-01
21	7.427E-01	1.436E+08	1.345E+09	5.189E-14	1.399E-12	8.903E-01
22	6.081E-01	1.070E+08	1.452E+09	3.148E-14	1.431E-12	9.103E-01
23	4.979E-01	1.219E+08	1.574E+09	4.831E-14	1.479E-12	9.411E-01
24	3.688E-01	1.130E+08	1.687E+09	2.335E-14	1.502E-12	9.559E-01
25	2.972E-01	1.327E+08	1.820E+09	2.661E-14	1.529E-12	9.729E-01
26	1.832E-01	1.172E+08	1.937E+09	1.652E-14	1.545E-12	9.834E-01
27	1.111E-01	7.506E+07	2.012E+09	9.706E-15	1.555E-12	9.896E-01
28	6.738E-02	6.140E+07	2.073E+09	3.977E-15	1.559E-12	9.921E-01
29	4.087E-02	1.926E+07	2.092E+09	1.559E-15	1.561E-12	9.931E-01
30	3.183E-02	6.918E+06	2.099E+09	1.967E-15	1.563E-12	9.943E-01
31	2.606E-02	3.126E+07	2.131E+09	6.302E-16	1.563E-12	9.947E-01
32	2.418E-02	1.582E+07	2.146E+09	6.929E-17	1.563E-12	9.948E-01
33	2.188E-02	3.394E+07	2.180E+09	2.780E-16	1.564E-12	9.949E-01
34	1.503E-02	5.610E+07	2.237E+09	1.052E-15	1.565E-12	9.956E-01
35	7.102E-03	6.681E+07	2.303E+09	5.943E-16	1.565E-12	9.960E-01
36	3.355E-03	5.667E+07	2.360E+09	1.995E-16	1.565E-12	9.961E-01
37	1.585E-03	9.795E+07	2.458E+09	1.647E-16	1.566E-12	9.962E-01
38	4.540E-04	4.904E+07	2.507E+09	4.835E-18	1.566E-12	9.962E-01
39	2.144E-04	5.799E+07	2.565E+09	8.316E-18	1.566E-12	9.962E-01
40	1.013E-04	7.762E+07	2.643E+09	1.732E-17	1.566E-12	9.962E-01
41	3.727E-05	9.402E+07	2.737E+09	3.703E-17	1.566E-12	9.963E-01
42	1.068E-05	5.270E+07	2.789E+09	3.387E-17	1.566E-12	9.963E-01
43	5.043E-06	6.412E+07	2.853E+09	6.412E-17	1.566E-12	9.963E-01
44	1.855E-06	4.158E+07	2.895E+09	6.391E-17	1.566E-12	9.964E-01
45	8.764E-07	3.558E+07	2.931E+09	7.984E-17	1.566E-12	9.964E-01
46	4.140E-07	6.985E+07	3.000E+09	2.866E-16	1.566E-12	9.966E-01
47	1.000E-07	5.249E+08	3.525E+09	5.338E-15	1.572E-12	1.000E+00

Table A.1.b. Absolute calculated neutron flux spectra
and dpa rate at the center of 3° surveillance capsule
and core axial midplane of Grand Gulf Cycle 2

G	Energy (MeV)	Group flux	Cumulative flux	Group dpa rate	Cumulative dpa rate	dpa fraction
1	1.733E+01	8.768E+05	8.768E+05	2.562E-15	2.562E-15	1.568E-03
2	1.419E+01	3.640E+06	4.517E+06	9.632E-15	1.219E-14	7.462E-03
3	1.221E+01	1.163E+07	1.615E+07	2.802E-14	4.022E-14	2.461E-02
4	1.000E+01	2.120E+07	3.735E+07	4.704E-14	8.726E-14	5.339E-02
5	8.607E+00	3.277E+07	7.012E+07	6.839E-14	1.556E-13	9.524E-02
6	7.408E+00	7.342E+07	1.435E+08	1.427E-13	2.983E-13	1.825E-01
7	6.065E+00	8.945E+07	2.330E+08	1.596E-13	4.579E-13	2.802E-01
8	4.966E+00	1.258E+06	3.588E+08	1.976E-13	6.555E-13	4.011E-01
9	3.679E+00	7.769E+07	4.364E+08	1.064E-13	7.619E-13	4.662E-01
10	3.012E+00	5.137E+07	4.878E+08	6.529E-14	8.272E-13	5.062E-01
11	2.725E+00	5.609E+07	5.439E+08	7.152E-14	8.987E-13	5.499E-01
12	2.466E+00	2.703E+07	5.709E+08	3.168E-14	9.304E-13	5.693E-01
13	2.365E+00	6.625E+06	5.776E+08	7.261E-15	9.376E-13	5.738E-01
14	2.346E+00	3.294E+07	6.105E+08	3.429E-14	9.719E-13	5.947E-01
15	2.231E+00	8.532E+07	6.958E+08	8.822E-14	1.060E-12	6.487E-01
16	1.920E+00	8.820E+07	7.840E+08	7.173E-14	1.132E-12	6.926E-01
17	1.653E+00	1.176E+08	9.016E+08	9.530E-14	1.227E-12	7.509E-01
18	1.353E+00	1.814E+08	1.083E+09	1.016E-13	1.329E-12	8.131E-01
19	1.003E+00	1.124E+08	1.195E+09	4.120E-14	1.370E-12	8.383E-01
20	8.208E-01	5.468E+07	1.250E+09	3.067E-14	1.401E-12	8.571E-01
21	7.427E-01	1.495E+08	1.400E+09	5.402E-14	1.455E-12	8.902E-01
22	6.081E-01	1.114E+08	1.511E+09	3.277E-14	1.487E-12	9.102E-01
23	4.979E-01	1.269E+08	1.638E+09	5.030E-14	1.538E-12	9.410E-01
24	3.688E-01	1.176E+08	1.755E+09	2.430E-14	1.562E-12	9.559E-01
25	2.972E-01	1.382E+08	1.894E+09	2.770E-14	1.590E-12	9.728E-01
26	1.832E-01	1.220E+08	2.016E+09	1.720E-14	1.607E-12	9.834E-01
27	1.111E-01	7.816E+07	2.094E+09	1.011E-14	1.617E-12	9.895E-01
28	6.738E-02	6.393E+07	2.158E+09	4.141E-15	1.621E-12	9.921E-01
29	4.087E-02	2.005E+07	2.178E+09	1.623E-15	1.623E-12	9.931E-01
30	3.183E-02	7.204E+06	2.185E+09	2.048E-15	1.625E-12	9.943E-01
31	2.606E-02	3.248E+07	2.217E+09	6.547E-16	1.626E-12	9.947E-01
32	2.418E-02	1.647E+07	2.234E+09	7.214E-17	1.626E-12	9.948E-01
33	2.188E-02	3.534E+07	2.269E+09	2.895E-16	1.626E-12	9.949E-01
34	1.503E-02	5.841E+07	2.328E+09	1.096E-15	1.627E-12	9.956E-01
35	7.102E-03	6.957E+07	2.397E+09	6.189E-16	1.628E-12	9.960E-01
36	3.355E-03	5.902E+07	2.456E+09	2.077E-16	1.628E-12	9.961E-01
37	1.585E-03	1.020E+08	2.558E+09	1.716E-16	1.628E-12	9.962E-01
38	4.540E-04	5.108E+07	2.609E+09	5.036E-18	1.628E-12	9.962E-01
39	2.144E-04	6.040E+07	2.670E+09	8.662E-18	1.628E-12	9.962E-01
40	1.013E-04	8.085E+07	2.751E+09	1.804E-17	1.628E-12	9.962E-01
41	3.727E-05	9.794E+07	2.849E+09	3.858E-17	1.628E-12	9.963E-01
42	1.068E-05	5.491E+07	2.903E+09	3.529E-17	1.628E-12	9.963E-01
43	5.043E-06	6.680E+07	2.970E+09	6.680E-17	1.628E-12	9.963E-01
44	1.855E-06	4.332E+07	3.014E+09	6.659E-17	1.628E-12	9.964E-01
45	8.764E-07	3.707E+07	3.051E+09	8.319E-07	1.628E-12	9.964E-01
46	4.140E-07	7.278E+07	3.123E+09	2.986E-06	1.629E-02	9.966E-01
47	1.000E-07	5.476E+08	3.671E+09	5.569E-05	1.634E-02	1.000E+00

Table A.2.a. Absolute calculated neutron flux spectra and dpa rate at the axial midplane, azimuthal peak and RPV-wetted surface wall of Grand Gulf Cycle 2

G	Energy (MeV)	Group flux	Cumulative flux	Group dpa rate	Cumulative dpa rate	dpa fraction
1	1.733E+01	1.310E+06	1.310E+06	3.827E-15	3.827E-15	1.428E-03
2	1.419E+01	5.449E+06	6.758E+06	1.442E-14	1.824E-14	6.807E-03
3	1.221E+01	1.855E+07	2.531E+07	4.469E-14	6.293E-14	2.348E-02
4	1.000E+01	3.450E+07	5.980E+07	7.655E-14	1.395E-13	5.204E-02
5	8.607E+00	5.475E+07	1.146E+08	1.143E-13	2.538E-13	9.468E-02
6	7.408E+00	1.245E+08	2.390E+08	2.419E-13	4.956E-13	1.849E-01
7	6.065E+00	1.543E+08	3.933E+08	2.753E-13	7.709E-13	2.876E-01
8	4.966E+00	2.214E+08	6.148E+08	3.479E-13	1.119E-12	4.174E-01
9	3.679E+00	1.351E+08	7.499E+08	1.851E-13	1.304E-12	4.865E-01
10	3.012E+00	8.815E+07	8.380E+08	1.120E-13	1.416E-12	5.283E-01
11	2.725E+00	9.464E+07	9.327E+08	1.207E-13	1.537E-12	5.733E-01
12	2.466E+00	4.552E+07	9.782E+08	5.334E-14	1.590E-12	5.932E-01
13	2.365E+00	1.114E+07	9.893E+08	1.221E-14	1.602E-12	5.978E-01
14	2.346E+00	5.399E+07	1.043E+09	5.621E-14	1.658E-12	6.187E-01
15	2.231E+00	1.338E+08	1.177E+09	1.383E-13	1.797E-12	6.703E-01
16	1.920E+00	1.344E+08	1.312E+09	1.093E-13	1.906E-12	7.111E-01
17	1.653E+00	1.761E+08	1.488E+09	1.427E-13	2.049E-12	7.644E-01
18	1.353E+00	2.614E+08	1.749E+09	1.464E-13	2.195E-12	8.190E-01
19	1.003E+00	1.640E+08	1.913E+09	6.011E-14	2.255E-12	8.414E-01
20	8.208E-01	8.400E+07	1.997E+09	4.712E-14	2.302E-12	8.590E-01
21	7.427E-01	2.096E+08	2.207E+09	7.576E-14	2.378E-12	8.873E-01
22	6.081E-01	1.641E+08	2.371E+09	4.829E-14	2.426E-12	9.053E-01
23	4.979E-01	1.861E+08	2.557E+09	7.376E-14	2.500E-12	9.328E-01
24	3.688E-01	1.691E+08	2.726E+09	3.494E-14	2.535E-12	9.459E-01
25	2.972E-01	2.216E+08	2.948E+09	4.444E-14	2.580E-12	9.624E-01
26	1.832E-01	1.880E+08	3.136E+09	2.650E-14	2.606E-12	9.723E-01
27	1.111E-01	1.356E+08	3.271E+09	1.753E-14	2.624E-12	9.789E-01
28	6.738E-02	1.148E+08	3.386E+09	7.436E-15	2.631E-12	9.816E-01
29	4.087E-02	4.666E+07	3.433E+09	3.776E-15	2.635E-12	9.831E-01
30	3.183E-02	3.210E+07	3.465E+09	9.127E-15	2.644E-12	9.865E-01
31	2.606E-02	3.725E+07	3.502E+09	7.510E-16	2.645E-12	9.867E-01
32	2.418E-02	2.292E+07	3.525E+09	1.004E-16	2.645E-12	9.868E-01
33	2.188E-02	6.198E+07	3.587E+09	5.076E-16	2.645E-12	9.870E-01
34	1.503E-02	1.218E+08	3.709E+09	2.284E-15	2.648E-12	9.878E-01
35	7.102E-03	1.270E+08	3.836E+09	1.130E-15	2.649E-12	9.882E-01
36	3.355E-03	1.206E+08	3.956E+09	4.246E-16	2.649E-12	9.884E-01
37	1.585E-03	1.997E+08	4.156E+09	3.359E-16	2.649E-12	9.885E-01
38	4.540E-04	1.153E+08	4.271E+09	1.137E-17	2.649E-12	9.885E-01
39	2.144E-04	1.194E+08	4.391E+09	1.713E-17	2.649E-12	9.885E-01
40	1.013E-04	1.587E+08	4.549E+09	3.542E-17	2.650E-12	9.885E-01
41	3.727E-05	1.961E+08	4.746E+09	7.723E-17	2.650E-12	9.886E-01
42	1.068E-05	1.151E+08	4.861E+09	7.396E-17	2.650E-12	9.886E-01
43	5.043E-06	1.486E+08	5.009E+09	1.486E-16	2.650E-12	9.887E-01
44	1.855E-06	1.064E+08	5.116E+09	1.635E-16	2.650E-12	9.887E-01
45	8.764E-07	1.013E+08	5.217E+09	2.273E-16	2.650E-12	9.888E-01
46	4.140E-07	3.027E+08	5.520E+09	1.242E-15	2.651E-12	9.893E-01
47	1.000E-07	2.828E+09	8.347E+09	2.876E-14	2.680E-12	1.000E+00

Table A.2.b. Absolute calculated neutron flux spectra
and dpa rate at the axial midplane, azimuthal peak, and
R = 0-T RPV wall of Grand Gulf Cycle 2

G	Energy (MeV)	Group flux	Cumulative flux	Group dpa rate	Cumulative dpa rate	dpa fraction
1	1.733E+01	1.240E+06	1.240E+06	3.624E-15	3.624E-15	1.386E-03
2	1.419E+01	5.164E+06	6.404E+06	1.366E-14	1.729E-14	6.611E-03
3	1.221E+01	1.750E+07	2.390E+07	4.215E-14	5.944E-14	2.273E-02
4	1.000E+01	3.255E+07	5.646E+07	7.223E-14	1.317E-13	5.036E-02
5	8.607E+00	5.164E+07	1.081E+08	1.078E-13	2.394E-13	9.157E-02
6	7.408E+00	1.173E+08	2.254E+08	2.280E-13	4.674E-13	1.788E-01
7	6.065E+00	1.455E+08	3.710E+08	2.596E-13	7.271E-13	2.780E-01
8	4.966E+00	2.095E+08	5.805E+08	3.291E-13	1.056E-12	4.039E-01
9	3.679E+00	1.286E+08	7.091E+08	1.762E-13	1.232E-12	4.713E-01
10	3.012E+00	8.473E+07	7.938E+08	1.077E-13	1.340E-12	5.125E-01
11	2.725E+00	9.157E+07	8.854E+08	1.168E-13	1.457E-12	5.571E-01
12	2.466E+00	4.422E+07	9.296E+08	5.182E-14	1.509E-12	5.770E-01
13	2.365E+00	1.085E+07	9.405E+08	1.189E-14	1.521E-12	5.815E-01
14	2.346E+00	5.294E+07	9.934E+08	5.511E-14	1.576E-12	6.026E-01
15	2.231E+00	1.330E+08	1.126E+09	1.375E-13	1.713E-12	6.552E-01
16	1.920E+00	1.351E+08	1.262E+09	1.099E-13	1.823E-12	6.972E-01
17	1.653E+00	1.789E+08	1.440E+09	1.449E-13	1.968E-12	7.526E-01
18	1.353E+00	2.719E+08	1.712E+09	1.523E-13	2.120E-12	8.109E-01
19	1.003E+00	1.710E+08	1.883E+09	6.266E-14	2.183E-12	8.348E-01
20	8.208E-01	8.601E+07	1.969E+09	4.824E-14	2.231E-12	8.533E-01
21	7.427E-01	2.259E+08	2.195E+09	8.165E-14	2.313E-12	8.845E-01
22	6.081E-01	1.736E+08	2.369E+09	5.108E-14	2.364E-12	9.040E-01
23	4.979E-01	1.981E+08	2.567E+09	7.853E-14	2.443E-12	9.341E-01
24	3.688E-01	1.828E+08	2.750E+09	3.779E-14	2.480E-12	9.485E-01
25	2.972E-01	2.255E+08	2.975E+09	4.522E-14	2.526E-12	9.658E-01
26	1.832E-01	1.928E+08	3.168E+09	2.719E-14	2.553E-12	9.762E-01
27	1.111E-01	1.330E+08	3.301E+09	1.720E-14	2.570E-12	9.828E-01
28	6.738E-02	1.117E+08	3.413E+09	7.234E-15	2.577E-12	9.856E-01
29	4.087E-02	4.265E+07	3.455E+09	3.452E-15	2.581E-12	9.869E-01
30	3.183E-02	2.665E+07	3.482E+09	7.578E-15	2.588E-12	9.898E-01
31	2.606E-02	4.367E+07	3.526E+09	8.804E-16	2.589E-12	9.901E-01
32	2.418E-02	2.356E+07	3.549E+09	1.032E-16	2.589E-12	9.902E-01
33	2.188E-02	5.710E+07	3.606E+09	4.677E-16	2.590E-12	9.903E-01
34	1.503E-02	1.119E+08	3.718E+09	2.100E-15	2.592E-12	9.911E-01
35	7.102E-03	1.219E+08	3.840E+09	1.084E-15	2.593E-12	9.916E-01
36	3.355E-03	1.133E+08	3.954E+09	3.990E-16	2.593E-12	9.917E-01
37	1.585E-03	1.899E+08	4.143E+09	3.193E-16	2.594E-12	9.918E-01
38	4.540E-04	1.067E+08	4.250E+09	1.052E-17	2.594E-12	9.918E-01
39	2.144E-04	1.136E+08	4.364E+09	1.629E-17	2.594E-12	9.918E-01
40	1.013E-04	1.512E+08	4.515E+09	3.374E-17	2.594E-12	9.918E-01
41	3.727E-05	1.859E+08	4.701E+09	7.322E-17	2.594E-12	9.919E-01
42	1.068E-05	1.079E+08	4.809E+09	6.933E-17	2.594E-12	9.919E-01
43	5.043E-06	1.373E+08	4.946E+09	1.373E-16	2.594E-12	9.920E-01
44	1.855E-06	9.620E+07	5.042E+09	1.479E-16	2.594E-12	9.920E-01
45	8.764E-07	8.963E+07	5.132E+09	2.011E-16	2.594E-12	9.921E-01
46	4.140E-07	2.435E+08	5.375E+09	9.989E-16	2.595E-12	9.925E-01
47	1.000E-07	1.936E+09	7.311E+09	1.969E-14	2.615E-12	1.000E+00

Table A.2.c. Absolute calculated neutron flux spectra
and dpa rate at the axial midplane, azimuthal peak, and
R = 1/4-T RPV wall of Grand Gulf Cycle 2

G	Energy (MeV)	Group flux	Cumulative flux	Group dpa rate	Cumulative dpa rate	dpa fraction
1	1.733E+01	6.868E+05	6.868E+05	2.007E-15	2.007E-15	1.092E-03
2	1.419E+01	2.865E+06	3.551E+06	7.580E-15	9.587E-15	5.214E-03
3	1.221E+01	9.423E+06	1.297E+07	2.270E-14	3.229E-14	1.756E-02
4	1.000E+01	1.773E+07	3.071E+07	3.935E-14	7.164E-14	3.897E-02
5	8.607E+00	2.787E+07	5.858E+07	5.817E-14	1.298E-13	7.061E-02
6	7.408E+00	6.187E+07	1.205E+08	1.202E-13	2.500E-13	1.360E-01
7	6.065E+00	7.555E+07	1.960E+08	1.348E-13	3.848E-13	2.093E-01
8	4.966E+00	1.081E+08	3.041E+08	1.699E-13	5.547E-13	3.017E-01
9	3.679E+00	6.924E+07	3.734E+08	9.487E-14	6.496E-13	3.533E-01
10	3.012E+00	4.836E+07	4.217E+08	5.147E-14	7.110E-13	3.868E-01
11	2.725E+00	5.502E+07	4.768E+08	7.015E-14	7.812E-13	4.249E-01
12	2.466E+00	2.733E+07	5.041E+08	3.203E-14	8.132E-13	4.423E-01
13	2.365E+00	7.102E+06	5.112E+08	7.783E-15	8.210E-13	4.466E-01
14	2.346E+00	3.532E+07	5.465E+08	3.677E-14	8.578E-13	4.666E-01
15	2.231E+00	9.446E+07	6.410E+08	9.767E-14	9.554E-13	5.197E-01
16	1.920E+00	1.049E+08	7.459E+08	8.534E-14	1.041E-12	5.661E-01
17	1.653E+00	1.475E+08	8.934E+08	1.195E-13	1.160E-12	6.311E-01
18	1.353E+00	2.595E+08	1.153E+09	1.454E-13	1.306E-12	7.102E-01
19	1.003E+00	1.727E+08	1.326E+09	6.330E-14	1.369E-12	7.446E-01
20	8.208E-01	8.155E+07	1.407E+09	4.574E-14	1.415E-12	7.695E-01
21	7.427E-01	2.727E+08	1.680E+09	9.857E-14	1.513E-12	8.231E-01
22	6.081E-01	2.040E+08	1.884E+09	6.004E-14	1.573E-12	8.558E-01
23	4.979E-01	2.431E+08	2.127E+09	9.635E-14	1.670E-12	9.082E-01
24	3.688E-01	2.453E+08	2.372E+09	5.071E-14	1.720E-12	9.358E-01
25	2.972E-01	2.533E+08	2.626E+09	5.078E-14	1.771E-12	9.634E-01
26	1.832E-01	2.318E+08	2.857E+09	3.269E-14	1.804E-12	9.812E-01
27	1.111E-01	1.335E+08	2.991E+09	1.726E-14	1.821E-12	9.906E-01
28	6.738E-02	1.033E+08	3.094E+09	6.691E-15	1.828E-12	9.942E-01
29	4.087E-02	2.766E+07	3.122E+09	2.238E-15	1.830E-12	9.954E-01
30	3.183E-02	9.654E+06	3.132E+09	2.745E-15	1.833E-12	9.969E-01
31	2.606E-02	5.720E+07	3.189E+09	1.153E-15	1.834E-12	9.976E-01
32	2.418E-02	2.941E+07	3.218E+09	1.288E-16	1.834E-12	9.976E-01
33	2.188E-02	5.062E+07	3.269E+09	4.146E-16	1.835E-12	9.979E-01
34	1.503E-02	6.866E+07	3.337E+09	1.288E-15	1.836E-12	9.986E-01
35	7.102E-03	8.967E+07	3.427E+09	7.976E-16	1.837E-12	9.990E-01
36	3.355E-03	6.809E+07	3.495E+09	2.397E-16	1.837E-12	9.991E-01
37	1.585E-03	1.181E+08	3.613E+09	1.986E-16	1.837E-12	9.992E-01
38	4.540E-04	5.241E+07	3.666E+09	5.166E-18	1.837E-12	9.992E-01
39	2.144E-04	6.468E+07	3.730E+09	9.275E-18	1.837E-12	9.992E-01
40	1.013E-04	8.915E+07	3.820E+09	1.989E-17	1.837E-12	9.992E-01
41	3.727E-05	1.067E+08	3.926E+09	4.204E-17	1.837E-12	9.993E-01
42	1.068E-05	5.698E+07	3.983E+09	3.662E-17	1.837E-12	9.993E-01
43	5.043E-06	6.319E+07	4.046E+09	6.319E-17	1.837E-12	9.993E-01
44	1.855E-06	3.596E+07	4.082E+09	5.527E-17	1.837E-12	9.993E-01
45	8.764E-07	2.608E+07	4.108E+09	5.853E-17	1.837E-12	9.994E-01
46	4.140E-07	2.771E+07	4.136E+09	1.137E-16	1.837E-12	9.994E-01
47	1.000E-07	1.012E+08	4.237E+09	1.030E-15	1.838E-12	1.000E+00

Table A.2.d. Absolute calculated neutron flux spectra
and dpa rate at the axial midplane, azimuthal peak, and
R = 3/4-T RPV wall of Grand Gulf Cycle 2

G	Energy (MeV)	Group flux	Cumulative flux	Group dpa rate	Cumulative dpa rate	dpa fraction
1	1.733E+01	1.913E+05	1.913E+05	5.591E-16	5.591E-16	7.635E-04
2	1.419E+01	7.851E+05	9.764E+05	2.077E-15	2.636E-15	3.600E-03
3	1.221E+01	2.455E+06	3.431E+06	5.914E-15	9.550E-15	1.168E-02
4	1.000E+01	4.593E+06	8.024E+06	1.019E-14	1.874E-14	2.560E-02
5	8.607E+00	6.952E+06	1.498E+07	1.451E-14	3.325E-14	4.541E-02
6	7.408E+00	1.438E+07	2.936E+07	2.795E-14	6.120E-14	8.358E-02
7	6.065E+00	1.710E+07	4.646E+07	3.050E-14	9.170E-14	1.252E-01
8	4.966E+00	2.455E+07	7.101E+07	3.857E-14	1.303E-13	1.779E-01
9	3.679E+00	1.697E+07	8.798E+07	2.325E-14	1.535E-13	2.097E-01
10	3.012E+00	1.236E+07	1.003E+08	1.571E-14	1.692E-13	2.311E-01
11	2.725E+00	1.479E+07	1.151E+08	1.886E-14	1.881E-13	2.569E-01
12	2.466E+00	7.570E+06	1.227E+08	8.873E-15	1.970E-13	2.690E-01
13	2.365E+00	2.125E+06	1.248E+08	2.329E-15	1.993E-13	2.722E-01
14	2.346E+00	1.075E+07	1.356E+08	1.119E-14	2.105E-13	2.875E-01
15	2.231E+00	3.016E+07	1.657E+08	3.118E-14	2.417E-13	3.300E-01
16	1.920E+00	3.775E+07	2.035E+08	3.070E-14	2.724E-13	3.720E-01
17	1.653E+00	5.700E+07	2.605E+08	4.619E-14	3.185E-13	4.350E-01
18	1.353E+00	1.215E+08	3.820E+08	6.810E-14	3.866E-13	5.281E-01
19	1.003E+00	9.228E+07	4.743E+08	3.382E-14	4.205E-13	5.742E-01
20	8.208E-01	4.193E+07	5.162E+08	2.352E-14	4.440E-13	6.064E-01
21	7.427E-01	1.727E+08	6.890E+08	6.243E-14	5.064E-13	6.916E-01
22	6.081E-01	1.346E+08	8.236E+08	3.963E-14	5.460E-13	7.457E-01
23	4.979E-01	1.635E+08	9.871E+08	6.481E-14	6.109E-13	8.343E-01
24	3.688E-01	1.851E+08	1.172E+09	3.826E-14	6.491E-13	8.865E-01
25	2.972E-01	1.810E+08	1.353E+09	3.630E-14	6.854E-13	9.361E-01
26	1.832E-01	1.755E+08	1.529E+09	2.475E-14	7.102E-13	9.699E-01
27	1.111E-01	9.426E+07	1.623E+09	1.219E-14	7.223E-13	9.865E-01
28	6.738E-02	6.657E+07	1.690E+09	4.312E-15	7.267E-13	9.924E-01
29	4.087E-02	1.634E+07	1.706E+09	1.323E-15	7.280E-13	9.942E-01
30	3.183E-02	5.653E+06	1.712E+09	1.607E-15	7.296E-13	9.964E-01
31	2.606E-02	4.174E+07	1.753E+09	8.415E-16	7.304E-13	9.976E-01
32	2.418E-02	2.248E+07	1.776E+09	9.843E-17	7.305E-13	9.977E-01
33	2.188E-02	3.434E+07	1.810E+09	2.812E-16	7.308E-13	9.981E-01
34	1.503E-02	3.558E+07	1.846E+09	6.674E-16	7.315E-13	9.990E-01
35	7.102E-03	4.552E+07	1.891E+09	4.049E-16	7.319E-13	9.995E-01
36	3.355E-03	3.161E+07	1.923E+09	1.113E-16	7.320E-13	9.997E-01
37	1.585E-03	5.132E+07	1.974E+09	8.632E-17	7.321E-13	9.998E-01
38	4.540E-04	2.134E+07	1.996E+09	2.104E-18	7.321E-13	9.998E-01
39	2.144E-04	2.491E+07	2.020E+09	3.573E-18	7.321E-13	9.998E-01
40	1.013E-04	3.357E+07	2.054E+09	7.489E-18	7.321E-13	9.998E-01
41	3.727E-05	3.887E+07	2.093E+09	1.531E-17	7.321E-13	9.998E-01
42	1.068E-05	1.977E+07	2.113E+09	1.271E-17	7.321E-13	9.999E-01
43	5.043E-06	1.977E+07	2.132E+09	1.977E-17	7.321E-13	9.999E-01
44	1.855E-06	9.857E+06	2.142E+09	1.515E-17	7.322E-13	9.999E-01
45	8.764E-07	5.950E+06	2.148E+09	1.335E-17	7.322E-13	9.999E-01
46	4.140E-07	3.437E+06	2.152E+09	1.410E-17	7.322E-13	1.000E+00
47	1.000E-07	3.587E+06	2.155E+09	3.648E-17	7.322E-13	1.000E+00

Table A.2.e. Absolute calculated neutron flux spectra
and dpa rate at the axial midplane, azimuthal peak, and
R = midcavity of Grand Gulf Cycle 2

G	Energy (MeV)	Group flux	Cumulative flux	Group dpa rate	Cumulative dpa rate	dpa fraction
1	1.733E+01	6.942E+04	6.942E+04	2.028E-16	2.028E-16	9.108E-04
2	1.419E+01	2.720E+05	3.414E+05	7.197E-16	9.226E-16	4.143E-03
3	1.221E+01	8.229E+05	1.164E+06	1.982E-15	2.905E-15	1.304E-02
4	1.000E+01	1.499E+06	2.664E+06	3.327E-15	6.232E-15	2.798E-02
5	8.607E+00	2.180E+06	4.844E+06	4.550E-15	1.078E-14	4.842E-02
6	7.408E+00	4.312E+06	9.156E+06	8.378E-15	1.916E-14	8.603E-02
7	6.065E+00	4.982E+06	1.414E+07	8.889E-15	2.805E-14	1.259E-01
8	4.966E+00	6.965E+06	2.110E+07	1.094E-14	3.899E-14	1.751E-01
9	3.679E+00	4.691E+06	2.579E+07	6.426E-15	4.542E-14	2.039E-01
10	3.012E+00	3.383E+06	2.918E+07	4.299E-15	4.972E-14	2.232E-01
11	2.725E+00	4.008E+06	3.318E+07	5.110E-15	5.483E-14	2.462E-01
12	2.466E+00	2.097E+06	3.528E+07	2.458E-15	5.729E-14	2.572E-01
13	2.365E+00	5.927E+05	3.587E+07	6.496E-16	5.794E-14	2.601E-01
14	2.346E+00	2.930E+06	3.881E+07	3.050E-15	6.099E-14	2.738E-01
15	2.231E+00	7.717E+06	4.652E+07	7.979E-15	6.896E-14	3.097E-01
16	1.920E+00	9.972E+06	5.649E+07	8.110E-15	7.707E-14	3.461E-01
17	1.653E+00	1.553E+07	7.202E+07	1.258E-14	8.966E-14	4.026E-01
18	1.353E+00	3.359E+07	1.056E+08	1.882E-14	1.085E-13	4.871E-01
19	1.003E+00	2.725E+07	1.329E+08	9.987E-15	1.185E-13	5.319E-01
20	8.208E-01	1.393E+07	1.468E+08	7.812E-15	1.263E-13	5.670E-01
21	7.427E-01	4.885E+07	1.956E+08	1.765E-14	1.439E-13	6.463E-01
22	6.081E-01	4.272E+07	2.384E+08	1.257E-14	1.565E-13	7.027E-01
23	4.979E-01	4.611E+07	2.845E+08	1.828E-14	1.748E-13	7.848E-01
24	3.688E-01	5.622E+07	3.407E+08	1.162E-14	1.864E-13	8.370E-01
25	2.972E-01	7.346E+07	4.141E+08	1.473E-14	2.011E-13	9.031E-01
26	1.832E-01	6.641E+07	4.805E+08	9.364E-15	2.105E-13	9.451E-01
27	1.111E-01	4.041E+07	5.210E+08	5.225E-15	2.157E-13	9.686E-01
28	6.738E-02	2.855E+07	5.495E+08	1.849E-15	2.176E-13	9.769E-01
29	4.087E-02	8.831E+06	5.583E+08	7.147E-16	2.183E-13	9.801E-01
30	3.183E-02	8.130E+06	5.665E+08	2.311E-15	2.206E-13	9.905E-01
31	2.606E-02	1.490E+07	5.814E+08	3.004E-16	2.209E-13	9.918E-01
32	2.418E-02	9.187E+06	5.905E+08	4.023E-17	2.209E-13	9.920E-01
33	2.188E-02	1.915E+07	6.097E+08	1.568E-16	2.211E-13	9.927E-01
34	1.503E-02	2.495E+07	6.346E+08	4.680E-16	2.216E-13	9.948E-01
35	7.102E-03	2.392E+07	6.586E+08	2.128E-16	2.218E-13	9.958E-01
36	3.355E-03	2.036E+07	6.789E+08	7.167E-17	2.218E-13	9.961E-01
37	1.585E-03	3.166E+07	7.106E+08	5.326E-17	2.219E-13	9.963E-01
38	4.540E-04	1.660E+07	7.272E+08	1.637E-18	2.219E-13	9.963E-01
39	2.144E-04	1.615E+07	7.433E+08	2.315E-18	2.219E-13	9.963E-01
40	1.013E-04	2.025E+07	7.636E+08	4.517E-18	2.219E-13	9.964E-01
41	3.727E-05	2.321E+07	7.868E+08	9.143E-18	2.219E-13	9.964E-01
42	1.068E-05	1.276E+07	7.995E+08	8.203E-18	2.219E-13	9.964E-01
43	5.043E-06	1.530E+07	8.148E+08	1.530E-17	2.219E-13	9.965E-01
44	1.855E-06	1.020E+07	8.250E+08	1.568E-17	2.219E-13	9.966E-01
45	8.764E-07	9.079E+06	8.341E+08	2.037E-17	2.220E-13	9.967E-01
46	4.140E-07	1.931E+07	8.534E+08	7.921E-17	2.220E-13	9.970E-01
47	1.000E-07	6.501E+07	9.184E+08	6.612E-16	2.227E-13	1.000E+00

Table A.2.f. Absolute calculated neutron flux spectra
and dpa rate at the axial midplane, azimuthal peak, and
R = front of the concrete shield wall of Grand Gulf Cycle 2

G	Energy (MeV)	Group flux	Cumulative flux	Group dpa rate	Cumulative dpa rate	dpa fraction
1	1.733E+01	4.366E+04	4.366E+04	1.276E-16	1.276E-16	7.413E-04
2	1.419E+01	1.772E+05	2.209E+05	4.689E-16	5.965E-16	3.466E-03
3	1.221E+01	5.485E+05	7.694E+05	1.321E-15	1.918E-15	1.114E-02
4	1.000E+01	1.018E+06	1.787E+06	2.259E-15	4.176E-15	2.427E-02
5	8.607E+00	1.521E+06	3.308E+06	3.174E-15	7.351E-15	4.271E-02
6	7.408E+00	3.111E+06	6.419E+06	6.045E-15	1.340E-14	7.784E-02
7	6.065E+00	3.778E+06	1.020E+07	6.740E-15	2.014E-14	1.170E-01
8	4.966E+00	5.542E+06	1.574E+07	8.707E-15	2.884E-14	1.676E-01
9	3.679E+00	3.801E+06	1.954E+07	5.208E-15	3.405E-14	1.978E-01
10	3.012E+00	2.753E+06	2.229E+07	3.498E-15	3.755E-14	2.182E-01
11	2.725E+00	3.309E+06	2.560E+07	4.220E-15	4.177E-14	2.427E-01
12	2.466E+00	1.781E+06	2.738E+07	2.087E-15	4.386E-14	2.548E-01
13	2.365E+00	4.926E+05	2.788E+07	5.399E-16	4.440E-14	2.580E-01
14	2.346E+00	2.377E+06	3.025E+07	2.474E-15	4.687E-14	2.723E-01
15	2.231E+00	5.784E+06	3.604E+07	5.981E-15	5.285E-14	3.071E-01
16	1.920E+00	7.366E+06	4.340E+07	5.990E-15	5.884E-14	3.419E-01
17	1.653E+00	1.158E+07	5.498E+07	9.379E-15	6.822E-14	3.964E-01
18	1.353E+00	2.346E+07	7.843E+07	1.314E-14	8.136E-14	4.727E-01
19	1.003E+00	1.856E+07	9.699E+07	6.801E-15	8.816E-14	5.123E-01
20	8.208E-01	1.181E+07	1.088E+08	6.627E-15	9.479E-14	5.508E-01
21	7.427E-01	3.399E+07	1.428E+08	1.228E-14	1.071E-13	6.221E-01
22	6.081E-01	3.314E+07	1.759E+08	9.754E-15	1.168E-13	6.788E-01
23	4.979E-01	3.369E+07	2.096E+08	1.335E-14	1.302E-13	7.564E-01
24	3.688E-01	3.827E+07	2.479E+08	7.910E-15	1.381E-13	8.024E-01
25	2.972E-01	6.168E+07	3.096E+08	1.237E-14	1.505E-13	8.742E-01
26	1.832E-01	5.860E+07	3.682E+08	8.263E-15	1.587E-13	9.222E-01
27	1.111E-01	3.955E+07	4.077E+08	5.114E-15	1.638E-13	9.519E-01
28	6.738E-02	3.056E+07	4.383E+08	1.979E-15	1.658E-13	9.634E-01
29	4.087E-02	1.140E+07	4.497E+08	9.226E-16	1.667E-13	9.688E-01
30	3.183E-02	9.432E+06	4.591E+08	2.682E-15	1.694E-13	9.844E-01
31	2.606E-02	8.181E+06	4.673E+08	1.649E-16	1.696E-13	9.853E-01
32	2.418E-02	7.369E+06	4.747E+08	3.227E-17	1.696E-13	9.855E-01
33	2.188E-02	2.023E+07	4.949E+08	1.657E-16	1.698E-13	9.865E-01
34	1.503E-02	3.038E+07	5.253E+08	5.699E-16	1.704E-13	9.898E-01
35	7.102E-03	2.744E+07	5.527E+08	2.441E-16	1.706E-13	9.912E-01
36	3.355E-03	2.449E+07	5.772E+08	8.621E-17	1.707E-13	9.917E-01
37	1.585E-03	3.769E+07	6.149E+08	6.339E-17	1.707E-13	9.921E-01
38	4.540E-04	2.024E+07	6.351E+08	1.995E-18	1.707E-13	9.921E-01
39	2.144E-04	1.922E+07	6.544E+08	2.757E-18	1.708E-13	9.921E-01
40	1.013E-04	2.402E+07	6.784E+08	5.359E-18	1.708E-13	9.922E-01
41	3.727E-05	2.764E+07	7.060E+08	1.089E-17	1.708E-13	9.922E-01
42	1.068E-05	1.541E+07	7.214E+08	9.902E-18	1.708E-13	9.923E-01
43	5.043E-06	1.889E+07	7.403E+08	1.889E-17	1.708E-13	9.924E-01
44	1.855E-06	1.297E+07	7.533E+08	1.994E-17	1.708E-13	9.925E-01
45	8.764E-07	1.189E+07	7.652E+08	2.668E-17	1.708E-13	9.927E-01
46	4.140E-07	2.786E+07	7.930E+08	1.143E-16	1.710E-13	9.933E-01
47	1.000E-07	1.131E+08	9.061E+08	1.150E-15	1.721E-13	1.000E+00

Table A.2.g. Absolute calculated neutron flux spectra
and dpa rate at the axial midplane, azimuthal peak, and
R = six inches in the concrete shield wall of Grand Gulf Cycle 2

G	Energy (MeV)	Group flux	Cumulative flux	Group dpa rate	Cumulative dpa rate	dpa fraction
1	1.733E+01	3.375E+03	3.375E+03	9.863E-18	9.863E-18	7.708E-04
2	1.419E+01	1.531E+04	1.869E+04	4.051E-17	5.038E-17	3.937E-03
3	1.221E+01	4.525E+04	6.394E+04	1.090E-16	1.594E-16	1.246E-02
4	1.000E+01	8.996E+04	1.539E+05	1.996E-16	3.590E-16	2.806E-02
5	8.607E+00	1.373E+05	2.912E+05	2.866E-16	6.456E-16	5.046E-02
6	7.408E+00	3.491E+05	6.403E+05	6.782E-16	1.324E-15	1.035E-01
7	6.065E+00	4.643E+05	1.105E+06	8.283E-16	2.152E-15	1.682E-01
8	4.966E+00	6.929E+05	1.797E+06	1.089E-15	3.241E-15	2.533E-01
9	3.679E+00	4.427E+05	2.240E+06	6.065E-16	3.847E-15	3.007E-01
10	3.012E+00	3.785E+05	2.619E+06	4.811E-16	4.328E-15	3.383E-01
11	2.725E+00	4.662E+05	3.085E+06	5.944E-16	4.923E-15	3.847E-01
12	2.466E+00	3.179E+05	3.403E+06	3.725E-16	5.295E-15	4.139E-01
13	2.365E+00	1.014E+05	3.504E+06	1.111E-16	5.406E-15	4.226E-01
14	2.346E+00	4.127E+05	3.917E+06	4.297E-16	5.836E-15	4.561E-01
15	2.231E+00	6.803E+05	4.597E+06	7.034E-16	6.539E-15	5.111E-01
16	1.920E+00	6.529E+05	5.250E+06	5.310E-16	7.070E-15	5.526E-01
17	1.653E+00	8.438E+05	6.094E+06	6.838E-16	7.754E-15	6.061E-01
18	1.353E+00	1.036E+06	7.130E+06	5.804E-16	8.335E-15	6.514E-01
19	1.003E+00	6.168E+05	7.747E+06	2.261E-16	8.561E-15	6.691E-01
20	8.208E-01	5.043E+05	8.251E+06	2.829E-16	8.844E-15	6.912E-01
21	7.427E-01	1.033E+06	9.284E+06	3.734E-16	9.217E-15	7.204E-01
22	6.081E-01	1.046E+06	1.033E+07	3.078E-16	9.525E-15	7.444E-01
23	4.979E-01	8.786E+05	1.121E+07	3.483E-16	9.873E-15	7.717E-01
24	3.688E-01	7.993E+05	1.201E+07	1.652E-16	1.004E-14	7.846E-01
25	2.972E-01	1.650E+06	1.366E+07	3.308E-16	1.037E-14	8.104E-01
26	1.832E-01	1.971E+06	1.563E+07	2.779E-16	1.065E-14	8.321E-01
27	1.111E-01	1.725E+06	1.735E+07	2.231E-16	1.087E-14	8.496E-01
28	6.738E-02	1.656E+06	1.901E+07	1.072E-16	1.098E-14	8.580E-01
29	4.087E-02	7.480E+05	1.976E+07	6.054E-17	1.104E-14	8.627E-01
30	3.183E-02	6.540E+05	2.041E+07	1.859E-16	1.122E-14	8.772E-01
31	2.606E-02	2.459E+05	2.066E+07	4.957E-18	1.123E-14	8.776E-01
32	2.418E-02	3.215E+05	2.098E+07	1.408E-18	1.123E-14	8.777E-01
33	2.188E-02	1.204E+06	2.218E+07	9.863E-18	1.124E-14	8.785E-01
34	1.503E-02	2.448E+06	2.463E+07	4.592E-17	1.129E-14	8.821E-01
35	7.102E-03	2.491E+06	2.712E+07	2.216E-17	1.131E-14	8.838E-01
36	3.355E-03	2.579E+06	2.970E+07	9.078E-18	1.132E-14	8.845E-01
37	1.585E-03	4.989E+06	3.469E+07	8.391E-18	1.133E-14	8.852E-01
38	4.540E-04	3.213E+06	3.790E+07	3.167E-19	1.133E-14	8.852E-01
39	2.144E-04	3.422E+06	4.132E+07	4.907E-19	1.133E-14	8.852E-01
40	1.013E-04	4.894E+06	4.622E+07	1.092E-18	1.133E-14	8.853E-01
41	3.727E-05	6.605E+06	5.282E+07	2.602E-18	1.133E-14	8.855E-01
42	1.068E-05	4.148E+06	5.697E+07	2.666E-18	1.133E-14	8.857E-01
43	5.043E-06	5.784E+06	6.276E+07	5.784E-18	1.134E-14	8.862E-01
44	1.855E-06	4.462E+06	6.722E+07	6.858E-18	1.135E-14	8.867E-01
45	8.764E-07	4.557E+06	7.177E+07	1.023E-17	1.136E-14	8.875E-01
46	4.140E-07	1.432E+07	8.610E+07	5.877E-17	1.141E-14	8.921E-01
47	1.000E-07	1.357E+08	2.218E+08	1.380E-15	1.279E-14	1.000E+00

Table A.2.h. Absolute calculated neutron flux spectra
and dpa rate at the axial midplane, azimuthal peak, and
R = one foot in the concrete shield wall of Grand Gulf Cycle 2

G	Energy (MeV)	Group flux	Cumulative flux	Group dpa rate	Cumulative dpa rate	dpa fraction
1	1.733E+01	2.206E+02	2.206E+02	6.446E-19	6.446E-19	5.894E-04
2	1.419E+01	1.082E+03	1.303E+03	2.864E-18	3.508E-18	3.208E-03
3	1.221E+01	3.102E+03	4.404E+03	7.472E-18	1.098E-17	1.004E-02
4	1.000E+01	6.540E+03	1.094E+04	1.451E-17	2.549E-17	2.331E-02
5	8.607E+00	9.975E+03	2.092E+04	2.082E-17	4.631E-17	4.234E-02
6	7.408E+00	2.976E+04	5.068E+04	5.783E-17	1.041E-16	9.521E-02
7	5.065E+00	4.030E+04	9.098E+04	7.189E-17	1.760E-16	1.609E-01
8	4.966E+00	5.953E+04	1.505E+05	9.353E-17	2.696E-16	2.465E-01
9	3.679E+00	3.800E+04	1.885E+05	5.206E-17	3.216E-16	2.941E-01
10	3.012E+00	3.356E+04	2.221E+05	4.265E-17	3.643E-16	3.330E-01
11	2.725E+00	4.213E+04	2.642E+05	5.371E-17	4.180E-16	3.822E-01
12	2.466E+00	3.205E+04	2.962E+05	3.756E-17	4.555E-16	4.165E-01
13	2.365E+00	1.170E+04	3.079E+05	1.283E-17	4.684E-16	4.282E-01
14	2.346E+00	4.380E+04	3.518E+05	4.560E-17	5.140E-16	4.699E-01
15	2.231E+00	6.588E+04	4.176E+05	6.812E-17	5.821E-16	5.322E-01
16	1.920E+00	5.992E+04	4.776E+05	4.873E-17	6.308E-16	5.768E-01
17	1.653E+00	7.333E+04	5.509E+05	5.942E-17	6.902E-16	6.311E-01
18	1.353E+00	8.513E+04	6.360E+05	4.770E-17	7.379E-16	6.747E-01
19	1.003E+00	4.988E+04	6.859E+05	1.828E-17	7.562E-16	6.914E-01
20	8.208E-01	3.965E+04	7.255E+05	2.224E-17	7.785E-16	7.118E-01
21	7.427E-01	7.397E+04	7.995E+05	2.673E-17	8.052E-16	7.362E-01
22	6.081E-01	7.156E+04	8.711E+05	2.106E-17	8.263E-16	7.555E-01
23	4.979E-01	5.969E+04	9.308E+05	2.366E-17	8.499E-16	7.771E-01
24	3.688E-01	5.304E+04	9.838E+05	1.096E-17	8.609E-16	7.871E-01
25	2.972E-01	1.075E+05	1.091E+06	2.155E-17	8.824E-16	8.068E-01
26	1.832E-01	1.192E+05	1.210E+06	1.681E-17	8.992E-16	8.222E-01
27	1.111E-01	9.895E+04	1.309E+06	1.279E-17	9.120E-16	8.339E-01
28	6.738E-02	9.121E+04	1.401E+06	5.907E-18	9.179E-16	8.393E-01
29	4.087E-02	4.042E+04	1.441E+06	3.271E-18	9.212E-16	8.423E-01
30	3.183E-02	3.514E+04	1.476E+06	9.991E-18	9.312E-16	8.514E-01
31	2.606E-02	1.281E+04	1.489E+06	2.582E-19	9.314E-16	8.516E-01
32	2.418E-02	1.677E+04	1.506E+06	7.341E-20	9.315E-16	8.517E-01
33	2.188E-02	6.148E+04	1.567E+06	5.035E-19	9.320E-16	8.522E-01
34	1.503E-02	1.218E+05	1.689E+06	2.284E-18	9.343E-16	8.543E-01
35	7.102E-03	1.207E+05	1.810E+06	1.074E-18	9.354E-16	8.552E-01
36	3.355E-03	1.229E+05	1.933E+06	4.327E-19	9.358E-16	8.556E-01
37	1.585E-03	2.287E+05	2.161E+06	3.847E-19	9.362E-16	8.560E-01
38	4.540E-04	1.456E+05	2.307E+06	1.435E-20	9.362E-16	8.560E-01
39	2.144E-04	1.537E+05	2.461E+06	2.204E-20	9.362E-16	8.560E-01
40	1.013E-04	2.206E+05	2.681E+06	4.922E-20	9.363E-16	8.561E-01
41	3.727E-05	3.027E+05	2.984E+06	1.192E-19	9.364E-16	8.562E-01
42	1.068E-05	1.940E+05	3.178E+06	1.247E-19	9.365E-16	8.563E-01
43	5.043E-06	2.782E+05	3.456E+06	2.782E-19	9.368E-16	8.565E-01
44	1.855E-06	2.206E+05	3.677E+06	3.391E-19	9.371E-16	8.568E-01
45	8.764E-07	2.325E+05	3.909E+06	5.217E-19	9.377E-16	8.573E-01
46	4.140E-07	7.995E+05	4.709E+06	3.280E-18	9.409E-16	8.603E-01
47	1.000E-07	1.502E+07	1.973E+07	1.528E-16	1.094E-15	1.000E+00

Table A.3.a. Absolute calculated neutron flux spectra
and dpa rate at the axial peak, azimuthal peak, and
RPV-wetted surface wall of Grand Gulf Cycle 2

G	Energy (MeV)	Group flux	Cumulative flux	Group dpa rate	Cumulative dpa rate	dpa fraction
1	1.733E+01	1.343E+06	1.343E+06	3.924E-15	3.924E-15	1.408E-03
2	1.419E+01	5.595E+06	6.938E+06	1.481E-14	1.873E-14	6.722E-03
3	1.221E+01	1.912E+07	2.606E+07	4.605E-14	6.478E-14	2.325E-02
4	1.000E+01	3.563E+07	6.168E+07	7.906E-14	1.438E-13	5.162E-02
5	8.607E+00	5.667E+07	1.184E+08	1.183E-13	2.621E-13	9.407E-02
6	7.408E+00	1.291E+08	2.475E+08	2.509E-13	5.130E-13	1.841E-01
7	6.065E+00	1.603E+08	4.078E+08	2.860E-13	7.990E-13	2.868E-01
8	4.966E+00	2.303E+08	6.381E+08	3.618E-13	1.161E-12	4.166E-01
9	3.679E+00	1.405E+08	7.786E+08	1.925E-13	1.353E-12	4.857E-01
10	3.012E+00	9.175E+07	8.704E+08	1.166E-13	1.470E-12	5.276E-01
11	2.725E+00	9.854E+07	9.689E+08	1.256E-13	1.596E-12	5.726E-01
12	2.466E+00	4.742E+07	1.016E+09	5.558E-14	1.651E-12	5.926E-01
13	2.365E+00	1.162E+07	1.028E+09	1.273E-14	1.664E-12	5.972E-01
14	2.346E+00	5.626E+07	1.084E+09	5.857E-14	1.722E-12	6.182E-01
15	2.231E+00	1.393E+08	1.224E+09	1.441E-13	1.867E-12	6.699E-01
16	1.920E+00	1.400E+08	1.364E+09	1.138E-13	1.980E-12	7.107E-01
17	1.653E+00	1.834E+08	1.547E+09	1.486E-13	2.129E-12	7.641E-01
18	1.353E+00	2.721E+08	1.819E+09	1.524E-13	2.281E-12	8.188E-01
19	1.003E+00	1.707E+08	1.990E+09	6.256E-14	2.344E-12	8.412E-01
20	8.208E-01	8.744E+07	2.077E+09	4.904E-14	2.393E-12	8.588E-01
21	7.427E-01	2.181E+08	2.295E+09	7.883E-14	2.472E-12	8.871E-01
22	6.081E-01	1.708E+08	2.466E+09	5.026E-14	2.522E-12	9.052E-01
23	4.979E-01	1.937E+08	2.660E+09	7.677E-14	2.599E-12	9.327E-01
24	3.688E-01	1.759E+08	2.836E+09	3.635E-14	2.635E-12	9.458E-01
25	2.972E-01	2.307E+08	3.066E+09	4.625E-14	2.681E-12	9.624E-01
26	1.832E-01	1.956E+08	3.262E+09	2.758E-14	2.709E-12	9.723E-01
27	1.111E-01	1.411E+08	3.403E+09	1.825E-14	2.727E-12	9.788E-01
28	6.738E-02	1.195E+08	3.523E+09	7.741E-15	2.735E-12	9.816E-01
29	4.087E-02	4.858E+07	3.571E+09	3.931E-15	2.739E-12	9.830E-01
30	3.183E-02	3.343E+07	3.605E+09	9.504E-15	2.748E-12	9.864E-01
31	2.606E-02	3.877E+07	3.643E+09	7.816E-16	2.749E-12	9.867E-01
32	2.418E-02	2.385E+07	3.667E+09	1.045E-16	2.749E-12	9.867E-01
33	2.188E-02	6.452E+07	3.732E+09	5.284E-16	2.750E-12	9.869E-01
34	1.503E-02	1.268E+08	3.858E+09	2.378E-15	2.752E-12	9.878E-01
35	7.102E-03	1.323E+08	3.991E+09	1.177E-15	2.753E-12	9.882E-01
36	3.355E-03	1.256E+08	4.116E+09	4.422E-16	2.754E-12	9.884E-01
37	1.585E-03	2.080E+08	4.324E+09	3.498E-16	2.754E-12	9.885E-01
38	4.540E-04	1.201E+08	4.444E+09	1.184E-17	2.754E-12	9.885E-01
39	2.144E-04	1.244E+08	4.569E+09	1.784E-17	2.754E-12	9.885E-01
40	1.013E-04	1.653E+08	4.734E+09	3.689E-17	2.754E-12	9.885E-01
41	3.727E-05	2.042E+08	4.938E+09	8.045E-17	2.754E-12	9.885E-01
42	1.068E-05	1.199E+08	5.058E+09	7.704E-17	2.754E-12	9.886E-01
43	5.043E-06	1.548E+08	5.213E+09	1.548E-16	2.755E-12	9.886E-01
44	1.855E-06	1.108E+08	5.324E+09	1.703E-16	2.755E-12	9.887E-01
45	8.764E-07	1.055E+08	5.429E+09	2.368E-16	2.755E-12	9.888E-01
46	4.140E-07	3.154E+08	5.745E+09	1.294E-15	2.756E-12	9.892E-01
47	1.000E-07	2.950E+09	8.695E+09	3.000E-14	2.786E-12	1.000E+00

Table A.3.b. Absolute calculated neutron flux spectra
and dpa rate at the axial peak, azimuthal peak, and
R = 0-T RPV wall of Grand Gulf Cycle 2

G	Energy (MeV)	Group flux	Cumulative flux	Group dpa rate	Cumulative dpa rate	dpa fraction
1	1.733E+01	1.272E+06	1.272E+06	3.716E-15	3.716E-15	1.367E-03
2	1.419E+01	5.303E+06	6.575E+06	1.403E-14	1.775E-14	6.529E-03
3	1.221E+01	1.803E+07	2.461E+07	4.344E-14	6.119E-14	2.251E-02
4	1.000E+01	3.362E+07	5.823E+07	7.461E-14	1.358E-13	4.995E-02
5	8.607E+00	5.344E+07	1.117E+08	1.115E-13	2.473E-13	9.099E-02
6	7.408E+00	1.217E+08	2.334E+08	2.365E-13	4.838E-13	1.780E-01
7	6.065E+00	1.512E+08	3.846E+08	2.698E-13	7.536E-13	2.772E-01
8	4.966E+00	2.179E+08	6.025E+08	3.423E-13	1.096E-12	4.032E-01
9	3.679E+00	1.338E+08	7.363E+08	1.833E-13	1.279E-12	4.706E-01
10	3.012E+00	8.819E+07	8.245E+08	1.121E-13	1.391E-12	5.118E-01
11	2.725E+00	9.534E+07	9.198E+08	1.216E-13	1.513E-12	5.565E-01
12	2.466E+00	4.606E+07	9.659E+08	5.399E-14	1.567E-12	5.764E-01
13	2.365E+00	1.131E+07	9.772E+08	1.240E-14	1.579E-12	5.809E-01
14	2.346E+00	5.516E+07	1.032E+09	5.742E-14	1.637E-12	6.021E-01
15	2.231E+00	1.385E+08	1.171E+09	1.432E-13	1.780E-12	6.547E-01
16	1.920E+00	1.407E+08	1.312E+09	1.144E-13	1.894E-12	6.968E-01
17	1.653E+00	1.862E+08	1.498E+09	1.509E-13	2.045E-12	7.523E-01
18	1.353E+00	2.830E+08	1.781E+09	1.586E-13	2.204E-12	8.107E-01
19	1.003E+00	1.779E+08	1.959E+09	6.521E-14	2.269E-12	8.347E-01
20	8.208E-01	8.952E+07	2.048E+09	5.021E-14	2.319E-12	8.531E-01
21	7.427E-01	2.351E+08	2.283E+09	8.496E-14	2.404E-12	8.844E-01
22	6.081E-01	1.806E+08	2.464E+09	5.315E-14	2.457E-12	9.039E-01
23	4.979E-01	2.061E+08	2.670E+09	8.171E-14	2.539E-12	9.340E-01
24	3.688E-01	1.902E+08	2.860E+09	3.930E-14	2.578E-12	9.485E-01
25	2.972E-01	2.347E+08	3.095E+09	4.706E-14	2.625E-12	9.658E-01
26	1.832E-01	2.007E+08	3.296E+09	2.829E-14	2.654E-12	9.762E-01
27	1.111E-01	1.384E+08	3.434E+09	1.790E-14	2.672E-12	9.828E-01
28	6.738E-02	1.163E+08	3.550E+09	7.530E-15	2.679E-12	9.855E-01
29	4.087E-02	4.441E+07	3.595E+09	3.594E-15	2.683E-12	9.868E-01
30	3.183E-02	2.775E+07	3.622E+09	7.890E-15	2.691E-12	9.898E-01
31	2.606E-02	4.544E+07	3.668E+09	9.160E-16	2.691E-12	9.901E-01
32	2.418E-02	2.452E+07	3.692E+09	1.074E-16	2.692E-12	9.901E-01
33	2.188E-02	5.944E+07	3.752E+09	4.868E-16	2.692E-12	9.903E-01
34	1.503E-02	1.165E+08	3.868E+09	2.186E-15	2.694E-12	9.911E-01
35	7.102E-03	1.269E+08	3.995E+09	1.129E-15	2.695E-12	9.915E-01
36	3.355E-03	1.180E+08	4.113E+09	4.154E-16	2.696E-12	9.917E-01
37	1.585E-03	1.977E+08	4.311E+09	3.326E-16	2.696E-12	9.918E-01
38	4.540E-04	1.111E+08	4.422E+09	1.095E-17	2.696E-12	9.918E-01
39	2.144E-04	1.183E+08	4.540E+09	1.697E-17	2.696E-12	9.918E-01
40	1.013E-04	1.575E+08	4.698E+09	3.514E-17	2.696E-12	9.918E-01
41	3.727E-05	1.936E+08	4.892E+09	7.627E-17	2.696E-12	9.918E-01
42	1.068E-05	1.124E+08	5.004E+09	7.221E-17	2.696E-12	9.919E-01
43	5.043E-06	1.431E+08	5.147E+09	1.431E-16	2.696E-12	9.919E-01
44	1.855E-06	1.002E+08	5.247E+09	1.540E-16	2.697E-12	9.920E-01
45	8.764E-07	9.338E+07	5.341E+09	2.096E-16	2.697E-12	9.921E-01
46	4.140E-07	2.537E+08	5.594E+09	1.041E-15	2.698E-12	9.924E-01
47	1.000E-07	2.020E+09	7.614E+09	2.054E-14	2.718E-12	1.000E+00

Table A.3.c. Absolute calculated neutron flux spectra
and dpa rate at the axial peak, azimuthal peak, and
R = 1/4-T RPV wall of Grand Gulf Cycle 2

G	Energy (MeV)	Group flux	Cumulative flux	Group dpa rate	Cumulative dpa rate	dpa fraction
1	1.733E+01	7.048E+05	7.048E+05	2.060E-15	2.060E-15	1.078E-03
2	1.419E+01	2.944E+06	3.649E+06	7.789E-15	9.849E-15	5.155E-03
3	1.221E+01	9.719E+06	1.337E+07	2.341E-14	3.326E-14	1.741E-02
4	1.000E+01	1.833E+07	3.170E+07	4.068E-14	7.394E-14	3.070E-02
5	8.607E+00	2.887E+07	6.057E+07	6.026E-14	1.342E-13	7.024E-02
6	7.408E+00	6.424E+07	1.248E+08	1.248E-13	2.590E-13	1.356E-01
7	6.065E+00	7.856E+07	2.034E+08	1.401E-13	3.992E-13	2.089E-01
8	4.966E+00	1.125E+08	3.159E+08	1.768E-13	5.759E-13	3.014E-01
9	3.679E+00	7.202E+07	3.879E+08	9.866E-14	6.746E-13	3.531E-01
10	3.012E+00	5.034E+07	4.382E+08	6.398E-14	7.386E-13	3.865E-01
11	2.725E+00	5.727E+07	4.955E+08	7.302E-14	8.116E-13	4.248E-01
12	2.466E+00	2.847E+07	5.240E+08	3.336E-14	8.449E-13	4.422E-01
13	2.365E+00	7.401E+06	5.314E+08	8.112E-15	8.530E-13	4.465E-01
14	2.346E+00	3.679E+07	5.682E+08	3.830E-14	8.914E-13	4.665E-01
15	2.231E+00	9.833E+07	6.665E+08	1.017E-13	9.930E-13	5.197E-01
16	1.920E+00	1.092E+08	7.757E+08	8.882E-14	1.082E-12	5.662E-01
17	1.653E+00	1.535E+08	9.292E+08	1.244E-13	1.206E-12	6.313E-01
18	1.353E+00	2.700E+08	1.199E+09	1.513E-13	1.357E-12	7.105E-01
19	1.003E+00	1.796E+08	1.379E+09	6.581E-14	1.423E-12	7.449E-01
20	8.208E-01	8.480E+07	1.464E+09	4.756E-14	1.471E-12	7.698E-01
21	7.427E-01	2.834E+08	1.747E+09	1.024E-13	1.573E-12	8.234E-01
22	6.081E-01	2.119E+08	1.959E+09	6.237E-14	1.636E-12	8.561E-01
23	4.979E-01	2.524E+08	2.211E+09	1.000E-13	1.736E-12	9.084E-01
24	3.688E-01	2.544E+08	2.466E+09	5.259E-14	1.788E-12	9.360E-01
25	2.972E-01	2.626E+08	2.728E+09	5.265E-14	1.841E-12	9.635E-01
26	1.832E-01	2.401E+08	2.968E+09	3.385E-14	1.875E-12	9.812E-01
27	1.111E-01	1.383E+08	3.107E+09	1.788E-14	1.893E-12	9.906E-01
28	6.738E-02	1.071E+08	3.214E+09	6.934E-15	1.900E-12	9.942E-01
29	4.087E-02	2.868E+07	3.242E+09	2.321E-15	1.902E-12	9.954E-01
30	3.183E-02	1.001E+07	3.252E+09	2.846E-15	1.905E-12	9.969E-01
31	2.606E-02	5.919E+07	3.312E+09	1.193E-15	1.906E-12	9.976E-01
32	2.418E-02	3.041E+07	3.342E+09	1.331E-16	1.906E-12	9.976E-01
33	2.188E-02	5.238E+07	3.394E+09	4.290E-16	1.907E-12	9.979E-01
34	1.503E-02	7.121E+07	3.466E+09	1.336E-15	1.908E-12	9.986E-01
35	7.102E-03	9.301E+07	3.559E+09	8.273E-16	1.909E-12	9.990E-01
36	3.355E-03	7.066E+07	3.629E+09	2.487E-16	1.909E-12	9.991E-01
37	1.585E-03	1.226E+08	3.752E+09	2.062E-16	1.909E-12	9.992E-01
38	4.540E-04	5.442E+07	3.806E+09	5.365E-18	1.909E-12	9.992E-01
39	2.144E-04	6.718E+07	3.873E+09	9.634E-18	1.909E-12	9.992E-01
40	1.013E-04	9.261E+07	3.966E+09	2.066E-17	1.909E-12	9.992E-01
41	3.727E-05	1.109E+08	4.077E+09	4.369E-17	1.909E-12	9.993E-01
42	1.068E-05	5.923E+07	4.136E+09	3.806E-17	1.909E-12	9.993E-01
43	5.043E-06	6.571E+07	4.202E+09	6.571E-17	1.909E-12	9.993E-01
44	1.855E-06	3.741E+07	4.239E+09	5.750E-17	1.909E-12	9.993E-01
45	8.764E-07	2.715E+07	4.266E+09	6.092E-17	1.909E-12	9.994E-01
46	4.140E-07	2.885E+07	4.295E+09	1.184E-16	1.910E-12	9.994E-01
47	1.000E-07	1.055E+08	4.401E+09	1.073E-15	1.911E-12	1.000E+00

Table A.3.d. Absolute calculated neutron flux spectra
and dpa rate at the axial peak, azimuthal peak, and
R = 3/4-T RPV wall of Grand Gulf Cycle 2

G	Energy (MeV)	Group flux	Cumulative flux	Group dpa rate	Cumulative dpa rate	dpa fraction
1	1.733E+01	1.960E+05	1.960E+05	5.728E-16	5.728E-16	7.554E-04
2	1.419E+01	8.055E+05	1.002E+06	2.131E-15	2.704E-15	3.566E-03
3	1.221E+01	2.527E+06	3.529E+06	6.088E-15	8.792E-15	1.159E-02
4	1.000E+01	4.738E+06	8.266E+06	1.051E-14	1.930E-14	2.546E-02
5	8.607E+00	7.186E+06	1.545E+07	1.500E-14	3.430E-14	4.524E-02
6	7.408E+00	1.490E+07	3.035E+07	2.895E-14	6.325E-14	8.342E-02
7	6.065E+00	1.774E+07	4.809E+07	3.165E-14	9.490E-14	1.251E-01
8	4.966E+00	2.549E+07	7.358E+07	4.004E-14	1.349E-13	1.780E-01
9	3.679E+00	1.761E+07	9.119E+07	2.413E-14	1.591E-13	2.098E-01
10	3.012E+00	1.283E+07	1.040E+08	1.631E-14	1.754E-13	2.313E-01
11	2.725E+00	1.536E+07	1.194E+08	1.958E-14	1.950E-13	2.571E-01
12	2.466E+00	7.863E+06	1.272E+08	9.215E-15	2.042E-13	2.693E-01
13	2.365E+00	2.208E+06	1.295E+08	2.420E-15	2.066E-13	2.724E-01
14	2.346E+00	1.117E+07	1.406E+08	1.163E-14	2.182E-13	2.878E-01
15	2.231E+00	3.132E+07	1.719E+08	3.239E-14	2.506E-13	3.305E-01
16	1.920E+00	3.920E+07	2.111E+08	3.188E-14	2.825E-13	3.725E-01
17	1.653E+00	5.917E+07	2.703E+08	4.795E-14	3.304E-13	4.358E-01
18	1.353E+00	1.261E+08	3.964E+08	7.066E-14	4.011E-13	5.290E-01
19	1.003E+00	9.569E+07	4.921E+08	3.507E-14	4.362E-13	5.752E-01
20	8.208E-01	4.345E+07	5.356E+08	2.437E-14	4.605E-13	6.073E-01
21	7.427E-01	1.789E+08	7.145E+08	6.467E-14	5.252E-13	6.926E-01
22	6.081E-01	1.393E+08	8.538E+08	4.100E-14	5.662E-13	7.467E-01
23	4.979E-01	1.691E+08	1.023E+09	6.702E-14	6.332E-13	8.351E-01
24	3.688E-01	1.912E+08	1.214E+09	3.953E-14	6.728E-13	8.872E-01
25	2.972E-01	1.866E+08	1.401E+09	3.741E-14	7.102E-13	9.365E-01
26	1.832E-01	1.806E+08	1.581E+09	2.547E-14	7.356E-13	9.701E-01
27	1.111E-01	9.688E+07	1.678E+09	1.253E-14	7.482E-13	9.866E-01
28	6.738E-02	6.837E+07	1.747E+09	4.429E-15	7.526E-13	9.925E-01
29	4.087E-02	1.678E+07	1.763E+09	1.358E-15	7.539E-13	9.943E-01
30	3.183E-02	5.805E+06	1.769E+09	1.650E-15	7.556E-13	9.964E-01
31	2.606E-02	4.293E+07	1.812E+09	8.655E-16	7.565E-13	9.976E-01
32	2.418E-02	2.311E+07	1.835E+09	1.012E-16	7.566E-13	9.977E-01
33	2.188E-02	3.522E+07	1.870E+09	2.884E-16	7.568E-13	9.981E-01
34	1.503E-02	3.643E+07	1.907E+09	6.833E-16	7.575E-13	9.990E-01
35	7.102E-03	4.662E+07	1.953E+09	4.147E-16	7.579E-13	9.995E-01
36	3.355E-03	3.236E+07	1.986E+09	1.139E-16	7.581E-13	9.997E-01
37	1.585E-03	5.252E+07	2.038E+09	8.834E-17	7.581E-13	9.998E-01
38	4.540E-04	2.183E+07	2.060E+09	2.152E-18	7.582E-13	9.998E-01
39	2.144E-04	2.549E+07	2.086E+09	3.655E-18	7.582E-13	9.998E-01
40	1.013E-04	3.437E+07	2.120E+09	7.668E-18	7.582E-13	9.998E-01
41	3.727E-05	3.983E+07	2.160E+09	1.569E-17	7.582E-13	9.999E-01
42	1.068E-05	2.026E+07	2.180E+09	1.302E-17	7.582E-13	9.999E-01
43	5.043E-06	2.025E+07	2.200E+09	2.025E-17	7.582E-13	9.999E-01
44	1.855E-06	1.009E+07	2.210E+09	1.551E-17	7.582E-13	9.999E-01
45	8.764E-07	6.084E+06	2.217E+09	1.365E-17	7.582E-13	9.999E-01
46	4.140E-07	3.490E+06	2.220E+09	1.432E-17	7.583E-13	1.000E+00
47	1.000E-07	3.607E+06	2.224E+09	3.668E-17	7.583E-13	1.000E+00

Table A.3.e. Absolute calculated neutron flux spectra
and dpa rate at the axial peak, azimuthal peak, and
R = midcavity of Grand Gulf Cycle 2

G	Energy (MeV)	Group flux	Cumulative flux	Group dpa rate	Cumulative dpa rate	dpa fraction
1	1.733E+01	7.024E+04	7.024E+04	2.052E-16	2.052E-16	9.087E-04
2	1.419E+01	2.754E+05	3.457E+05	7.288E-16	9.340E-16	4.135E-03
3	1.221E+01	8.356E+05	1.181E+06	2.013E-15	2.947E-15	1.305E-02
4	1.000E+01	1.524E+06	2.706E+06	3.383E-15	6.330E-15	2.803E-02
5	8.607E+00	2.219E+06	4.925E+06	4.631E-15	1.096E-14	4.853E-02
6	7.408E+00	4.395E+06	9.320E+06	8.540E-15	1.950E-14	8.634E-02
7	6.065E+00	5.079E+06	1.440E+07	9.060E-15	2.856E-14	1.265E-01
8	4.966E+00	7.090E+06	2.149E+07	1.114E-14	3.970E-14	1.758E-01
9	3.679E+00	4.768E+06	2.626E+07	6.532E-15	4.623E-14	2.047E-01
10	3.012E+00	3.439E+06	2.970E+07	4.371E-15	5.060E-14	2.241E-01
11	2.725E+00	4.072E+06	3.377E+07	5.192E-15	5.580E-14	2.470E-01
12	2.466E+00	2.131E+06	3.590E+07	2.498E-15	5.829E-14	2.581E-01
13	2.365E+00	6.035E+05	3.650E+07	6.614E-16	5.895E-14	2.610E-01
14	2.346E+00	2.981E+06	3.948E+07	3.103E-15	6.206E-14	2.748E-01
15	2.231E+00	7.849E+06	4.733E+07	8.115E-15	7.017E-14	3.107E-01
16	1.920E+00	1.014E+07	5.747E+07	8.246E-15	7.842E-14	3.472E-01
17	1.653E+00	1.577E+07	7.324E+07	1.278E-14	9.120E-14	4.038E-01
18	1.353E+00	3.410E+07	1.073E+08	1.911E-14	1.103E-13	4.884E-01
19	1.003E+00	2.766E+07	1.350E+08	1.014E-14	1.204E-13	5.333E-01
20	8.208E-01	1.409E+07	1.491E+08	7.905E-15	1.283E-13	5.683E-01
21	7.427E-01	4.952E+07	1.986E+08	1.790E-14	1.462E-13	6.475E-01
22	6.081E-01	4.324E+07	2.418E+08	1.273E-14	1.590E-13	7.038E-01
23	4.979E-01	4.666E+07	2.885E+08	1.850E-14	1.775E-13	7.857E-01
24	3.688E-01	5.689E+07	3.454E+08	1.176E-14	1.892E-13	8.378E-01
25	2.972E-01	7.416E+07	4.196E+08	1.487E-14	2.041E-13	9.036E-01
26	1.832E-01	6.704E+07	4.866E+08	9.452E-15	2.135E-13	9.455E-01
27	1.111E-01	4.074E+07	5.273E+08	5.268E-15	2.188E-13	9.688E-01
28	6.738E-02	2.877E+07	5.561E+08	1.863E-15	2.207E-13	9.771E-01
29	4.087E-02	8.884E+06	5.650E+08	7.190E-16	2.214E-13	9.802E-01
30	3.183E-02	8.175E+06	5.732E+08	2.324E-15	2.237E-13	9.905E-01
31	2.606E-02	1.506E+07	5.882E+08	3.037E-16	2.240E-13	9.919E-01
32	2.418E-02	9.278E+06	5.975E+08	4.063E-17	2.241E-13	9.921E-01
33	2.188E-02	1.930E+07	6.168E+08	1.581E-16	2.242E-13	9.928E-01
34	1.503E-02	2.511E+07	6.419E+08	4.711E-16	2.247E-13	9.948E-01
35	7.102E-03	2.409E+07	6.660E+08	2.143E-16	2.249E-13	9.958E-01
36	3.355E-03	2.051E+07	6.865E+08	7.219E-17	2.250E-13	9.961E-01
37	1.585E-03	3.190E+07	7.184E+08	5.366E-17	2.250E-13	9.963E-01
38	4.540E-04	1.673E+07	7.351E+08	1.649E-18	2.250E-13	9.964E-01
39	2.144E-04	1.628E+07	7.514E+08	2.334E-18	2.250E-13	9.964E-01
40	1.013E-04	2.042E+07	7.718E+08	4.556E-18	2.250E-13	9.964E-01
41	3.727E-05	2.342E+07	7.953E+08	9.226E-18	2.250E-13	9.964E-01
42	1.068E-05	1.288E+07	8.081E+08	8.280E-18	2.251E-13	9.965E-01
43	5.043E-06	1.544E+07	8.236E+08	1.544E-17	2.251E-13	9.965E-01
44	1.855E-06	1.030E+07	8.339E+08	1.583E-17	2.251E-13	9.966E-01
45	8.764E-07	9.166E+06	8.431E+08	2.057E-17	2.251E-13	9.967E-01
46	4.140E-07	1.949E+07	8.626E+08	7.998E-17	2.252E-13	9.970E-01
47	1.000E-07	6.568E+07	9.282E+08	6.680E-16	2.259E-13	1.000E+00

Table A.3.f. Absolute calculated neutron flux spectra
and dpa rate at the axial peak, azimuthal peak, and
R = front of the concrete shield wall of Grand Gulf Cycle 2

G	Energy (MeV)	Group flux	Cumulative flux	Group dpa rate	Cumulative dpa rate	dpa fraction
1	1.733E+01	4.360E+04	4.360E+04	1.274E-16	1.274E-16	7.344E-04
2	1.419E+01	1.772E+05	2.208E+05	4.688E-16	5.962E-16	3.437E-03
3	1.221E+01	5.497E+05	7.705E+05	1.324E-15	1.921E-15	1.107E-02
4	1.000E+01	1.022E+06	1.792E+06	2.267E-15	4.188E-15	2.414E-02
5	8.607E+00	1.529E+06	3.322E+06	3.192E-15	7.380E-15	4.254E-02
6	7.408E+00	3.134E+06	6.456E+06	6.090E-15	1.347E-14	7.764E-02
7	6.065E+00	3.813E+06	1.027E+07	6.802E-15	2.027E-14	1.169E-01
8	4.966E+00	5.598E+06	1.587E+07	8.794E-15	2.907E-14	1.675E-01
9	3.679E+00	3.838E+06	1.970E+07	5.258E-15	3.432E-14	1.979E-01
10	3.012E+00	2.778E+06	2.248E+07	3.531E-15	3.785E-14	2.182E-01
11	2.725E+00	3.340E+06	2.582E+07	4.259E-15	4.211E-14	2.428E-01
12	2.466E+00	1.797E+06	2.762E+07	2.106E-15	4.422E-14	2.549E-01
13	2.365E+00	4.975E+05	2.812E+07	5.452E-16	4.476E-14	2.580E-01
14	2.346E+00	2.399E+06	3.052E+07	2.497E-15	4.726E-14	2.724E-01
15	2.231E+00	5.837E+06	3.635E+07	6.036E-15	5.330E-14	3.072E-01
16	1.920E+00	7.432E+06	4.379E+07	6.045E-15	5.934E-14	3.421E-01
17	1.653E+00	1.168E+07	5.546E+07	9.463E-15	6.880E-14	3.966E-01
18	1.353E+00	2.365E+07	7.911E+07	1.325E-14	8.206E-14	4.730E-01
19	1.003E+00	1.871E+07	9.782E+07	6.857E-15	8.891E-14	5.125E-01
20	8.208E-01	1.191E+07	1.097E+08	6.680E-15	9.559E-14	5.510E-01
21	7.427E-01	3.425E+07	1.440E+08	1.238E-14	1.080E-13	6.224E-01
22	6.081E-01	3.339E+07	1.774E+08	9.827E-15	1.178E-13	6.790E-01
23	4.979E-01	3.394E+07	2.113E+08	1.346E-14	1.313E-13	7.566E-01
24	3.688E-01	3.855E+07	2.499E+08	7.968E-15	1.392E-13	8.025E-01
25	2.972E-01	6.212E+07	3.120E+08	1.246E-14	1.517E-13	8.743E-01
26	1.832E-01	5.902E+07	3.710E+08	8.321E-15	1.600E-13	9.223E-01
27	1.111E-01	3.982E+07	4.108E+08	5.149E-15	1.651E-13	9.520E-01
28	6.738E-02	3.078E+07	4.416E+08	1.994E-15	1.671E-13	9.635E-01
29	4.087E-02	1.148E+07	4.531E+08	9.292E-16	1.681E-13	9.688E-01
30	3.183E-02	9.497E+06	4.626E+08	2.700E-15	1.708E-13	9.844E-01
31	2.606E-02	8.253E+06	4.708E+08	1.664E-16	1.709E-13	9.853E-01
32	2.418E-02	7.423E+06	4.783E+08	3.251E-17	1.710E-13	9.855E-01
33	2.188E-02	2.038E+07	4.986E+08	1.669E-16	1.711E-13	9.865E-01
34	1.503E-02	3.060E+07	5.292E+08	5.740E-16	1.717E-13	9.898E-01
35	7.102E-03	2.765E+07	5.569E+08	2.459E-16	1.720E-13	9.912E-01
36	3.355E-03	2.468E+07	5.816E+08	8.686E-17	1.720E-13	9.917E-01
37	1.585E-03	3.798E+07	6.195E+08	6.387E-17	1.721E-13	9.921E-01
38	4.540E-04	2.039E+07	6.399E+08	2.010E-18	1.721E-13	9.921E-01
39	2.144E-04	1.938E+07	6.593E+08	2.779E-18	1.721E-13	9.921E-01
40	1.013E-04	2.421E+07	6.835E+08	5.402E-18	1.721E-13	9.921E-01
41	3.727E-05	2.787E+07	7.114E+08	1.098E-17	1.721E-13	9.922E-01
42	1.068E-05	1.554E+07	7.269E+08	9.986E-18	1.721E-13	9.923E-01
43	5.043E-06	1.905E+07	7.460E+08	1.905E-17	1.722E-13	9.924E-01
44	1.855E-06	1.309E+07	7.591E+08	2.011E-17	1.722E-13	9.925E-01
45	8.764E-07	1.199E+07	7.711E+08	2.691E-17	1.722E-13	9.926E-01
46	4.140E-07	2.811E+07	7.992E+08	1.153E-16	1.723E-13	9.933E-01
47	1.000E-07	1.141E+08	9.133E+08	1.160E-15	1.735E-13	1.000E+00

Table A.3.g. Absolute calculated neutron flux spectra
and dpa rate at the axial peak, azimuthal peak, and
R = six inches in the concrete shield wall of Grand Gulf Cycle 2

G	Energy (MeV)	Group flux	Cumulative flux	Group dpa rate	Cumulative dpa rate	dpa fraction
1	1.733E+01	3.411E+03	3.411E+03	9.968E-18	9.968E-18	7.677E-04
2	1.419E+01	1.548E+04	1.889E+04	4.096E-17	5.093E-17	3.923E-03
3	1.221E+01	4.590E+04	6.479E+04	1.106E-16	1.615E-16	1.244E-02
4	1.000E+01	9.133E+04	1.561E+05	2.027E-16	3.642E-16	2.805E-02
5	8.607E+00	1.395E+05	2.957E+05	2.912E-16	6.554E-16	5.047E-02
6	7.408E+00	3.548E+05	6.505E+05	6.894E-16	1.345E-15	1.036E-01
7	6.065E+00	4.722E+05	1.123E+06	8.425E-16	2.187E-15	1.685E-01
8	4.966E+00	7.048E+05	1.828E+06	1.107E-15	3.294E-15	2.537E-01
9	3.679E+00	4.503E+05	2.278E+06	6.169E-16	3.911E-15	3.012E-01
10	3.012E+00	3.849E+05	2.663E+06	4.892E-16	4.401E-15	3.389E-01
11	2.725E+00	4.739E+05	3.137E+06	6.042E-16	5.005E-15	3.855E-01
12	2.466E+00	3.228E+05	3.459E+06	3.784E-16	5.383E-15	4.146E-01
13	2.365E+00	1.029E+05	3.562E+06	1.128E-16	5.496E-15	4.233E-01
14	2.346E+00	4.190E+05	3.981E+06	4.362E-16	5.932E-15	4.569E-01
15	2.231E+00	6.910E+05	4.672E+06	7.145E-16	6.647E-15	5.119E-01
16	1.920E+00	6.630E+05	5.335E+06	5.392E-16	7.186E-15	5.534E-01
17	1.653E+00	8.566E+05	6.192E+06	6.941E-16	7.880E-15	6.069E-01
18	1.353E+00	1.051E+06	7.243E+06	5.891E-16	8.469E-15	6.523E-01
19	1.003E+00	6.260E+05	7.869E+06	2.294E-16	8.698E-15	6.699E-01
20	8.208E-01	5.117E+05	8.381E+06	2.870E-16	8.986E-15	6.920E-01
21	7.427E-01	1.048E+06	9.429E+06	3.788E-16	9.364E-15	7.212E-01
22	6.081E-01	1.061E+06	1.049E+07	3.122E-16	9.677E-15	7.452E-01
23	4.979E-01	8.912E+05	1.138E+07	3.533E-16	1.003E-14	7.725E-01
24	3.688E-01	8.106E+05	1.219E+07	1.676E-16	1.020E-14	7.854E-01
25	2.972E-01	1.673E+06	1.386E+07	3.354E-16	1.053E-14	8.112E-01
26	1.832E-01	1.998E+06	1.586E+07	2.817E-16	1.081E-14	8.329E-01
27	1.111E-01	1.748E+06	1.761E+07	2.260E-16	1.104E-14	8.503E-01
28	6.738E-02	1.677E+06	1.929E+07	1.086E-16	1.115E-14	8.587E-01
29	4.087E-02	7.576E+05	2.005E+07	6.132E-17	1.121E-14	8.634E-01
30	3.183E-02	6.623E+05	2.071E+07	1.883E-16	1.140E-14	8.779E-01
31	2.606E-02	2.490E+05	2.096E+07	5.020E-18	1.140E-14	8.783E-01
32	2.418E-02	3.256E+05	2.128E+07	1.426E-18	1.141E-14	8.784E-01
33	2.188E-02	1.219E+06	2.250E+07	9.987E-18	1.142E-14	8.791E-01
34	1.503E-02	2.477E+06	2.498E+07	4.648E-17	1.146E-14	8.827E-01
35	7.102E-03	2.521E+06	2.750E+07	2.242E-17	1.148E-14	8.844E-01
36	3.355E-03	2.609E+06	3.011E+07	9.184E-18	1.149E-14	8.852E-01
37	1.585E-03	5.045E+06	3.515E+07	8.486E-18	1.150E-14	8.858E-01
38	4.540E-04	3.248E+06	3.840E+07	3.202E-19	1.150E-14	8.858E-01
39	2.144E-04	3.458E+06	4.186E+07	4.959E-19	1.150E-14	8.859E-01
40	1.013E-04	4.944E+06	4.680E+07	1.103E-18	1.150E-14	8.860E-01
41	3.727E-05	6.671E+06	5.347E+07	2.628E-18	1.151E-14	8.862E-01
42	1.068E-05	4.189E+06	5.766E+07	2.692E-18	1.151E-14	8.864E-01
43	5.043E-06	5.840E+06	6.350E+07	5.840E-18	1.151E-14	8.868E-01
44	1.855E-06	4.505E+06	6.801E+07	6.925E-18	1.152E-14	8.873E-01
45	8.764E-07	4.601E+06	7.261E+07	1.032E-17	1.153E-14	8.881E-01
46	4.140E-07	1.446E+07	8.707E+07	5.933E-17	1.159E-14	8.927E-01
47	1.000E-07	1.370E+08	2.240E+08	1.393E-15	1.298E-14	1.000E+00

Table A.3.h. Absolute calculated neutron flux spectra
and dpa rate at the axial peak, azimuthal peak, and
R = one foot in the concrete shield wall of Grand Gulf Cycle 2

G	Energy (MeV)	Group flux	Cumulative flux	Group dpa rate	Cumulative dpa rate	dpa fraction
1	1.733E+01	2.222E+02	2.222E+02	6.493E-19	6.493E-19	5.868E-04
2	1.419E+01	1.092E+03	1.314E+03	2.889E-18	3.539E-18	3.198E-03
3	1.221E+01	3.136E+03	4.450E+03	7.555E-18	1.109E-17	1.003E-02
4	1.000E+01	6.636E+03	1.109E+04	1.473E-17	2.582E-17	2.333E-02
5	8.607E+00	1.013E+04	2.121E+04	2.113E-17	4.695E-17	4.243E-02
6	7.408E+00	3.032E+04	5.154E+04	5.892E-17	1.059E-16	9.568E-02
7	6.065E+00	4.093E+04	9.247E+04	7.302E-17	1.789E-16	1.617E-01
8	4.966E+00	5.998E+04	1.525E+05	9.423E-17	2.731E-16	2.468E-01
9	3.679E+00	3.814E+04	1.906E+05	5.226E-17	3.254E-16	2.940E-01
10	3.012E+00	3.378E+04	2.244E+05	4.294E-17	3.683E-16	3.329E-01
11	2.725E+00	4.244E+04	2.668E+05	5.411E-17	4.224E-16	3.818E-01
12	2.466E+00	3.257E+04	2.994E+05	3.817E-17	4.606E-16	4.162E-01
13	2.365E+00	1.196E+04	3.114E+05	1.311E-17	4.737E-16	4.281E-01
14	2.346E+00	4.471E+04	3.561E+05	4.654E-17	5.203E-16	4.702E-01
15	2.231E+00	6.683E+04	4.229E+05	6.911E-17	5.894E-16	5.326E-01
16	1.920E+00	6.076E+04	4.837E+05	4.942E-17	6.388E-16	5.773E-01
17	1.653E+00	7.442E+04	5.581E+05	6.030E-17	6.991E-16	6.318E-01
18	1.353E+00	8.612E+04	6.442E+05	4.825E-17	7.473E-16	6.754E-01
19	1.003E+00	5.034E+04	6.945E+05	1.845E-17	7.658E-16	6.920E-01
20	8.208E-01	4.007E+04	7.346E+05	2.247E-17	7.883E-16	7.123E-01
21	7.427E-01	7.463E+04	8.092E+05	2.697E-17	8.152E-16	7.367E-01
22	6.081E-01	7.217E+04	8.814E+05	2.124E-17	8.365E-16	7.559E-01
23	4.979E-01	6.020E+04	9.416E+05	2.386E-17	8.603E-16	7.775E-01
24	3.688E-01	5.342E+04	9.950E+05	1.104E-17	8.714E-16	7.875E-01
25	2.972E-01	1.083E+05	1.103E+06	2.171E-17	8.931E-16	8.071E-01
26	1.832E-01	1.201E+05	1.223E+06	1.693E-17	9.100E-16	8.224E-01
27	1.111E-01	9.971E+04	1.323E+06	1.289E-17	9.229E-16	8.340E-01
28	6.738E-02	9.197E+04	1.415E+06	5.957E-18	9.289E-16	8.394E-01
29	4.087E-02	4.081E+04	1.456E+06	3.303E-18	9.322E-16	8.424E-01
30	3.183E-02	3.550E+04	1.491E+06	1.009E-17	9.423E-16	8.515E-01
31	2.606E-02	1.292E+04	1.504E+06	2.605E-19	9.425E-16	8.517E-01
32	2.418E-02	1.692E+04	1.521E+06	7.408E-20	9.426E-16	8.518E-01
33	2.188E-02	6.204E+04	1.583E+06	5.081E-19	9.431E-16	8.523E-01
34	1.503E-02	1.230E+05	1.706E+06	2.307E-18	9.454E-16	8.544E-01
35	7.102E-03	1.219E+05	1.828E+06	1.084E-18	9.465E-16	8.553E-01
36	3.355E-03	1.241E+05	1.952E+06	4.370E-19	9.469E-16	8.557E-01
37	1.585E-03	2.313E+05	2.183E+06	3.890E-19	9.473E-16	8.561E-01
38	4.540E-04	1.472E+05	2.331E+06	1.451E-20	9.473E-16	8.561E-01
39	2.144E-04	1.555E+05	2.486E+06	2.229E-20	9.474E-16	8.561E-01
40	1.013E-04	2.232E+05	2.709E+06	4.980E-20	9.474E-16	8.562E-01
41	3.727E-05	3.064E+05	3.016E+06	1.207E-19	9.475E-16	8.563E-01
42	1.068E-05	1.963E+05	3.212E+06	1.262E-19	9.476E-16	8.564E-01
43	5.043E-06	2.816E+05	3.494E+06	2.816E-19	9.479E-16	8.566E-01
44	1.855E-06	2.234E+05	3.717E+06	3.433E-19	9.483E-16	8.569E-01
45	8.764E-07	2.354E+05	3.952E+06	5.283E-19	9.488E-16	8.574E-01
46	4.140E-07	8.093E+05	4.762E+06	3.320E-18	9.521E-16	8.604E-01
47	1.000E-07	1.519E+07	1.995E+07	1.544E-16	1.107E-15	1.000E+00

Table A.4.a. Absolute calculated neutron flux spectra and dpa rate
at the axial feed water nozzle elevation, azimuthal peak, and
RPV-wetted surface wall of Grand Gulf Cycle 2

G	Energy (MeV)	Group flux	Cumulative flux	Group dpa rate	Cumulative dpa rate	dpa fraction
1	1.733E+01	1.901E+02	1.901E+02	5.553E-19	5.553E-19	4.812E-03
2	1.419E+01	7.674E+02	9.574E+02	2.030E-18	2.586E-18	2.240E-02
3	1.221E+01	1.711E+03	2.668E+03	4.122E-18	6.708E-18	5.812E-02
4	1.000E+01	2.488E+03	5.156E+03	5.521E-18	1.223E-17	1.060E-01
5	8.607E+00	3.225E+03	8.382E+03	6.731E-18	1.896E-17	1.643E-01
6	7.408E+00	5.923E+03	1.430E+04	1.151E-17	3.047E-17	2.640E-01
7	6.065E+00	6.474E+03	2.078E+04	1.155E-17	4.202E-17	3.641E-01
8	4.966E+00	8.760E+03	2.954E+04	1.376E-17	5.578E-17	4.833E-01
9	3.679E+00	5.360E+03	3.490E+04	7.344E-18	6.312E-17	5.469E-01
10	3.012E+00	3.360E+03	3.826E+04	4.271E-18	6.739E-17	5.839E-01
11	2.725E+00	3.565E+03	4.182E+04	4.546E-18	7.194E-17	6.233E-01
12	2.466E+00	1.664E+03	4.349E+04	1.951E-18	7.389E-17	6.402E-01
13	2.365E+00	3.922E+02	4.388E+04	4.299E-19	7.432E-17	6.439E-01
14	2.346E+00	1.967E+03	4.585E+04	2.048E-18	7.637E-17	6.617E-01
15	2.231E+00	5.000E+03	5.085E+04	5.170E-18	8.154E-17	7.065E-01
16	1.920E+00	5.065E+03	5.591E+04	4.119E-18	8.566E-17	7.422E-01
17	1.653E+00	6.644E+03	6.256E+04	5.384E-18	9.104E-17	7.888E-01
18	1.353E+00	1.003E+04	7.259E+04	5.620E-18	9.666E-17	8.375E-01
19	1.003E+00	6.376E+03	7.896E+04	2.337E-18	9.900E-17	8.578E-01
20	8.208E-01	3.230E+03	8.219E+04	1.812E-18	1.008E-16	8.735E-01
21	7.427E-01	8.198E+03	9.039E+04	2.963E-18	1.038E-16	8.991E-01
22	6.081E-01	6.390E+03	9.678E+04	1.881E-18	1.057E-16	9.154E-01
23	4.979E-01	7.247E+03	1.040E+05	2.873E-18	1.085E-16	9.403E-01
24	3.688E-01	6.739E+03	1.108E+05	1.393E-18	1.099E-16	9.524E-01
25	2.972E-01	8.648E+03	1.194E+05	1.734E-18	1.117E-16	9.674E-01
26	1.832E-01	7.323E+03	1.267E+05	1.033E-18	1.127E-16	9.764E-01
27	1.111E-01	5.208E+03	1.319E+05	6.734E-19	1.134E-16	9.822E-01
28	6.738E-02	4.383E+03	1.363E+05	2.839E-19	1.136E-16	9.846E-01
29	4.087E-02	1.769E+03	1.381E+05	1.432E-19	1.138E-16	9.859E-01
30	3.183E-02	1.212E+03	1.393E+05	3.445E-19	1.141E-16	9.889E-01
31	2.606E-02	1.465E+03	1.408E+05	2.954E-20	1.142E-16	9.891E-01
32	2.418E-02	9.005E+02	1.417E+05	3.943E-21	1.142E-16	9.892E-01
33	2.188E-02	2.377E+03	1.441E+05	1.947E-20	1.142E-16	9.893E-01
34	1.503E-02	4.618E+03	1.487E+05	8.663E-20	1.143E-16	9.901E-01
35	7.102E-03	4.807E+03	1.535E+05	4.276E-20	1.143E-16	9.905E-01
36	3.355E-03	4.546E+03	1.580E+05	1.600E-20	1.143E-16	9.906E-01
37	1.585E-03	7.498E+03	1.655E+05	1.261E-20	1.143E-16	9.907E-01
38	4.540E-04	4.314E+03	1.698E+05	4.253E-20	1.143E-16	9.907E-01
39	2.144E-04	4.456E+03	1.743E+05	6.390E-20	1.143E-16	9.907E-01
40	1.013E-04	5.910E+03	1.802E+05	1.318E-21	1.143E-16	9.907E-01
41	3.727E-05	7.268E+03	1.875E+05	2.863E-21	1.143E-16	9.907E-01
42	1.068E-05	4.254E+03	1.917E+05	2.734E-21	1.143E-16	9.908E-01
43	5.043E-06	5.481E+03	1.972E+05	5.481E-21	1.144E-16	9.908E-01
44	1.855E-06	3.915E+03	2.011E+05	6.017E-21	1.144E-16	9.909E-01
45	8.764E-07	3.716E+03	2.048E+05	8.339E-21	1.144E-16	9.909E-01
46	4.140E-07	1.103E+04	2.159E+05	4.527E-20	1.144E-16	9.913E-01
47	1.000E-07	9.835E+04	3.142E+05	1.000E-18	1.154E-16	1.000E+00

Table A.4.b. Absolute calculated neutron flux spectra and dpa rate
at the axial feed water nozzle elevation, azimuthal peak, and
R = 0-T RPV wall of Grand Gulf Cycle 2

G	Energy (MeV)	Group flux	Cumulative flux	Group dpa rate	Cumulative dpa rate	dpa fraction
1	1.733E+01	1.794E+02	1.794E+02	5.242E-19	5.242E-19	4.657E-03
2	1.419E+01	7.258E+02	9.052E+02	1.921E-18	2.445E-18	2.172E-02
3	1.221E+01	1.615E+03	2.520E+03	3.890E-18	6.335E-18	5.628E-02
4	1.000E+01	2.352E+03	4.872E+03	5.218E-18	1.155E-17	1.026E-01
5	8.607E+00	3.042E+03	7.914E+03	6.350E-18	1.790E-17	1.590E-01
6	7.408E+00	5.578E+03	1.349E+04	1.084E-17	2.874E-17	2.553E-01
7	6.065E+00	6.100E+03	1.959E+04	1.088E-17	3.962E-17	3.520E-01
8	4.966E+00	8.295E+03	2.789E+04	1.303E-17	5.265E-17	4.678E-01
9	3.679E+00	5.122E+03	3.301E+04	7.017E-18	5.967E-17	5.301E-01
10	3.012E+00	3.245E+03	3.625E+04	4.124E-18	6.380E-17	5.668E-01
11	2.725E+00	3.467E+03	3.972E+04	4.421E-18	6.822E-17	6.060E-01
12	2.466E+00	1.627E+03	4.135E+04	1.907E-18	7.012E-17	6.230E-01
13	2.365E+00	3.850E+02	4.173E+04	4.220E-19	7.055E-17	6.267E-01
14	2.346E+00	1.941E+03	4.367E+04	2.020E-18	7.257E-17	6.447E-01
15	2.231E+00	5.001E+03	4.867E+04	5.171E-18	7.774E-17	6.906E-01
16	1.920E+00	5.124E+03	5.380E+04	4.167E-18	8.190E-17	7.276E-01
17	1.653E+00	6.788E+03	6.059E+04	5.500E-18	8.740E-17	7.765E-01
18	1.353E+00	1.050E+04	7.109E+04	5.885E-18	9.329E-17	8.288E-01
19	1.003E+00	6.692E+03	7.778E+04	2.452E-18	9.574E-17	8.506E-01
20	8.208E-01	3.329E+03	8.111E+04	1.867E-18	9.761E-17	8.672E-01
21	7.427E-01	8.887E+03	9.000E+04	3.212E-18	1.008E-16	8.957E-01
22	6.081E-01	6.801E+03	9.680E+04	2.001E-18	1.028E-16	9.135E-01
23	4.979E-01	7.766E+03	1.046E+05	3.079E-18	1.059E-16	9.408E-01
24	3.688E-01	7.334E+03	1.119E+05	1.516E-18	1.074E-16	9.543E-01
25	2.972E-01	8.858E+03	1.208E+05	1.776E-18	1.092E-16	9.701E-01
26	1.832E-01	7.561E+03	1.283E+05	1.066E-18	1.103E-16	9.795E-01
27	1.111E-01	5.130E+03	1.334E+05	6.632E-19	1.109E-16	9.854E-01
28	6.738E-02	4.275E+03	1.377E+05	2.769E-19	1.112E-16	9.879E-01
29	4.087E-02	1.619E+03	1.393E+05	1.310E-19	1.113E-16	9.891E-01
30	3.183E-02	1.005E+03	1.403E+05	2.857E-19	1.116E-16	9.916E-01
31	2.606E-02	1.724E+03	1.421E+05	3.475E-20	1.116E-16	9.919E-01
32	2.418E-02	9.338E+02	1.430E+05	4.089E-21	1.117E-16	9.919E-01
33	2.188E-02	2.200E+03	1.452E+05	1.802E-20	1.117E-16	9.921E-01
34	1.503E-02	4.249E+03	1.495E+05	7.971E-20	1.118E-16	9.928E-01
35	7.102E-03	4.617E+03	1.541E+05	4.107E-20	1.118E-16	9.932E-01
36	3.355E-03	4.273E+03	1.583E+05	1.504E-20	1.118E-16	9.933E-01
37	1.585E-03	7.132E+03	1.655E+05	1.200E-20	1.118E-16	9.934E-01
38	4.540E-04	3.991E+03	1.695E+05	3.934E-22	1.118E-16	9.934E-01
39	2.144E-04	4.241E+03	1.737E+05	6.081E-22	1.118E-16	9.934E-01
40	1.013E-04	5.631E+03	1.793E+05	1.256E-21	1.118E-16	9.934E-01
41	3.727E-05	6.892E+03	1.862E+05	2.715E-21	1.118E-16	9.935E-01
42	1.068E-05	3.988E+03	1.902E+05	2.563E-21	1.118E-16	9.935E-01
43	5.043E-06	5.066E+03	1.953E+05	5.066E-21	1.118E-16	9.935E-01
44	1.855E-06	3.539E+03	1.988E+05	5.439E-21	1.118E-16	9.936E-01
45	8.764E-07	3.286E+03	2.021E+05	7.374E-21	1.118E-16	9.936E-01
46	4.140E-07	8.857E+03	2.110E+05	3.634E-20	1.119E-16	9.940E-01
47	1.000E-07	6.689E+04	2.779E+05	6.803E-19	1.126E-16	1.000E+00

Table A.4.c. Absolute calculated neutron flux spectra and dpa rate
at the axial feed water nozzle elevation, azimuthal peak, and
R = 1/4-T RPV wall of Grand Gulf Cycle 2

G	Energy (MeV)	Group flux	Cumulative flux	Group dpa rate	Cumulative dpa rate	dpa fraction
1	1.733E+01	9.118E+01	9.118E+01	2.664E-19	2.664E-19	2.295E-04
2	1.419E+01	3.749E+02	4.661E+02	9.920E-19	1.258E-18	1.084E-03
3	1.221E+01	8.199E+02	1.286E+03	1.975E-18	3.234E-18	2.786E-03
4	1.000E+01	1.226E+03	2.512E+03	2.720E-18	5.953E-18	5.129E-03
5	8.607E+00	1.621E+03	4.133E+03	3.383E-18	9.337E-18	8.044E-03
6	7.408E+00	3.011E+03	7.143E+03	5.849E-18	1.519E-17	1.308E-02
7	6.065E+00	3.608E+03	1.075E+04	6.436E-18	2.162E-17	1.863E-02
8	4.966E+00	5.926E+03	1.668E+04	9.310E-18	3.093E-17	2.665E-02
9	3.679E+00	4.492E+03	2.117E+04	6.154E-18	3.709E-17	3.195E-02
10	3.012E+00	3.321E+03	2.449E+04	4.221E-18	4.131E-17	3.559E-02
11	2.725E+00	4.336E+03	2.883E+04	5.528E-18	4.683E-17	4.035E-02
12	2.466E+00	2.322E+03	3.115E+04	2.721E-18	4.956E-17	4.269E-02
13	2.365E+00	6.504E+02	3.180E+04	7.129E-19	5.027E-17	4.331E-02
14	2.346E+00	3.429E+03	3.523E+04	3.570E-18	5.384E-17	4.638E-02
15	2.231E+00	9.726E+03	4.495E+04	1.006E-17	6.390E-17	5.505E-02
16	1.920E+00	1.367E+04	5.862E+04	1.111E-17	7.501E-17	6.463E-02
17	1.653E+00	2.441E+04	8.303E+04	1.978E-17	9.479E-17	8.166E-02
18	1.353E+00	7.560E+04	1.586E+05	4.236E-17	1.371E-16	1.182E-01
19	1.003E+00	7.541E+04	2.340E+05	2.764E-17	1.648E-16	1.420E-01
20	8.208E-01	3.732E+04	2.714E+05	2.093E-17	1.857E-16	1.600E-01
21	7.427E-01	2.526E+05	5.239E+05	9.128E-17	2.770E-16	2.386E-01
22	6.081E-01	2.708E+05	7.947E+05	7.969E-17	3.567E-16	3.073E-01
23	4.979E-01	3.980E+05	1.193E+06	1.578E-16	5.145E-16	4.432E-01
24	3.688E-01	6.301E+05	1.823E+06	1.302E-16	6.447E-16	5.554E-01
25	2.972E-01	8.301E+05	2.653E+06	1.664E-16	8.111E-16	6.988E-01
26	1.832E-01	1.161E+06	3.814E+06	1.637E-16	9.748E-16	8.398E-01
27	1.111E-01	7.090E+05	4.523E+06	9.167E-17	1.066E-15	9.188E-01
28	6.738E-02	5.687E+05	5.091E+06	3.683E-17	1.103E-15	9.506E-01
29	4.087E-02	1.402E+05	5.232E+06	1.135E-17	1.115E-15	9.603E-01
30	3.183E-02	4.818E+04	5.280E+06	1.370E-17	1.128E-15	9.721E-01
31	2.606E-02	4.583E+05	5.738E+06	9.239E-18	1.138E-15	9.801E-01
32	2.418E-02	2.912E+05	6.029E+06	1.275E-18	1.139E-15	9.812E-01
33	2.188E-02	4.815E+05	6.511E+06	3.944E-18	1.143E-15	9.846E-01
34	1.503E-02	4.395E+05	6.950E+06	8.246E-18	1.151E-15	9.917E-01
35	7.102E-03	6.078E+05	7.558E+06	5.407E-18	1.156E-15	9.964E-01
36	3.355E-03	4.266E+05	7.985E+06	1.501E-18	1.158E-15	9.977E-01
37	1.585E-03	7.148E+05	8.700E+06	1.202E-18	1.159E-15	9.987E-01
38	4.540E-04	2.958E+05	8.995E+06	2.916E-20	1.159E-15	9.987E-01
39	2.144E-04	3.512E+05	9.347E+06	5.037E-20	1.159E-15	9.988E-01
40	1.013E-04	4.883E+05	9.835E+06	1.089E-19	1.159E-15	9.988E-01
41	3.727E-05	5.793E+05	1.041E+07	2.282E-19	1.160E-15	9.990E-01
42	1.068E-05	2.966E+05	1.071E+07	1.906E-19	1.160E-15	9.992E-01
43	5.043E-06	2.908E+05	1.100E+07	2.908E-19	1.160E-15	9.995E-01
44	1.855E-06	1.391E+05	1.114E+07	2.138E-19	1.160E-15	9.996E-01
45	8.764E-07	7.722E+04	1.122E+07	1.733E-19	1.160E-15	9.998E-01
46	4.140E-07	2.986E+04	1.125E+07	1.225E-19	1.161E-15	9.999E-01
47	1.000E-07	1.163E+04	1.126E+07	1.183E-19	1.161E-15	1.000E+00

Table A.4.d. Absolute calculated neutron flux spectra and dpa rate
at the axial feed water nozzle elevation, azimuthal peak, and
R = 3/4-T RPV wall of Grand Gulf Cycle 2

G	Energy (MeV)	Group flux	Cumulative flux	Group dpa rate	Cumulative dpa rate	dpa fraction
1	1.733E+01	2.285E+01	2.285E+01	6.677E-20	6.677E-20	2.738E-05
2	1.419E+01	1.135E+02	1.364E+02	3.003E-19	3.671E-19	1.506E-04
3	1.221E+01	3.066E+02	4.429E+02	7.385E-19	1.106E-18	4.534E-04
4	1.000E+01	5.720E+02	1.015E+03	1.269E-18	2.375E-18	9.740E-04
5	8.607E+00	1.053E+03	2.068E+03	2.198E-18	4.573E-18	1.875E-03
6	7.408E+00	2.590E+03	4.659E+03	5.033E-18	9.606E-18	3.940E-03
7	6.065E+00	4.917E+03	9.576E+03	8.772E-18	1.838E-17	7.537E-03
8	4.966E+00	1.235E+04	2.193E+04	1.940E-17	3.778E-17	1.549E-02
9	3.679E+00	1.144E+04	3.337E+04	1.567E-17	5.345E-17	2.192E-02
10	3.012E+00	9.002E+03	4.237E+04	1.144E-17	6.489E-17	2.661E-02
11	2.725E+00	1.298E+04	5.534E+04	1.655E-17	8.144E-17	3.340E-02
12	2.466E+00	7.438E+03	6.278E+04	8.717E-18	9.016E-17	3.697E-02
13	2.365E+00	2.016E+03	6.480E+04	2.210E-18	9.237E-17	3.788E-02
14	2.346E+00	1.079E+04	7.559E+04	1.123E-17	1.036E-16	4.249E-02
15	2.231E+00	2.932E+04	1.049E+05	3.032E-17	1.339E-16	5.492E-02
16	1.920E+00	4.115E+04	1.461E+05	3.347E-17	1.674E-16	6.865E-02
17	1.653E+00	7.557E+04	2.216E+05	6.123E-17	2.286E-16	9.376E-02
18	1.353E+00	2.115E+05	4.331E+05	1.185E-16	3.471E-16	1.424E-01
19	1.003E+00	1.848E+05	6.179E+05	6.773E-17	4.148E-16	1.701E-01
20	8.208E-01	1.123E+05	7.302E+05	6.300E-17	4.778E-16	1.960E-01
21	7.427E-01	5.444E+05	1.275E+06	1.967E-16	6.746E-16	2.767E-01
22	6.081E-01	5.883E+05	1.863E+06	1.731E-16	8.477E-16	3.477E-01
23	4.979E-01	8.517E+05	2.715E+06	3.376E-16	1.185E-15	4.861E-01
24	3.688E-01	1.086E+06	3.801E+06	2.246E-16	1.410E-15	5.782E-01
25	2.972E-01	1.699E+06	5.500E+06	3.407E-16	1.751E-15	7.179E-01
26	1.832E-01	2.092E+06	7.593E+06	2.950E-16	2.046E-15	8.389E-01
27	1.111E-01	1.431E+06	9.024E+06	1.851E-16	2.231E-15	9.148E-01
28	6.738E-02	1.212E+06	1.024E+07	7.851E-17	2.309E-15	9.470E-01
29	4.087E-02	3.106E+05	1.055E+07	2.514E-17	2.334E-15	9.573E-01
30	3.183E-02	1.084E+05	1.065E+07	3.082E-17	2.365E-15	9.700E-01
31	2.606E-02	7.342E+05	1.139E+07	1.480E-17	2.380E-15	9.760E-01
32	2.418E-02	4.358E+05	1.182E+07	1.908E-18	2.382E-15	9.768E-01
33	2.188E-02	8.465E+05	1.267E+07	6.933E-18	2.389E-15	9.797E-01
34	1.503E-02	1.064E+06	1.374E+07	1.997E-17	2.409E-15	9.879E-01
35	7.102E-03	1.418E+06	1.515E+07	1.261E-17	2.421E-15	9.930E-01
36	3.355E-03	1.097E+06	1.625E+07	3.860E-18	2.425E-15	9.946E-01
37	1.585E-03	1.937E+06	1.819E+07	3.259E-18	2.428E-15	9.960E-01
38	4.540E-04	8.598E+05	1.905E+07	8.476E-20	2.429E-15	9.960E-01
39	2.144E-04	1.043E+06	2.009E+07	1.496E-19	2.429E-15	9.960E-01
40	1.013E-04	1.429E+06	2.152E+07	3.187E-19	2.429E-15	9.962E-01
41	3.727E-05	1.688E+06	2.321E+07	6.649E-19	2.430E-15	9.965E-01
42	1.068E-05	8.838E+05	2.409E+07	5.680E-19	2.430E-15	9.967E-01
43	5.043E-06	9.477E+05	2.504E+07	9.477E-19	2.431E-15	9.971E-01
44	1.855E-06	5.180E+05	2.556E+07	7.962E-19	2.432E-15	9.974E-01
45	8.764E-07	3.557E+05	2.591E+07	7.982E-19	2.433E-15	9.977E-01
46	4.140E-07	2.869E+05	2.620E+07	1.177E-18	2.434E-15	9.982E-01
47	1.000E-07	4.296E+05	2.663E+07	4.369E-18	2.438E-15	1.000E+00

Table A.4.e. Absolute calculated neutron flux spectra and dpa rate
at the axial feed water nozzle elevation, azimuthal peak, and
R = midcavity of Grand Gulf Cycle 2

G	Energy (MeV)	Group flux	Cumulative flux	Group dpa rate	Cumulative dpa rate	dpa fraction
1	1.733E+01	7.846E+01	7.846E+01	2.293E-19	2.293E-19	3.525E-05
2	1.419E+01	6.758E+02	7.543E+02	1.788E-18	2.017E-18	3.102E-04
3	1.221E+01	2.708E+03	3.462E+03	6.523E-18	8.540E-18	1.313E-03
4	1.000E+01	6.201E+03	9.663E+03	1.376E-17	2.230E-17	3.428E-03
5	8.607E+00	1.288E+04	2.254E+04	2.688E-17	4.918E-17	7.561E-03
6	7.408E+00	3.319E+04	5.573E+04	6.449E-17	1.137E-16	1.747E-02
7	6.065E+00	5.931E+04	1.150E+05	1.058E-16	2.195E-16	3.374E-02
8	4.966E+00	1.225E+05	2.375E+05	1.924E-16	4.119E-16	6.332E-02
9	3.679E+00	9.776E+04	3.353E+05	1.339E-16	5.458E-16	8.391E-02
10	3.012E+00	7.058E+04	4.059E+05	8.971E-17	6.355E-16	9.770E-02
11	2.725E+00	9.133E+04	4.972E+05	1.164E-16	7.520E-16	1.156E-01
12	2.466E+00	5.247E+04	5.496E+05	6.150E-17	8.134E-16	1.251E-01
13	2.365E+00	1.287E+04	5.625E+05	1.411E-17	8.276E-16	1.272E-01
14	2.346E+00	6.614E+04	6.287E+05	6.885E-17	8.964E-16	1.378E-01
15	2.231E+00	1.614E+05	7.901E+05	1.669E-16	1.063E-15	1.635E-01
16	1.920E+00	2.067E+05	9.967E+05	1.681E-16	1.231E-15	1.893E-01
17	1.653E+00	3.516E+05	1.348E+06	2.849E-16	1.516E-15	2.331E-01
18	1.353E+00	7.859E+05	2.134E+06	4.404E-16	1.957E-15	3.008E-01
19	1.003E+00	6.016E+05	2.736E+06	2.205E-16	2.177E-15	3.347E-01
20	8.208E-01	4.689E+05	3.205E+06	2.630E-16	2.440E-15	3.751E-01
21	7.427E-01	1.264E+06	4.468E+06	4.566E-16	2.897E-15	4.453E-01
22	6.081E-01	1.470E+06	5.938E+06	4.326E-16	3.329E-15	5.118E-01
23	4.979E-01	1.706E+06	7.645E+06	6.764E-16	4.006E-15	6.158E-01
24	3.688E-01	1.729E+06	9.374E+06	3.575E-16	4.363E-15	6.708E-01
25	2.972E-01	3.449E+06	1.282E+07	6.914E-16	5.055E-15	7.771E-01
26	1.832E-01	3.438E+06	1.626E+07	4.848E-16	5.540E-15	8.516E-01
27	1.111E-01	2.593E+06	1.885E+07	3.353E-16	5.875E-15	9.032E-01
28	6.738E-02	2.136E+06	2.099E+07	1.384E-16	6.013E-15	9.244E-01
29	4.087E-02	7.672E+05	2.176E+07	6.209E-17	6.075E-15	9.340E-01
30	3.183E-02	7.045E+05	2.246E+07	2.003E-16	6.276E-15	9.648E-01
31	2.606E-02	7.273E+05	2.319E+07	1.466E-17	6.290E-15	9.670E-01
32	2.418E-02	5.691E+05	2.376E+07	2.492E-18	6.293E-15	9.674E-01
33	2.188E-02	1.478E+06	2.524E+07	1.211E-17	6.305E-15	9.693E-01
34	1.503E-02	2.379E+06	2.762E+07	4.462E-17	6.350E-15	9.761E-01
35	7.102E-03	2.309E+06	2.992E+07	2.054E-17	6.370E-15	9.793E-01
36	3.355E-03	2.149E+06	3.207E+07	7.566E-18	6.378E-15	9.804E-01
37	1.585E-03	3.491E+06	3.556E+07	5.872E-18	6.383E-15	9.813E-01
38	4.540E-04	1.917E+06	3.748E+07	1.890E-19	6.384E-15	9.814E-01
39	2.144E-04	1.917E+06	3.940E+07	2.749E-19	6.384E-15	9.814E-01
40	1.013E-04	2.476E+06	4.188E+07	5.525E-19	6.385E-15	9.815E-01
41	3.727E-05	2.943E+06	4.482E+07	1.159E-18	6.386E-15	9.817E-01
42	1.068E-05	1.668E+06	4.649E+07	1.072E-18	6.387E-15	9.818E-01
43	5.043E-06	2.068E+06	4.855E+07	2.068E-18	6.389E-15	9.822E-01
44	1.855E-06	1.421E+06	4.998E+07	2.183E-18	6.391E-15	9.825E-01
45	8.764E-07	1.294E+06	5.127E+07	2.904E-18	6.394E-15	9.829E-01
46	4.140E-07	2.841E+06	5.411E+07	1.166E-17	6.406E-15	9.847E-01
47	1.000E-07	9.761E+06	6.387E+07	9.927E-17	6.505E-15	1.000E+00

Table A.4.f. Absolute calculated neutron flux spectra and dpa rate
at the axial feed water nozzle elevation, azimuthal peak, and
R = front of the concrete shield wall of Grand Gulf Cycle 2

G	Energy (MeV)	Group flux	Cumulative flux	Group dpa rate	Cumulative dpa rate	dpa fraction
1	1.733E+01	1.192E+02	1.192E+02	3.483E-19	3.483E-19	7.139E-05
2	1.419E+01	7.333E+02	8.525E+02	1.940E-18	2.289E-18	4.691E-04
3	1.221E+01	2.544E+03	3.397E+03	6.129E-18	8.418E-18	1.725E-03
4	1.000E+01	5.848E+03	9.245E+03	1.298E-17	2.140E-17	4.385E-03
5	8.607E+00	1.141E+04	2.066E+04	2.381E-17	4.521E-17	9.266E-03
6	7.408E+00	2.961E+04	5.026E+04	5.753E-17	1.027E-16	2.106E-02
7	6.065E+00	4.968E+04	9.994E+04	8.862E-17	1.914E-16	3.922E-02
8	4.966E+00	9.763E+04	1.976E+05	1.534E-16	3.447E-16	7.066E-02
9	3.679E+00	7.523E+04	2.728E+05	1.031E-16	4.478E-16	9.178E-02
10	3.012E+00	5.994E+04	3.327E+05	7.618E-17	5.240E-16	1.074E-01
11	2.725E+00	7.729E+04	4.100E+05	9.854E-17	6.225E-16	1.276E-01
12	2.466E+00	4.553E+04	4.556E+05	5.336E-17	6.759E-16	1.385E-01
13	2.365E+00	1.145E+04	4.670E+05	1.255E-17	6.884E-16	1.411E-01
14	2.346E+00	5.710E+04	5.241E+05	5.944E-17	7.479E-16	1.533E-01
15	2.231E+00	1.345E+05	6.586E+05	1.390E-16	8.869E-16	1.818E-01
16	1.920E+00	1.642E+05	8.228E+05	1.335E-16	1.020E-15	2.091E-01
17	1.653E+00	2.748E+05	1.098E+06	2.226E-16	1.243E-15	2.548E-01
18	1.353E+00	5.658E+05	1.663E+06	3.170E-16	1.560E-15	3.198E-01
19	1.003E+00	4.336E+05	2.097E+06	1.589E-16	1.719E-15	3.523E-01
20	8.208E-01	3.414E+05	2.438E+06	1.915E-16	1.911E-15	3.916E-01
21	7.427E-01	9.230E+05	3.361E+06	3.336E-16	2.244E-15	4.599E-01
22	6.081E-01	1.029E+06	4.390E+06	3.027E-16	2.547E-15	5.220E-01
23	4.979E-01	1.095E+06	5.485E+06	4.340E-16	2.981E-15	6.109E-01
24	3.688E-01	1.198E+06	6.682E+06	2.475E-16	3.228E-15	6.617E-01
25	2.972E-01	2.423E+06	9.106E+06	4.859E-16	3.714E-15	7.612E-01
26	1.832E-01	2.565E+06	1.167E+07	3.616E-16	4.076E-15	8.354E-01
27	1.111E-01	1.977E+06	1.365E+07	2.556E-16	4.331E-15	8.877E-01
28	6.738E-02	1.659E+06	1.531E+07	1.074E-16	4.439E-15	9.097E-01
29	4.087E-02	6.396E+05	1.594E+07	5.176E-17	4.491E-15	9.204E-01
30	3.183E-02	5.694E+05	1.651E+07	1.619E-16	4.652E-15	9.535E-01
31	2.606E-02	4.313E+05	1.695E+07	8.696E-18	4.661E-15	9.553E-01
32	2.418E-02	3.941E+05	1.734E+07	1.726E-18	4.663E-15	9.557E-01
33	2.188E-02	1.158E+06	1.850E+07	9.487E-18	4.672E-15	9.576E-01
34	1.503E-02	1.959E+06	2.046E+07	3.675E-17	4.709E-15	9.651E-01
35	7.102E-03	1.888E+06	2.235E+07	1.679E-17	4.726E-15	9.686E-01
36	3.355E-03	1.798E+06	2.414E+07	6.329E-18	4.732E-15	9.699E-01
37	1.585E-03	2.985E+06	2.713E+07	5.022E-18	4.737E-15	9.709E-01
38	4.540E-04	1.690E+06	2.882E+07	1.666E-19	4.737E-15	9.709E-01
39	2.144E-04	1.678E+06	3.050E+07	2.406E-19	4.738E-15	9.710E-01
40	1.013E-04	2.186E+06	3.268E+07	4.877E-19	4.738E-15	9.711E-01
41	3.727E-05	2.633E+06	3.531E+07	1.037E-18	4.739E-15	9.713E-01
42	1.068E-05	1.514E+06	3.683E+07	9.728E-19	4.740E-15	9.715E-01
43	5.043E-06	1.911E+06	3.874E+07	1.911E-18	4.742E-15	9.719E-01
44	1.855E-06	1.342E+06	4.008E+07	2.063E-18	4.744E-15	9.723E-01
45	8.764E-07	1.251E+06	4.133E+07	2.807E-18	4.747E-15	9.729E-01
46	4.140E-07	2.960E+06	4.429E+07	1.214E-17	4.759E-15	9.754E-01
47	1.000E-07	1.181E+07	5.610E+07	1.201E-16	4.879E-15	1.000E+00

Table A.4.g. Absolute calculated neutron flux spectra and dpa rate
at the axial feed water nozzle elevation, azimuthal peak, and
R = six inches in the concrete shield wall of Grand Gulf Cycle 2

G	Energy (MeV)	Group flux	Cumulative flux	Group dpa rate	Cumulative dpa rate	dpa fraction
1	1.733E+01	1.615E+00	1.615E+00	4.720E-21	4.720E-21	3.613E-05
2	1.419E+01	9.114E+00	1.073E+01	2.411E-20	2.883E-20	2.207E-04
3	1.221E+01	2.689E+01	3.762E+01	6.478E-20	9.362E-20	7.167E-04
4	1.000E+01	5.984E+01	9.746E+01	1.328E-19	2.264E-19	1.733E-03
5	8.607E+00	1.183E+02	2.157E+02	2.468E-19	4.732E-19	3.622E-03
6	7.408E+00	4.374E+02	6.531E+02	8.499E-19	1.323E-18	1.013E-02
7	6.065E+00	9.375E+02	1.591E+03	1.672E-18	2.995E-18	2.293E-02
8	4.966E+00	2.182E+03	3.773E+03	3.428E-18	6.423E-18	4.917E-02
9	3.679E+00	1.662E+03	5.434E+03	2.277E-18	8.700E-18	6.660E-02
10	3.012E+00	1.681E+03	7.116E+03	2.137E-18	1.084E-17	8.296E-02
11	2.725E+00	2.314E+03	9.430E+03	2.951E-18	1.379E-17	1.056E-01
12	2.466E+00	1.829E+03	1.126E+04	2.143E-18	1.593E-17	1.220E-01
13	2.365E+00	6.054E+02	1.186E+04	6.635E-19	1.659E-17	1.270E-01
14	2.346E+00	2.484E+03	1.435E+04	2.586E-18	1.918E-17	1.468E-01
15	2.231E+00	4.101E+03	1.845E+04	4.241E-18	2.342E-17	1.793E-01
16	1.920E+00	4.057E+03	2.251E+04	3.300E-18	2.672E-17	2.046E-01
17	1.653E+00	5.500E+03	2.801E+04	4.457E-18	3.118E-17	2.387E-01
18	1.353E+00	7.065E+03	3.507E+04	3.958E-18	3.514E-17	2.690E-01
19	1.003E+00	4.256E+03	3.933E+04	1.560E-18	3.670E-17	2.809E-01
20	8.208E-01	3.693E+03	4.302E+04	2.072E-18	3.877E-17	2.968E-01
21	7.427E-01	8.345E+03	5.137E+04	3.016E-18	4.178E-17	3.199E-01
22	6.081E-01	9.196E+03	6.056E+04	2.706E-18	4.449E-17	3.406E-01
23	4.979E-01	7.696E+03	6.826E+04	3.051E-18	4.754E-17	3.639E-01
24	3.688E-01	7.230E+03	7.549E+04	1.494E-18	4.903E-17	3.754E-01
25	2.972E-01	1.567E+04	9.116E+04	3.142E-18	5.218E-17	3.994E-01
26	1.832E-01	2.172E+04	1.129E+05	3.062E-18	5.524E-17	4.229E-01
27	1.111E-01	2.115E+04	1.340E+05	2.734E-18	5.797E-17	4.438E-01
28	6.738E-02	2.214E+04	1.562E+05	1.434E-18	5.941E-17	4.548E-01
29	4.087E-02	1.030E+04	1.665E+05	8.337E-19	6.024E-17	4.612E-01
30	3.183E-02	9.344E+03	1.758E+05	2.656E-18	6.290E-17	4.815E-01
31	2.606E-02	3.604E+03	1.794E+05	7.266E-20	6.297E-17	4.821E-01
32	2.418E-02	4.744E+03	1.842E+05	2.077E-20	6.299E-17	4.822E-01
33	2.188E-02	1.845E+04	2.026E+05	1.511E-19	6.314E-17	4.834E-01
34	1.503E-02	4.017E+04	2.428E+05	7.536E-19	6.390E-17	4.891E-01
35	7.102E-03	4.372E+04	2.865E+05	3.889E-19	6.428E-17	4.921E-01
36	3.355E-03	4.732E+04	3.338E+05	1.666E-19	6.445E-17	4.934E-01
37	1.585E-03	1.024E+05	4.362E+05	1.722E-19	6.462E-17	4.947E-01
38	4.540E-04	7.085E+04	5.070E+05	6.984E-21	6.463E-17	4.948E-01
39	2.144E-04	8.001E+04	5.870E+05	1.147E-20	6.464E-17	4.949E-01
40	1.013E-04	1.224E+05	7.095E+05	2.732E-20	6.467E-17	4.951E-01
41	3.727E-05	1.788E+05	8.883E+05	7.044E-20	6.474E-17	4.956E-01
42	1.068E-05	1.184E+05	1.007E+06	7.609E-20	6.482E-17	4.962E-01
43	5.043E-06	1.741E+05	1.181E+06	1.741E-19	6.499E-17	4.975E-01
44	1.855E-06	1.401E+05	1.321E+06	2.154E-19	6.521E-17	4.992E-01
45	8.764E-07	1.485E+05	1.469E+06	3.333E-19	6.554E-17	5.017E-01
46	4.140E-07	5.103E+05	1.980E+06	2.094E-18	6.763E-17	5.177E-01
47	1.000E-07	6.194E+06	8.174E+06	6.300E-17	1.306E-16	1.000E+00

Table A.4.h. Absolute calculated neutron flux spectra and dpa rate at the axial feed water nozzle elevation, azimuthal peak, and R = one foot in the concrete shield wall of Grand Gulf Cycle 2

G	Energy (MeV)	Group flux	Cumulative flux	Group dpa rate	Cumulative dpa rate	dpa fraction
1	1.733E+01	8.778E-02	8.778E-02	2.565E-22	2.565E-22	3.267E-05
2	1.419E+01	5.232E-01	6.110E-01	1.385E-21	1.641E-21	2.090E-04
3	1.221E+01	1.466E+00	2.077E+00	3.532E-21	5.173E-21	6.589E-04
4	1.000E+01	3.308E+00	5.385E+00	7.340E-21	1.251E-20	1.594E-03
5	8.607E+00	6.434E+00	1.182E+01	1.343E-20	2.594E-20	3.305E-03
6	7.408E+00	2.810E+01	3.992E+01	5.460E-20	8.054E-20	1.026E-02
7	6.065E+00	6.130E+01	1.012E+02	1.094E-19	1.899E-19	2.419E-02
8	4.966E+00	1.290E+02	2.302E+02	2.027E-19	3.926E-19	5.001E-02
9	3.679E+00	9.022E+01	3.204E+02	1.236E-19	5.162E-19	6.575E-02
10	3.012E+00	1.010E+02	4.214E+02	1.284E-19	6.445E-19	8.211E-02
11	2.725E+00	1.409E+02	5.624E+02	1.797E-19	8.242E-19	1.050E-01
12	2.466E+00	1.340E+02	6.963E+02	1.570E-19	9.812E-19	1.250E-01
13	2.365E+00	5.443E+01	7.507E+02	5.965E-20	1.041E-18	1.326E-01
14	2.346E+00	2.010E+02	9.518E+02	2.093E-19	1.250E-18	1.593E-01
15	2.231E+00	2.909E+02	1.243E+03	3.008E-19	1.551E-18	1.976E-01
16	1.920E+00	2.673E+02	1.510E+03	2.174E-19	1.768E-18	2.253E-01
17	1.653E+00	3.302E+02	1.840E+03	2.676E-19	2.036E-18	2.594E-01
18	1.353E+00	3.789E+02	2.219E+03	2.123E-19	2.248E-18	2.864E-01
19	1.003E+00	2.191E+02	2.438E+03	8.029E-20	2.329E-18	2.966E-01
20	8.208E-01	1.774E+02	2.616E+03	9.950E-20	2.428E-18	3.093E-01
21	7.427E-01	3.402E+02	2.956E+03	1.230E-19	2.551E-18	3.250E-01
22	6.081E-01	3.386E+02	3.294E+03	9.965E-20	2.651E-18	3.377E-01
23	4.979E-01	2.804E+02	3.575E+03	1.112E-19	2.762E-18	3.518E-01
24	3.688E-01	2.503E+02	3.825E+03	5.175E-20	2.814E-18	3.584E-01
25	2.972E-01	5.145E+02	4.340E+03	1.032E-19	2.917E-18	3.716E-01
26	1.832E-01	5.953E+02	4.935E+03	8.394E-20	3.001E-18	3.822E-01
27	1.111E-01	5.125E+02	5.447E+03	6.627E-20	3.067E-18	3.907E-01
28	6.738E-02	4.879E+02	5.935E+03	3.160E-20	3.098E-18	3.947E-01
29	4.087E-02	2.188E+02	6.154E+03	1.771E-20	3.116E-18	3.970E-01
30	3.183E-02	1.943E+02	6.348E+03	5.525E-20	3.171E-18	4.040E-01
31	2.606E-02	7.083E+01	6.419E+03	1.428E-21	3.173E-18	4.042E-01
32	2.418E-02	9.363E+01	6.513E+03	4.100E-22	3.173E-18	4.042E-01
33	2.188E-02	3.498E+02	6.863E+03	2.865E-21	3.176E-18	4.046E-01
34	1.503E-02	7.197E+02	7.582E+03	1.350E-20	3.190E-18	4.063E-01
35	7.102E-03	7.418E+02	8.324E+03	6.599E-21	3.196E-18	4.072E-01
36	3.355E-03	7.783E+02	9.103E+03	2.740E-21	3.199E-18	4.075E-01
37	1.585E-03	1.583E+03	1.069E+04	2.663E-21	3.202E-18	4.079E-01
38	4.540E-04	1.069E+03	1.175E+04	1.054E-22	3.202E-18	4.079E-01
39	2.144E-04	1.205E+03	1.296E+04	1.728E-22	3.202E-18	4.079E-01
40	1.013E-04	1.874E+03	1.483E+04	4.181E-22	3.202E-18	4.079E-01
41	3.727E-05	2.852E+03	1.769E+04	1.124E-21	3.203E-18	4.081E-01
42	1.068E-05	1.959E+03	1.965E+04	1.259E-21	3.205E-18	4.082E-01
43	5.043E-06	3.059E+03	2.270E+04	3.059E-21	3.208E-18	4.086E-01
44	1.855E-06	2.593E+03	2.530E+04	3.986E-21	3.212E-18	4.091E-01
45	8.764E-07	2.903E+03	2.820E+04	6.514E-21	3.218E-18	4.100E-01
46	4.140E-07	1.189E+04	4.009E+04	4.880E-20	3.267E-18	4.162E-01
47	1.000E-07	4.506E+05	4.907E+05	4.583E-18	7.850E-18	1.000E+00

EXTERNAL DISTRIBUTION

M. E. Mayfield, U. S. Nuclear Regulatory Commission, Division of Engineering,
Mail Stop NL/S 217/C, Washington DC 20555

C. Z. Serpan, Jr., U.S. Nuclear Regulatory Commission, Division of Engineering,
Mail Stop NL/S-217C, Washington DC 20555

A. Taboada, U.S. Nuclear Regulatory Commission, Division of Engineering, Mail
Stop NL/S-217C, Washington DC 20555

Assistant Manager for Energy Research and Development, U.S. Department of
Energy, Oak Ridge Operations Office, P. O. Box E, Oak Ridge TN 37831

U.S. Department of Energy, Technical Information Center, Office of Information
Services, P. O. Box 62, Oak Ridge TN 37831

Given distribution under Category RL (10 copies - NTIS)

INTERNAL DISTRIBUTION

- | | | | |
|--------|-----------------|--------|--------------------------------|
| 1. | J. A. Bucholz | 22. | J. A. Wang |
| 2. | R. L. Childs | 23. | R. M. Westfall |
| 3. | W. R. Corwin | 24. | G. E. Whitesides |
| 4-14. | F. B. K. Kam | 25. | A. Zucker |
| 15. | R. K. Nanstad | 26. | Document Reference Section |
| 16. | C. E. Pugh | 27. | Central Research Library |
| 17-19. | C. H. Shappert | 28-30. | Laboratory Records Department |
| 20. | F. W. Stallmann | 31. | Laboratory Records - ORNL R.C. |
| 21. | J. S. Tang | 32. | ORNL Patent Office |

BIBLIOGRAPHIC DATA SHEET

(See instructions on the reverse)

1. REPORT NUMBER
(Assigned by NRC. Add Vol., Supp., Rev.,
and Addendum Numbers, if any.)

NUREG/CR-5449
ORNL/TM-11350

2. TITLE AND SUBTITLE

Determination of the Neutron and Gamma Flux Distribution in the
Pressure Vessel and Cavity of a Boiling Water Reactor

3. DATE REPORT PUBLISHED

MONTH | YEAR
June | 1990

4. FIN OR GRANT NUMBER

B0415

5. AUTHOR(S)

M. Asgari, M. L. Williams, and F. B. K. Kam

6. TYPE OF REPORT

Technical

7. PERIOD COVERED (Inclusive Dates)

8. PERFORMING ORGANIZATION - NAME AND ADDRESS (If NRC, provide Division, Office or Region, U.S. Nuclear Regulatory Commission, and mailing address; if contractor, provide name and mailing address.)

Oak Ridge National Laboratory
P. O. Box 2008
Oak Ridge TN 37831

9. SPONSORING ORGANIZATION - NAME AND ADDRESS (If NRC, type "Same as above"; if contractor, provide NRC Division, Office or Region, U.S. Nuclear Regulatory Commission, and mailing address.)

Division of Engineering
Office of Nuclear Regulatory Research
U.S. Nuclear Regulatory Commission
Washington DC 20555

10. SUPPLEMENTARY NOTES

11. ABSTRACT (200 words or less)

The Grand Gulf Boiling Water Reactor (BWR/6), owned and operated by Mississippi Power & Light Company has been analyzed to determine the neutron and gamma energy spectrum and flux levels in regions from the reactor vessel throughout the concrete shield wall. Several two-dimensional and one-dimensional transport calculations were performed for the Grand Gulf reactor configuration. The results from these calculations were synthesized to obtain the three-dimensional neutron flux spectra and dosimeter activities. The results from the transport calculations indicate the flux above 1 MeV peaks near the axial midplane and azimuthal angle between 40° and 45°, depending on the radial locations. The peak flux above 1 MeV incident on the vessel and at midcavity is about 1.82×10^9 and 1.07×10^8 n·cm⁻²·s⁻¹, respectively. The vessel fluence accumulated during Cycle 2 and after 32 effective full power years is about 4.41×10^{16} and 1.84×10^{18} n·cm⁻²·s⁻¹, respectively. The peak flux above 1 MeV at the front of the concrete shield wall, 15.24 cm (6 in.) into the concrete wall, and 30.48 cm (1 ft) into the concrete wall is about 7.91×10^7 , 7.24×10^6 , and 6.44×10^5 n·cm⁻²·s⁻¹, respectively.

The results obtained from the gamma calculations show that the peak gamma heating at the 0-T location of the reactor pressure vessel has a value of 2.54×10^{-3} W/g of stainless steel (SS 304). The peak gamma absorbed dose rate at the midcavity is about 7.31×10^3 rad/h at full power operation.

12. KEY WORDS/DESCRIPTORS (List words or phrases that will assist researchers in locating the report.)

boiling water reactor
neutron transport calculations
surveillance dosimetry

13. AVAILABILITY STATEMENT

Unlimited

14. SECURITY CLASSIFICATION

(This Page)

Unclassified

(This Report)

Unclassified

15. NUMBER OF PAGES

16. PRICE

UNITED STATES
NUCLEAR REGULATORY COMMISSION
WASHINGTON, D.C. 20555

OFFICIAL BUSINESS
PENALTY FOR PRIVATE USE, \$300

SPECIAL FOURTH-CLASS RATE
POSTAGE & FEES PAID
USNRC
PERMIT No. G-67